# ANALYSIS OF PULSE DIVERSITY IN RADAR SYSTEMS

A THESIS SUBMITTED TO
THE GRADUATE SCHOOL OF NATURAL AND APPLIED SCIENCES
OF
MIDDLE EAST TECHNICAL UNIVERSITY

BY

UMUT KEÇELİOĞLU

IN PARTIAL FULFILLMENT OF THE REQUIREMENTS
FOR
THE DEGREE OF MASTER OF SCIENCE
IN
ELECTRICAL AND ELECTRONICS ENGINEERING

SEPTEMBER 2006

Approval of the Graduate School of Natural And Applied Science

Prof. Dr. Canan ÖZGEN
Director

I certify that this thesis satisfies all the requirements as a thesis for the degree of Master of Science.

Prof. Dr. İsmet ERKMEN
Head of Department

This is to certify that we have read this thesis and that in our opinion it is fully adequate, in scope and quality, as a thesis for the degree of Master of Science.

Assoc. Prof. Dr. S. Sencer KOÇ
Supervisor

**Examining Committee Members**

Prof. Dr. Yalçın TANIK (METU, EEE) _____

Assoc. Prof. Dr. S. Sencer KOÇ (METU, EEE) _____

Prof. Dr. Altunkan HIZAL (METU, EEE) _____

Prof. Dr. Fatih CANATAN (METU, EEE) _____

Assoc. Prof. Dr. S. Gökhun TANYER (TÜBİTAK-UEKAE) _____

**I hereby declare that all information in this document has been obtained and presented in accordance with academic rules and ethical conduct. I also declare that, as required by these rules and conduct, I have fully cited and referenced all material and results that are not original to this work.**

Name, Last name : KEÇELİOĞLU, Umut

Signature :

# ABSTRACT

## ANALYSIS OF PULSE DIVERSITY IN RADAR SYSTEMS

**KEÇELİOĞLU, Umut**

**M.S., Department of Electrical and Electronics Engineering**
**Supervisor: Assoc. Prof. Dr. S. Sencer KOÇ**

**September 2006, 120 pages**

In this thesis, the pulse diversity technique in radar systems in high clutter environments is investigated. In this technique, different pulse compression methods are used in each pulse in the transmitted burst to increase the unambiguous range.

In pulse diversity, the design of filters used in the receiver is as important as designing the transmitted waveform. At the output of pulse-burst filter that processes pulse-by-pulse, as many channels as the pulses in the burst occur. Each of these channels is matched to a certain range interval.

In order to improve the detector performance, the phase codes used in the transmitted pulse-burst waveform and their corresponding filters must have good auto-correlation and cross-correlation properties, either individually or as their sum.

In the literature some phase codes, having mentioned properties, are present. However, the performance of these codes in radar applications is not fully

evaluated. The studies in the thesis show that the codes in the literature cannot be used directly in radar applications. In the scope of thesis, optimization criteria suitable for radar applications are defined and applied according to the mentioned requirements. Then, the obtained phase codes are tested in the radar simulator and the obtained results of the simulations are evaluated.

**Keywords:** pulse diversity, pulse-burst waveform, pulse compression, radar simulator

# ÖZ

## RADAR SİSTEMLERİNDE DARBE ÇEŞİTLİLİĞİ ANALİZİ

**KEÇELİOĞLU, Umut**

**Yüksek Lisans, Elektrik ve Elektronik Mühendisliği Bölümü**
**Tez Yöneticisi: Doç. Dr. S. Sencer KOÇ**

**Eylül 2006, 120 sayfa**

Bu tezde radar sistemlerinde yüksek kargaşa ortamlarında darbe çeşitliliği yöntemi incelenmiştir. Bu teknikte, gönderilen çoğuşmadaki her darbede belirli menzili arttırmak için farklı darbe sıkıştırma yöntemleri kullanılmıştır.

Darbe çeşitliliğinde almaçta kullanılan süzgeçlerin tasarımı gönderilen dalgabiçiminin tasarlanması kadar önemlidir. Darbeden-darbeye çalışan darbe-çoğuşmalı süzgeç çıkışında çoğuşma içindeki darbelerin sayısı kadar kanal oluşur. Bu kanalların herbiri belirli bir menzil aralığına uyumludur.

Sezici başarımını artırmak için gönderilen darbe-çoğuşmalı dalga biçiminde ve onların karşılığı olan süzgeçlerde kullanılan faz kodlarının bireysel veya toplamda iyi özilinti ve karşılıklı-ilinti özellikleri olmalıdır.

Literatürde bahsedilen özelliklere sahip bazı faz kodları bulunmaktadır. Ancak, bu kodların radar uygulamalarındaki başarımları tam olarak değerlendirilmemiştir. Bu tezdeki çalışmalar göstermektedir ki; literatürdeki

kodlar radar uygulamarında doğrudan kullanılamazlar. Tez kapsamında, radar uygulamaları için uygun olan optimizasyon ölçütleri tanımlanmış ve bahsedilen gereksinimlere göre uygulanmıştır. Sonrasında elde edilen faz kodları radar benzetimcisinde test edilmiş ve elde edilen benzetim sonuçları değerlendirilmiştir.

**Anahtar kelimeler:** darbe çeşitliliği, darbe-çoğuşmalı dalga biçimi, darbe sıkıştırması, radar benzetimcisi

***To my family***

# ACKNOWLEDGEMENTS

I wish to express my sincere gratitude to my supervisor Assoc. Prof. Dr. Seyit Sencer Koç for his guidance, advice, criticism, encouragements and insight throughout the research.

I would like to express my thanks and appreciation to Dr. Mehmet Alper Kutay for his suggestions and comments. I would like to thank Özgur İnce for his help in writing this thesis.

I am also grateful to my colleagues from TÜBİTAK-UEKAE (İLTAREN) department for their encouragement.

Finally, special appreciation and gratitude are also for my family and Nesrin Güler for their encouragement, reassurance, endless love and understanding of spending lots of time on this thesis.

# TABLE OF CONTENTS

# LIST OF TABLES

# LIST OF FIGURES

# LIST OF ABBREVIATIONS

| | |
|---|---|
| ACV | Aperiodic Correlation Vector |
| AACF | Aperiodic Auto-Correlation Function |
| ACCF | Aperiodic Cross-Correlation Functions |
| AACV | Aperiodic Auto-Correlation Vector |
| ACCV | Aperiodic Cross-Correlation Vector |
| CA-CFAR | Cell Averaging Constant False Alarm Rate |
| CCF | Cross-Correlation Function |
| CFAR | Constant False Alarm Rate |
| ISL | Integrated Sidelobe Level |
| MTI | Moving Target Indicator |
| PCV | Periodic Correlation Vector |
| PACF | Periodic Auto-Correlation Function |
| PCCF | Periodic Cross-Correlation Functions |
| PACV | Periodic Auto-Correlation Vector |
| PCCV | Periodic Cross-Correlation Vector |
| PSL | Peak to Sidelobe Ratio |
| PRI | Pulse Repetition Interval |
| PRF | Pulse Repetition Frequency |
| RCS | Radar Cross section |
| SCR | Signal to Clutter Ratio |
| SNR | Signal to Noise Ratio |
| SPR | Sidelobe to Peak Ratio |
| SQP | Sequential Quadratic Programming |
| ZCC | Zero-Cross Correlation |
| ZSPC | Zero Sidelobe Periodic Code |

# CHAPTER 1

# INTRODUCTION

## 1.1 PROBLEM DEFINITION

Radar is an electromagnetic system, used for detecting and tracking objects in different environments. In pulse Doppler radar, the distance of an object is determined by observing the time delay between transmitted and received pulses. The velocity of an object is measured by comparing the transmitted and received waveforms carrier frequencies. However, in pulse radar systems, periodicity of transmitted waveform in time domain and limitation of sampling frequency in frequency domain cause ambiguous intervals in range and velocity. In range measurement, if a target echo of any transmitted pulse reaches to the receiver after the following pulse is transmitted, the target range will be measured ambiguously. Similarly, when the Doppler frequency shift is larger than half of the sampling frequency, the target velocity will be decided ambiguously.

All radar systems are required to have high unambiguous interval and high resolution in range and velocity. However, it is difficult to obtain improvement both in range and velocity concurrently [33], [34]. For example, in pulse radar systems good velocity resolution requires a wider signal; on the other hand, minimizing eclipsing and obtaining high resolution in range requires a shorter transmission time.

In order to get the required properties in radar systems, waveforms with different characteristics can be transmitted and received signals can be processed through different methods. Coding of the transmitted waveform, coherent processing of the pulse-burst waveform or using diversity would result in various improvements in pulse Doppler radar systems.

Modulating the transmitted pulses increases the range resolution. Using a long burst increases Doppler frequency resolution. However, neither of these two methods affects the ambiguous intervals occurring in range and velocity. Pulse repetition interval (PRI) value can be increased to increase the unambiguous range. This method decreases the unambiguous Doppler frequency interval as well. Furthermore; increasing the PRI needs high peak power. In order to increase the unambiguous range without increasing the PRI, diversity may be applied to the transmitted waveform by some of its parameters.

Diversity in the pulse-burst waveform can be done with various parameters. The first method is to diversify the identical pulse train by using different pulse separation periods [30], [31]. This is called PRF diversity. PRF diversity maximizes the unambiguous range and unambiguous Doppler frequency, while minimizing blind range and speed, [5]. The second method is changing the radar carrier frequency used in each pulse [32]. This is called frequency diversity. Frequency diversity forces a potential jammer to spread the available energy across a wider bandwidth, thereby decreasing the jammer energy density, [5]. However, it is quite difficult to achieve coherent integration in both methods when these parameters change in pulse-to-pulse basis. Besides, there are various ineffectiveness and loss in signal processing. Another method for increasing the unambiguous range is using pulses with different waveforms in the transmitted pulse-burst waveform. This is called pulse diversity or waveform agility. Pulse diversity can be considered as a

way to improve the radar ambiguity function according to the needs. The unambiguous range can be increased to the product of PRI range and the number of different pulses used in the burst by pulse diversity.

In pulse diverse radar, coherent integration is achieved easily and effectively with pulse-burst matched filtering [5]. Pulse-burst matched filtering process can be done in two ways. In the first method, all of the received pulses are kept until whole burst waveform is received. Then, it is filtered through the matched filter, which has the same length as the transmitted pulse-burst waveform [1]. In the second method, received pulses are processed individually through single matched filters of the pulses in the pulse-burst waveform. After the single-pulse matched filter outputs of all of the pulses inside the burst are obtained, the outputs are time aligned and summed [1], [23], [24], [25]. This method is called pulse-by-pulse processing [1]. In pulse-by-pulse processing; there should be as many single-pulse matched filters as the number of different pulses in the burst. Despite the fact that more than one filter are used in pulse-by-pulse processing, filtering process is more efficient since the no-signal intervals in the burst are eliminated. In pulse-by-pulse processing as many channels as the number of different pulses in the burst are constructed at the filter output. Each of these channels is matched to a certain PRI interval. In other words; the echo of a target whose delay time is between [$nPRI$, ($n$+1)$PRI$], occurs in the $(n+1)^{th}$ channel. Therefore, the targets in the pulse-burst waveform range can be detected unambiguously.

In order to be able to detect the targets unambiguously, the properties listed below should be obtained at the end of the filtering process.

1. The number of channels, i.e., the number of different pulses in the burst should be large.

2. The signal level should be low in the channels that are not matched to the target range.
3. The time sidelobe level should be low in the channel that is matched to the target range.
4. The peak level of the echo signal should be high in the channel that is matched to the target range.

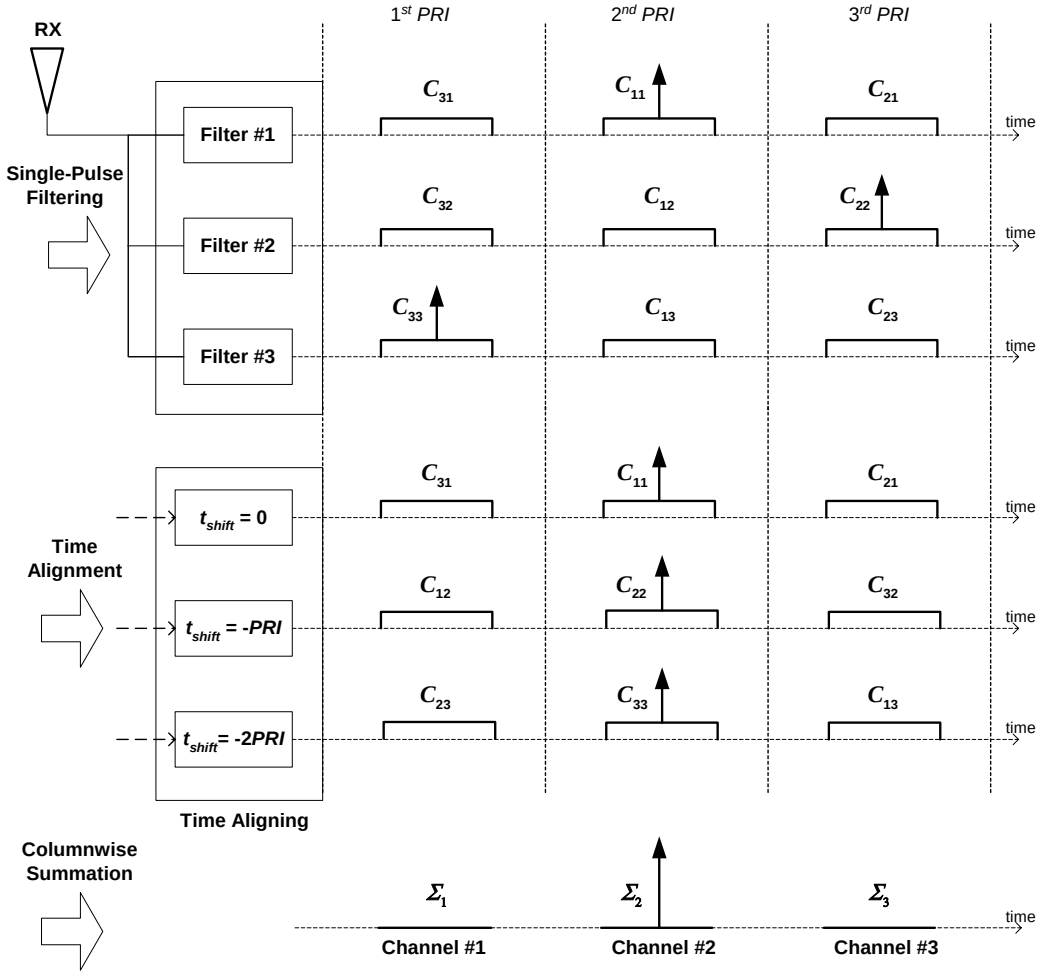


**Figure 1-1** Phases of pulse-by-pulse processing

In Figure 1-1 the phases of the processing of 3-pulsed burst waveform with a pulse-by-pulse processing pulse-burst filter are given. $C_{mn}$ is the correlation

function between the $m^{th}$ pulse and the $n^{th}$ filter. The target is in the $c$[$PRI$ 2$PRI$]/2 range interval. Therefore, the order of the pulses in the received pulse-burst waveform is as [$p_3$ $p_1$ $p_2$]. If the single-pulse filters are matched to the transmitted pulses, the signal appearing in the Channel #2, which is matched channel, is equal to the sum of the auto-correlation functions of the transmitted pulses. The range sidelobes of the correlation function of a single-pulse cannot be reduced below certain bounds that can be found in literature [16], [17]. However, the sum of correlation functions is not restricted in this. $\Sigma_1$ and $\Sigma_3$ sum signals are expected to be equal to 0 and the sum signal $\Sigma_2$ is expected to have zero-sidelobe level. This condition will decrease the false alarms, increase the unambiguous range from $cPRI$/2 to $c3PRI$/2 and suppress the clutter signal, coming from multiple ranges, inherently in each channel. In each channel only the clutter signal coming from its matched range interval occurs. This clutter signal can be suppressed by MTI as well. Even if the target is stationary, the characteristics of the $\Sigma_1$, $\Sigma_2$ and $\Sigma_3$ sum signals are different from each other. Therefore, the MTI process cannot be done between the sum signals that occur in the same burst. However, characteristics of the $\Sigma_1$, $\Sigma_2$ and $\Sigma_3$ sum signals occurring in any burst are the same with the characteristics of the sum signals with the same number occurring in another burst. Consequently, MTI processing is executed between the sum signals that occur in the channels with the same numbers in the consecutive bursts.

Increasing the number of the pulses used in pulse-burst waveform increases the number of channels constructed at the filter output [23], [24], [25]. Thus, unambiguous range increases. However, increasing the number of pulses in the burst prolongs the time interval between the pulses used in cancellation process. Since the clutter inevitably has an internal fluctuation, the fluctuation between the pulses used in the MTI will increase and clutter suppression will be reduced. Consequently, the number of pulses that will be used in the burst should be specified under the requirements and the environmental conditions.

High peak level in the matched channel make the detection of the target echo easier in high clutter background. If the sidelobe level in matched channel is low, smaller targets will be prevented from shadowing by a large one. To get high peak level and zero sidelobe level in the matched channel, the code matrix is supposed to comprise of complementary code sequences [18]-[25].

Low signal level in mismatched channels ensures that the clutter signal, coming from the mismatched range intervals, can be suppressed in each channel. Therefore, only the clutter signal from the matched range interval exists in each channel. To get low signal level in the mismatched channels, the code matrix is supposed to comprise of zero cross-correlation (ZCC) code sequences [22].

It seems that in pulse diverse radar systems, in which complementary and ZCC code sequences are used, unambiguous range will be shifted and target detection will be done more easily [22]. However, target motion can cause significant phase shift between the consecutive pulses in the burst. This phase shift reduces the signal level at matched point and increases the signal level at undesired points after the coherent integration of pulses in the burst. Thus; the target cannot be detected and false alarms occur. The distortion due to the Doppler shift in the coherent processing of pulse diverse waveform is more serious than the distortion in the processing of single pulse. The phase shift between code elements in the pulse is equal to the integration of Doppler frequency during chipwidth. However, the phase shift between the pulses in the burst is equal to the integration of Doppler frequency during the PRI.

In burst processing it is very difficult for a single filter to tolerate all possible Doppler shifts. More than one filter should be used in the receiver to tolerate all possible Doppler shifts. Each of the filters is expected to provide the required properties mentioned above in a certain Doppler interval. In order to

achieve high PSL value, mismatched filters may be used instead of matched filters in the receiver. Consequently, the distortion in the integration of the pulses in the burst due to the Doppler shift will decrease. At the filter outputs low sidelobe level will be obtained and unambiguous range will increase.

## 1.2 LITERATURE SURVEY

The studies in the scope of this thesis are included in the pulse compression concept of radar signal processing. However, nearly all of the pulse compression studies of radar signal processing in the literature are on coding a single pulse.

In the literature all of the code matrices, which can be used in coding pulse-burst waveform, are studied according to the information theory. In some studies, it is claimed that complementary, ZCC and ZCC-Complementary code matrices can be used in radar applications. However, the results of these code matrices in radar applications are not evaluated in any of these studies.

Complementary series are first defined by Golay in the literature [16]. Golay composed pairs of binary codes that can be used especially for solving optical problems. Afterwards, Tseng and Liu [19] define the binary complementary codes that are made up of more than two sequences. Sivaswamy [20] describes multiphase complementary sequences as well. Some studies are done on multiphase complementary sequences in information theory. The studies on using these codes in radar applications is done only by Kretschmer and Gerlach, [23], [24], [25]. Also; Anderson, Temple, Brown and Crossley introduce a nonlinear suppression technique for range ambiguity resolution in pulse Doppler radars, [26].

Kretschmer and Gerlach stated that wrong detections caused by the signal sources around the target could be avoided by using complementary code sequences. Since, the sum of the auto-correlations of the complementary code sequences has zero sidelobe level. Furthermore, they obtained some code series, shifted sums of whose cross-correlation functions are nearly zero [25]. They stated that low value of the sum of cross correlation functions inherently suppresses the clutter signals coming from the mismatched range intervals. Finally, they identified the ZCC-complementary code series [23]. The sidelobe of the sum of the auto-correlation functions and sum of cross correlation functions are equal to zero in ZCC-complementary sequences. Consequently, ZCC-complementary code sequences have zero sidelobe level in the matched channel and zero signal level in mismatched channels at the output of the matched filter. This property is the point that is aimed in radar applications. In this way; the unambiguous range increases, the clutter signals coming from mismatched range intervals are inherently suppressed and detections can be made more correctly. Kretschmer and Gerlach mentioned all of these advantages of ZCC-complementary codes, however; they did not evaluate the results of these codes under Doppler effect with clutter signal.

In the scope of this thesis pulse diverse radar systems, in which pulse-burst waveform is transmitted and received waveform is processed coherently, are studied. The studies particularly focused on the codes used in transmitted waveform and their corresponding filters in the receiver. The received signal is processed through pulse-burst filter, which has pulse-by pulse processing. The codes, which have low sidelobe level in the matched channel and low signal level in the mismatched channels after filtering under Doppler effect, are searched. Furthermore, performances of the code matrices in the literature and code matrices obtained by some optimizations are evaluated.

In Chapter 2, fundamentals of matched filter and pulse compression concepts are mentioned. Afterwards, some functions, defined on code sequences, are given. The properties of complementary, ZCC and ZCC-complementary codes that can be used in pulse diversity are given. Besides; orthogonal code matrices are studied to be able to make comparison.

In Chapter 3, the pulse-burst matched filter outputs of orthogonal, complementary, ZCC and ZCC-Complementary code matrices, which are defined in Chapter 2, are simulated. Ambiguity diagrams of these code matrices are formed and their performances are evaluated on the condition of having different Doppler shifts.

In Chapter 4, it is decided to use more than one mismatched filter in the receiver to tolerate all possible Doppler shifts. Four different optimization methods are defined in accordance with the needs determined as a result of the observations that are made in Chapter 3. Suitable waveform and mismatched filter code matrices are searched by these optimization methods. Pulse-burst mismatched filter outputs of the code matrices, obtained through optimizations, are formed. Then, the conditions in which these codes can be used are evaluated.

In Chapter 5, the radar model, which is formed to carry out experiments in scope of the thesis, is mentioned. The features of the clutter signal formed in the radar model and the modeling techniques are given. Then some scenarios of the radar applications, in which optimized code matrices of waveform and mismatched filters are used, are simulated. The performances of these code matrices under clutter and Doppler effect are evaluated with MTI and constant false alarm rate (CFAR) systems.

Finally, in Chapter 6 the conclusion of thesis and possible future works are discussed.

# CHAPTER 2

# BACKGROUND

## 2.1 PULSE COMPRESSION

Pulse compression involves the transmission of a long duration coded pulse and the processing of the received echo to obtain a relatively narrow pulse. The use of long duration coded pulses provides some advantages to the radar system, listed below.

- Increased detection capability is obtained,
- Generation of high peak power signals is avoided,
- Increased resolving capability in range is obtained,
- The vulnerability to interfering signal is suppressed.

The disadvantage of using long duration pulse is that in radar systems using single antenna, the period in which the receiver is off during transmission gets longer. This situation extends the blind range in which the target cannot be detected.

Modulating the signal within the transmitted pulse increases the radar signal bandwidth to be transmitted. This modulation may be applied to the signal with its amplitude, phase or frequency. In radar applications target echo signals are passed through filters matched to the transmitted signal to compress the echo energy into a time duration $\tau_c$. This duration is inversely

proportional to the transmitted bandwidth. The ratio of the transmitted to compressed pulse lengths is called pulse compression ratio [10].

$$\rho = B_t \tau_t = \frac{\tau_t}{\tau_c} \qquad \textbf{(2.1)}$$

where $\rho$ : pulse compression ratio; $B_t$ : transmitted bandwidth; $\tau_t$ : transmitted pulsewidth; $\tau_c$ : compressed pulsewidth.

When compressing $\tau_t$ to $\tau_c$, the resultant signal is not in the form of only a single pulse in time. There are other components of compressed pulse waveform in time domain called range sidelobes. The ratio of the main peak to sidelobe peak depends on the characteristics of the modulation used in the signal. Time sidelobes on the radar pulses are not desired, since a time sidelobe of a strong echo may hide a weaker target return [10].

### 2.1.1 Phase Coded Pulses

Phase-coded waveforms are subdivided into a number of subpulses. The subpulses are of equal duration, and each has a particular phase. The phase of each subpulse is selected in accordance with a given code sequence. If the phase sequence consists of only 0º or 180º phases, it is called *binary phase coding*. If the elements of the phase sequence differ from 0º to 360º, then it is called *polyphase coding*. In the reception, the compressed pulse is obtained by either matched filtering or correlation processing [2]. The width of the compressed pulse at the half-amplitude point is nominally equal to the subpulsewidth. Hence, the range resolution is proportional to the time duration of one element of the code. It is also concluded that compression ratio is equal to the number of subpulses in the waveform.

The choice of waveform directly determines the signal-to-noise ratio (SNR), the range resolution, the Doppler resolution, ambiguities in range and Doppler domain, range and Doppler domain sidelobes, and range Doppler coupling in the radar system. There are many types of codes in the literature. Some of them used in this thesis are provided with their properties in Section 2.2.1.2.

## 2.2 MATCHED FILTER

In the radar systems the probability of detection is related to the SNR rather than to the waveform or average power of the signal received [5]. Consequently, maximizing the SNR is the main concern in the filtering process. Matched filter is a linear filter whose impulse response is determined by a specific signal to obtain maximum attainable SNR at the end of the filtering process. In Figure 2-1 the usage of the matched filter is given.

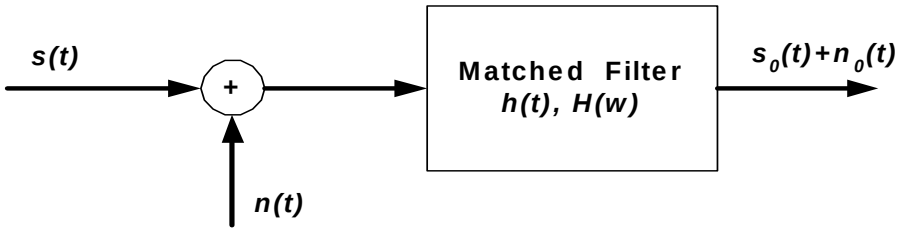


**Figure 2-1** Matched filter definition

The signal power at the output of the matched filter is given in (2.2).

$$\left|s_0(t)\right|^2 = \left|h(t) * s(t)\right|^2 = \left|\frac{1}{2\pi}\int_{-\infty}^{\infty} H(\omega)S(\omega)e^{j\omega t}d\omega\right|^2 \qquad \textbf{(2.2)}$$

where $s_0(t)$ : output signal; $h(t)$ : matched filter impulse response; $s(t)$ : input signal; $H(\omega)$ : Fourier transform of $h(t)$; $S(\omega)$ : Fourier transform of $s(t)$.

The noise power spectral density at the input of the filter is equal to $N_0/2$ per Hertz and the total noise power at the output of the filter is given in (2.3).

$$n_0(t) = \frac{1}{2\pi}\frac{N_0}{2}\int_{-\infty}^{\infty}\left|H(\omega)\right|^2 d\omega \tag{2.3}$$

where $n_o(t)$ : total noise power at the output of the matched filter.

The output *SNR* of the filter at time $t_0$ is given in (2.4).

$$SNR_{out} = \frac{\left|s_0(t_0)\right|^2}{n(t_0)} = \frac{\left|\int_{-\infty}^{\infty} H(\omega)S(\omega)e^{j\omega t_0}d\omega\right|^2}{\pi N_0\int_{-\infty}^{\infty}\left|H(\omega)\right|^2 d\omega} \tag{2.4}$$

The Schwarz inequality for any two complex signals is given in (2.5).

$$\left|\int_{-\infty}^{\infty} X(\omega)Y(\omega)d\omega\right|^2 \le \int_{-\infty}^{\infty}\left|X(\omega)\right|^2 d\omega\int_{-\infty}^{\infty}\left|Y(\omega)\right|^2 d\omega \tag{2.5}$$

The inequality in (2.5) holds if and only if the equation in (2.6) is satisfied.

$$X(\omega) = \alpha Y^*(\omega), \qquad \alpha \ : \ \textit{arbitrary constant} \tag{2.6}$$

$X(\omega)$ and $Y(\omega)$ can be chosen as in (2.7).

$$\begin{aligned} X(\omega) &= H(\omega) \\ Y(\omega) &= S(\omega)e^{j\omega t} \end{aligned} \tag{2.7}$$

From (2.6) and (2.7), maximum $SNR_{out}$ is obtained when the condition specified in (2.8) is satisfied.

$$H(\omega) = \alpha S^*(\omega)e^{-j\omega t} \tag{2.8}$$

Thus the frequency response of the matched filter is obtained. By taking the inverse Fourier transform of the $H(\omega)$, the impulse response of the matched filter is also obtained.

$$h(t) = \alpha s^*(t_0 - t) \tag{2.9}$$

where $h(t)$ must be zero for $t<0$ for the filter to be casual. This is correct only if $t_0$ is equal or longer than the duration of the signal $s(t)$.

The $SNR_{out}$ at time $t_0$ under the condition (2.8) is expressed in (2.10).

$$\begin{aligned} SNR_{out} &= \frac{|s_0(t_0)|^2}{n(t_0)} = \frac{\left|\int_{-\infty}^{\infty} \alpha S^*(\omega) e^{-j\omega t_0} S(\omega) e^{j\omega t_0} d\omega\right|^2}{\pi N_0 \int_{-\infty}^{\infty} \left|\alpha S^*(\omega) e^{-j\omega t_0}\right|^2 d\omega} \\ &= \frac{\left|\alpha \int_{-\infty}^{\infty} |S(\omega)|^2 d\omega\right|^2}{\pi N_0 \int_{-\infty}^{\infty} \left|\alpha S^*(\omega) e^{-j\omega t_0}\right|^2 d\omega} = \frac{\left|\alpha \int_{-\infty}^{\infty} |S(\omega)|^2 d\omega\right|^2}{\pi N_0 |\alpha|^2 \int_{-\infty}^{\infty} |S^*(\omega)|^2 d\omega} \\ &= \frac{\int_{-\infty}^{\infty} |S(\omega)|^2 d\omega}{\pi N_0} \end{aligned} \tag{2.10}$$

The energy of the signal $s(t)$ is represented in (2.11) by using Persaval's relation.

$$E = \int_{-\infty}^{\infty} |s(t)|^2 dt = \frac{1}{2\pi} \int_{-\infty}^{\infty} |S(\omega)|^2 d\omega \tag{2.11}$$

The $SNR_{out}$ representation in (2.10) can also be given as in (2.12).

$$SNR_{out} = \frac{\int_{-\infty}^{\infty} |S(\omega)|^2 \, d\omega}{\pi N_0} = \frac{2E}{N_0} \qquad \textbf{(2.12)}$$

The result in (2.12) states that the maximum achievable *SNR* depends only on the energy of the input signal, but not on other details such as its modulation. Two waveforms having the same energy will produce the same maximum *SNR*, provided each is processed through its own matched filter.

### 2.2.1 Pulse-Burst Matched Filter

In radar systems it is very difficult to obtain the required information from a single pulse. To overcome this problem, pulse-burst waveform is used and all pulses in the burst are processed instead of processing a single pulse to obtain the available information. Whether the pulses in the burst are coherent or incoherent, affects the processing method. Besides, the coding technique in the pulses can be the same for all the pulses or each pulse can be coded differently as well. Precisely, the matched filter which should be used if all pulses are coded differently in the burst, is required to be matched to the whole burst waveform. Consequently, the coherent integration of pulses in the burst is achieved by using pulse-burst matched filter.

In the pulse-burst waveform shown in Figure 2-2, there is a periodicity of $MT_r$. For example; $(k\text{-}1)^{th}$ burst's last pulse is followed by the first pulse of the $k^{th}$ burst.

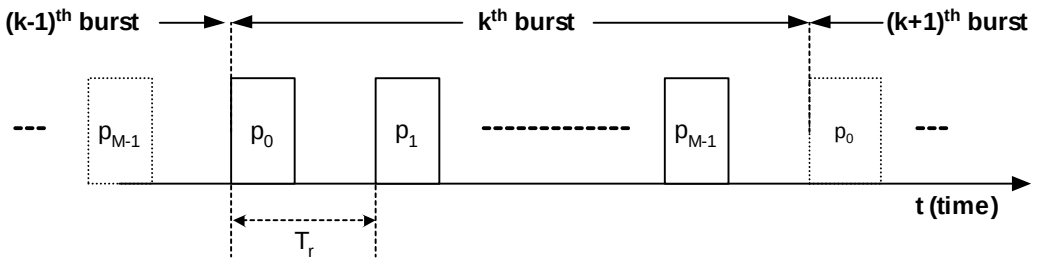


**Figure 2-2** Pulse-burst waveform with pulse diversity

The mathematical representation of a single burst is given in (2.13).

$$s(t)=\sum_{m=0}^{M-1} p_m(t)\ , \quad p_m(t)=\begin{cases}\neq 0, & mT_r \le t \le mT_r+\tau \\ =0, & otherwise\end{cases} \tag{2.13}$$

where s*(t)* : transmitted pulse-burst waveform; $p_m(t)$ : $m^{th}$ pulse in the burst; $M$ : number of pulses in the burst; $T_r$ : PRI of the pulse radar system.

The matched filter for the pulse-burst waveform is given in (2.14), when the scalars, used in (2.9), $\alpha=1$ and $t_0=0$ . The time reversal of the pulse-burst waveform results in both pulse order reversal in the burst and time reversal of code sequence used in each pulses as presented in (2.14) and Figure 2-3.

$$\begin{aligned} h(t)=s^*(-t)=\sum_{m=0}^{M-1} h_m(t)=\sum_{m=0}^{M-1} p^*_{M-1-m}((M-1)T_r+\tau-t), \\ h_m(t)=\begin{cases}\neq 0, & (M-1-m)T_r \le t \le (M-1-m)T_r+\tau \\ =0, & otherwise\end{cases} \end{aligned} \tag{2.14}$$

where $h(t)$ : pulse-burst matched filter; $h_m(t)$ : single-pulse matched filter of the $m^{th}$ pulse in the burst.

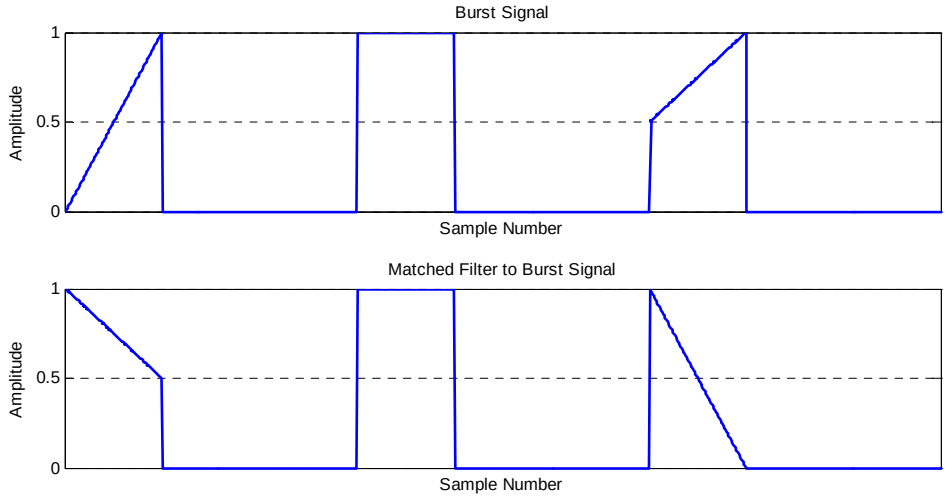


**Figure 2-3** An example of burst waveform amplitude and its matched filter amplitude

According to the definition in (2.13) and (2.14) the vector of pulses in a burst and the vector of single-pulse matched filters in pulse-burst matched filter can be defined as in (2.15).

$$\begin{aligned} \hat{s} &= [p_0, p_1, p_2 \ldots p_{M\text{-}1}] \\ \hat{h} &= [h_{M-1}, h_{M-2}, \ldots h_1, h_0] \end{aligned} \qquad \textbf{(2.15)}$$

where $h_n = (p'_n)^*$; $\hat{s}$ : the vector of pulses in the burst; $\hat{h}$ : the vector of single-pulse matched filters in a pulse-burst matched filter; $(p'_n)^*$ : complex conjugate of the time reversal of the $n^{th}$ pulse.

The elements of the output signal vector are provided in (2.16).

$$\begin{aligned} y_n &= \hat{s} \otimes \hat{h} \\ &= \sum_{m=0}^{M-1} p_m * h_{((m-n))M} = p_0 * h_{((-n))M} + p_1 * h_{((1-n))M} \ldots p_{M-1} * h_{((M-1-n))M} \end{aligned} \qquad \textbf{(2.16)}$$

where $n$ : the number of the PRI; $\otimes$ : circular convolution; $((n))M$ : $n$ modulo of $M$.

The output of the matched filter in each PRI in the burst is shown in Table 1.

**Table 1** The output of the matched filter under zero delay in the signal

| | |
|---|---|
| In $1^{st}$ PRI | $y_0 = s_0 * h_0 + s_1 * h_1 + s_2 * h_2 \quad ... \quad s_{M-2} * h_{M-2} + s_{M-1} * h_{M-1}$ |
| In $2^{nd}$ PRI | $y_1 = s_0 * h_{(M-1)} + s_1 * h_0 + s_2 * h_1 \quad ... \quad s_{M-2} * h_{M-3} + s_{M-1} * h_{M-2}$ |
| … | … |
| In $M^{th}$ PRI | $y_{M-1} = s_0 * h_1 + s_1 * h_2 + s_2 * h_3 \quad ... \quad s_{M-2} * h_{M-1} + s_{M-1} * h_0$ |

The pulse-burst matched filter is made up of single-pulse matched filters matched to the pulses in the burst. Therefore, when the pulse-burst matched filter is matched to the burst waveform, all of the pulses in the burst are matched with their own single-pulse matched filters. The peak value of the signal at the pulse-burst matched filter output is equal to the sum of the peak values of each pulse at their own single-pulse matched filter output. Since; the peak value at the output of single-pulse matched filter is related to the pulse energy, the peak value of the signal at the pulse-burst matched filter is proportional to the sum of the energy of the pulses in the burst.

#### 2.2.1.1 Pulse-by-pulse Processing

The pulse-burst matched filter output, shown in Table 1, illustrates that it is not necessary to construct an explicit matched filter for the entire pulse-burst waveform. The pulse-burst matched filter can be implemented by filtering each pulse with its own single-pulse matched filter with appropriate time aligning and simple addition. This convenient implementation is called pulse-by-pulse processing [1].

In pulse-by-pulse processing, $M$ single pulse matched filters are used in parallel and the received pulse is processed through all single-pulse matched filters at the same time as shown in Figure 2-4. The advantage of this method is using $M$ single-pulse matched filters of size $\tau$, instead of using one pulse-burst matched filter of size $MT_r$.

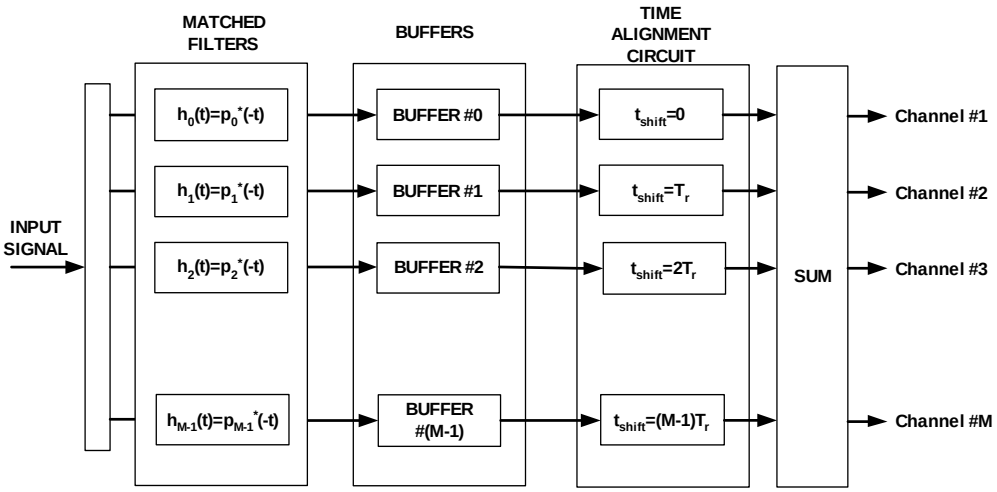


**Figure 2-4** Pulse-burst matched filter implementation with pulse-by-pulse processing

The output of each single-pulse matched filter should be kept in the corresponding buffer during the burst duration. There are single-pulse matched filter outputs of all pulses in the burst in the buffers, accordingly. The signals in each buffer are indicated in Table 2.

**Table 2** The contents of the buffers

| **Buffer Number** | **Output of the Single-Pulse Matched Filter** | | | |
|---|---|---|---|---|
| | **in the 1$^{st}$ PRI** | **in the 2$^{nd}$ PRI** | **...** | **in the $M^{th}$ PRI** |
| Buffer #0 | $p_0 * h_0$ | $p_1 * h_0$ | ... | $p_{M-1} * h_0$ |
| Buffer #1 | $p_0 * h_1$ | $p_1 * h_1$ | ... | $p_{M-1} * h_1$ |
| ... | ... | ... | ... | ... |
| Buffer #($M$-2) | $p_0 * h_{M-2}$ | $p_1 * h_{M-2}$ | ... | $p_{M-1} * h_{M-2}$ |
| Buffer #($M$-1) | $p_0 * h_{M-1}$ | $p_1 * h_{M-1}$ | ... | $p_{M-1} * h_{M-1}$ |

Once the buffers are filled by the processing of the whole burst waveform, the signals kept in the corresponding buffers are shifted circularly according to the given amounts in Figure 2-4. The circularly shifted and time aligned signals are given in Table 3.

**Table 3** The contents of the buffers after time alignment

| **Buffer Number** | **at 1$^{st}$ Channel** | **at 2$^{nd}$ Channel** | | **at $M^{th}$ Channel** |
|---|---|---|---|---|
| Buffer #0 | $p_0 * h_0$ | $p_1 * h_0$ | ... | $p_{M-1} * h_0$ |
| Buffer #1 | $p_1 * h_1$ | $p_2 * h_1$ | ... | $p_0 * h_1$ |
| ... | ... | ... | ... | ... |
| Buffer #($M$-2) | $p_{M-2} * h_{M-2}$ | $p_{M-1} * h_{M-2}$ | ... | $p_{M-3} * h_{M-2}$ |
| Buffer #($M$-1) | $p_{M-1} * h_{M-1}$ | $p_0 * h_{M-1}$ | ... | $p_{M-2} * h_{M-1}$ |

When the time aligned signals given in Table 3 are added up columnwise, the summed signals, appearing in any channel, is given in (2.17).

$$y_n = \hat{s} \otimes \hat{h}$$
$$= \sum_{m=0}^{M-1} p_m * h_{((m-n))M} = p_0 * h_{((-n))M} + p_1 * h_{((1-n))M} \cdots p_{M-1} * h_{((M-1-n))M} \quad \textbf{(2.17)}$$

where $n$ : number of the channel; $((n))M$ : $n$ modulo of $M$; $y_n$ : signal in the $n^{th}$ channel.

When (2.16) and (2.17) are examined, it is observed that the signals, obtained in each channel at the end of pulse-by-pulse processing, are equal to the signals obtained in the related PRI interval of the pulse-burst matched filter.

#### 2.2.1.2 Some Types of Phase Coded Pulses

**Definition 1 :** A code sequence is defined as a vector of $N$ code elements. The symbolization of a code sequence is given in (2.18).

$$c = [c_0, c_1, c_2, \ldots c_{N-1}] \quad \textbf{(2.18)}$$

where $c$ : code sequence; $c_n$ , $n$ = 1,2,3,...$N$-1 : elements of the code sequence.

**Definition 2 :** The Aperiodic Correlation Function (ACF) between the codes $c$ and $d$ is given in the expression in (2.19) [23].

$$R_{cd}(k) = r_k^{cd} = \begin{cases} \sum_{i=0}^{N-1-k} c_{i+k} d_i^*, & 0 \le k \le N-1 \\ \sum_{i=0}^{N-1+k} c_i d_{i-k}^*, & -(N-1) \le k < 0 \end{cases} \quad \textbf{(2.19)}$$

where $R_{cd}$ : Aperiodic Correlation Vector (ACV) between $c$ and $d$; $N$ : length of $c$ and $d$; * : complex conjugation; $r_k^{cd}$ : $k^{th}$ sample of the ACV of $c$.

The correlation between $c$ and $d$ is named as auto-correlation if the code sequence $c$ is equal to the code sequence $d$. Also if $c$ is not equal to $d$, the correlation between these code sequences is named as cross-correlation.

The matched filter output of a code sequence is equal to the aperiodic auto-correlation function of the corresponding code sequence.

**Definition 3 :** A periodic code repeats the code sequence infinitely. The symbolization of the periodic code associated with code sequence, $c$, is given in (2.20) [23].

$$c_{pc} = \left[ c \;\; c \;\; c \;\; c ... \right] \tag{2.20}$$

where $c_{pc}$ : periodic code.

If a periodic code sequence is match filtered with its aperiodic code sequence, the output of the matched filter is also periodic with the period of code sequence.

**Definition 4 :** The Periodic Auto-Correlation Function (PACF) of a code sequence, c, is given in (2.21) [23].

$$R_c^p(k) = \sum_{i=0}^{N-1} c_i^* c_{((i+k))N}, \qquad k = 0,1,2,...., N-1 \tag{2.21}$$

where $R_c^p$ : Periodic Auto-Correlation Vector (PACV) of $c$.

The PACF can also be defined in terms of vectors as given in (2.22).

$$R_c^p(k) = h_0^* h_k^T, \qquad k = 0,1,2,....,N-1$$
$$h_0 = (c_0, c_1, c_2, ..., c_{N-1})$$
$$h_1 = (c_1, c_2, ..., c_{N-1}, c_0)$$
$$h_2 = (c_2, c_3, ..., c_{N-1}, c_0, c_1) \qquad \textbf{(2.22)}$$
$$...$$
$$h_{N-1} = (c_{N-1}, c_0, c_1 ... c_{N-2})$$

**Definition 5 :** The code sequence defined in (2.18) is a Zero Sidelobe Periodic Code (ZSPC) if it has the property given in (2.23) [23].

$$R_c^p(k) = \sum_{i=0}^{N-1} c_i^* c_{((i+k))N} = 0 \qquad for\ k \neq 0 \qquad \textbf{(2.23)}$$

#### 2.2.1.2.1 Orthogonal Codes

Consider a set, *C*, of finite length code sequences, symbolized in (2.24).

$$C = \begin{bmatrix} c_0 \\ c_1 \\ ... \\ c_{M-1} \end{bmatrix} = \begin{bmatrix} c_{00} & c_{01} & c_{02} & ... & c_{0,N-1} \\ c_{10} & c_{11} & c_{12} & ... & c_{1,N-1} \\ ... & & & & \\ c_{M-1,0} & c_{M-1,1} & c_{M-1,2} & ... & c_{M-1,N-1} \end{bmatrix} \qquad \textbf{(2.24)}$$

where $C$ : the code matrix; $c_m$ : the $m^{th}$ code sequence; $c_{mn}$ : the $n^{th}$ element of the $m^{th}$ code sequence.

*C* is an orthogonal code matrix if the Cross Correlation Functions (CCF) between all code sequences in *C* are equal to zero.

The Periodic Cross Correlation Functions (PCCF) between all code sequences in *C* are possible to equal to 0. However, the first and the last elements of ACCF identified between two code sequences are equal to the multiplication

of the first and the last elements of the code sequences. Since the elements of the code sequences are non-zero, the first and the last elements of ACCF are non-zero as well. Therefore, it is not possible for ACCF of the code sequences in $C$ matrix to be 0. Welch [16] and Sarwate [17] have determined lower bounds of ACCF between two discrete and complex code sequences as given in (2.25) and (2.26).

**Theorem 1 :** Welch Bound Theorem [16]

$$SPR_{\min} = \frac{C_{\max}^2}{N} = \max\left\{\frac{C_a^2}{N}, \frac{C_c^2}{N}\right\} \geq \frac{N(M-1)}{(2NM-M-1)}$$
$$where \quad C_a = \max\left\{\left|R_{(nn)}(l)\right| : 1 \leq l \leq N-1\right\} \qquad \textbf{(2.25)}$$
$$C_c = \max\left\{\left|R_{(mn)}(l)\right| : -(N-1) \leq l \leq N-1\right\}$$

where $SPR_{min}$ : minimum value of maximum sidelobe to peak ratio; $C_{max}$ : maximum correlation level; $C_a$ : maximum AACF sidelobe level; $C_c$ : maximum ACCF level; $N$: code length; $M$ : number of code sequences in the code matrix.

**Theorem 2 :** Sarwate Bound Theorem [17]

$$\frac{2(N-1)}{N}\left(\frac{C_c^2}{N}\right) + \frac{2(N-1)}{N(M-1)}\left(\frac{C_a^2}{N}\right) \geq 1 \qquad \textbf{(2.26)}$$

where $C_a$ : maximum AACF sidelobe level; $C_c$ : maximum ACCF level; $N$ : code length; $M$ : number of code sequences in the code matrix.

In Welch Bound and Sarwate Bound Theorems, the maximum limit of the peak to sidelobe ratio that the code sequences in a code matrix can have is calculated.

#### 2.2.1.2.2 Complementary Codes

$C$ is a complementary code matrix if the sum of the AACV of each code sequence in the $C$ is zero everywhere except at the matched point as given in (2.27).

$$\sum_{m=0}^{M-1} c_m^* * \tilde{c}_m = \sum_{m=0}^{M-1} R_{(mm)} = \{0,0,....,k,....0,0\} \quad where\ k \neq 0 \qquad \textbf{(2.27)}$$

Figure 2-5 shows the normalized amplitude of the AACV of code sequences in a 2x7 complementary code matrix and the amplitude of sum of these AACV's.

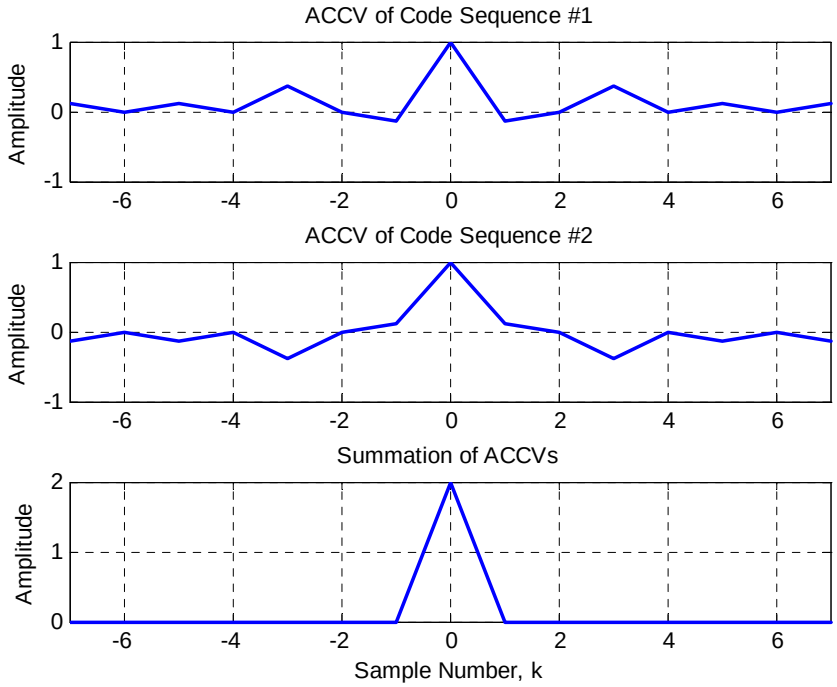


**Figure 2-5** Complementary code example

Complementary sets can be generated directly or by recursive steps based on complementary sets with fewer elements in each sequences or fewer members

in the set. More detailed information about complementary codes and their construction is stated in [16], [19], [20].

#### 2.2.1.2.3 Zero Cross Correlation Codes

The code matrix given in (2.24) is a Zero-Cross Correlation (ZCC) code matrix if the condition in (2.28) is satisfied.

$$\sum_{m=0}^{M-1} c_m^* * \tilde{c}_{m+l} = \sum_{m=0}^{M-1} R_{m((m+l))M} = \{0,0,....,0,....0,0\}, \qquad l \neq 0 \tag{2.28}$$

**Theorem 3 :** The code matrix $C_2$, given in (2.29) is a ZCC code matrix if the code sequence $a = \{ a_0, a_1, ...a_{M-1}\}$ is a ZSPC [23]. The code sequence $b = \{b_0, b_1, ... b_{M-1}\}$ can be an arbitrary code sequence.

$$C_2 = a^T b = \begin{bmatrix} a_0 \\ a_1 \\ ... \\ a_{M-1} \end{bmatrix} \begin{bmatrix} b_0 & b_1 & ... & b_{N-1} \end{bmatrix} = \begin{bmatrix} a_0 b_0 & a_0 b_1 & ... & a_1 b_{N-1} \\ a_1 b_0 & a_1 b_1 & ... & a_1 b_{N-1} \\ ... & & & \\ a_{M-1} b_0 & a_{M-1} b_1 & ... & a_{M-1} b_{N-1} \end{bmatrix} \tag{2.29}$$

**Proof :** The code elements in $C_2$ are $c_{mi} = a_m b_i$; $m = 0,1...M-1$ and $i = 0,1..N-1$.

The elements of the ACV of $m^{th}$ code sequence in $C_2$ and $n^{th}$ code sequence in $C_2$ is given in (2.30).

$$R_{mn}(k) = r_k^{mn} = \begin{cases} \sum_{i=0}^{N-1-k} a_m^* b_i^* a_n b_{i+k}, & 0 \le k \le N-1 \\ \sum_{i=0}^{N-1+k} a_m^* b_{i-k}^* a_n b_i, & -(N-1) \le k < 0 \end{cases} \tag{2.30}$$

After setting $n=m+l$ in (2.30), the equation in (2.31) is obtained.

$$R_{m(m+l)}(k) = r_k^{m(m+l)} = \begin{cases} \sum_{i=0}^{N-1-k} a_m{}^* b_i^* a_{m+l} b_{i+k}, & 0 \le k \le N-1 \\ \sum_{i=0}^{N-1+k} a_m^* b_{i-k}{}^* a_{m+l} b_i, & -(N-1) \le k < 0 \end{cases} \quad \textbf{(2.31)}$$

The elements of the vector summation of the ACV for all $m$ values are calculated in (2.32).

$$\begin{aligned} q_k^l &= \sum_{m=0}^{M-1} R_{m(m+l)}(k) = \sum_{m=0}^{M-1} r_k^{m(m+l)} \\ &= \begin{cases} \left( \sum_{m=0}^{M-1} a_m{}^* a_{m+l} \right) \times \left( \sum_{i=0}^{N-1-k} b_i^* b_{i+k} \right), & 0 \le k \le N-1 \\ \left( \sum_{m=0}^{M-1} a_m^* a_{m+l} \right) \times \left( \sum_{i=0}^{N-1+k} b_{i-k}{}^* b_i \right), & -(N-1) \le k < 0 \end{cases} \end{aligned} \quad \textbf{(2.32)}$$

Since the code sequence *"a"* is a ZSPC, the first summation in (2.32) is equal to zero for $l \neq 0$. Consequently, the property defined in (2.28) is satisfied.

ZCC code matrix given in (2.29) is made up of 2 code sequences. The code sequence, which is same for each column, can be called slowtime code sequence and the code sequence same for each row can be called fasttime code sequence. Slowtime code sequence PACF determines the signal ratio between the channels and; fasttime code sequence ACCF determines the characteristics of the signals in any channel at the matched filter output.

In Figure 2-6 the summations of the normalized correlation vectors of a 4x13 ZCC code are shown.

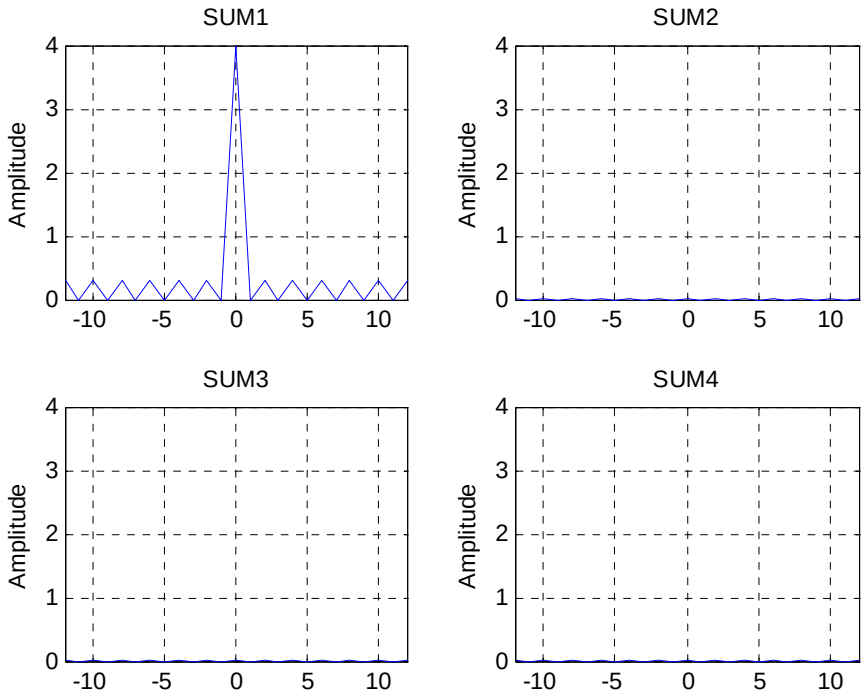


**Figure 2-6** ZCC code example

In the ZCC code sample, whose pulse-burst matched filter output is given in Figure 2-6, Barker 13 code is used as the fasttime code sequence. In this example matched point appears in Channel 1. The characteristic of Barker 13 code is observed in the output signal in Channel 1. The characteristic of Barker 13 code is formed in other channels in the same way. However, the characteristics of Barker 13 code cannot be observed in mismatched channels, since the signal level in these channels is very low.

#### 2.2.1.2.4 ZCC-Complementary Codes

The ZCC-Complementary codes are the combination of the ZCC codes and complementary codes. A code matrix is ZCC-Complementary if it is a ZCC

code matrix and also a complementary code matrix. The ZCC-Complementary code matrix should satisfy the conditions specified in (2.33), accordingly.

$$\sum_{m=0}^{N-1} c_m^* * \tilde{c}_{m+l} = \sum_{m=0}^{N-1} R_{m(m+l)}$$
$$= \begin{cases} \{0,0...0...0,0\},\ l \neq 0 \rightarrow \text{ZCC code property} \\ \{0,0...k...0,0\},\ l = 0 \rightarrow \text{Complementary code property} \end{cases} \quad \textbf{(2.33)}$$
$$\text{where } k \neq 0$$

**Theorem 4 :** The *N*x*N* code matrix *C* is a ZCC-Complementary code matrix if their elements have the form given in (2.34) [23].

$$c_{mi} = \lambda_m d_{i+1} W_N^{Mmi}, \quad m = 0,1,2,...N\text{-}1; \quad i = 0,1,2,...N\text{-}1$$
$$W_N = e^{j2\pi/N} \quad \textbf{(2.34)}$$
$$\lambda \in \left\{1, W_N, W_N^2, ...W_N^{N-1}\right\}$$

where $c_{mi}$ : $i^{th}$ element of the $m^{th}$ code sequence in *C*; $\{d_1, d_2, ... d_{N\text{-}1}\}$ : arbitrary numbers and *M* : an integer relatively prime to *N*.

**Proof :** The elements of the ACV of $m^{th}$ code sequence and $n^{th}$ code sequence is given in (2.35).

$$R_{mn}(k) = r_k^{mn} = \begin{cases} \sum_{i=0}^{N-1-k} \left(\lambda^m d_{i+1} W_N^{Mmi}\right)^* \left(\lambda^n d_{i+k+1} W_N^{Mn(i+k)}\right) \\ \sum_{i=0}^{N-1+k} \left(\lambda^m d_{i-k+1} W_N^{Mm(i-k)}\right)^* \left(\lambda^n d_{i+1} W_N^{Mni}\right) \end{cases}$$
$$= \begin{cases} \lambda^{n-m} W_N^{Mnk} \sum_{i=0}^{N-1-k} d_{i+1}^* d_{i+k+1} W_N^{M(n-m)i}, & 0 \le k \le N-1 \\ \lambda^{n-m} W_N^{Mnk} \sum_{i=0}^{N-1+k} d_{i-k+1}^* d_{i+1} W_N^{M(n-m)i}, & -(N-1) \le k < 0 \end{cases} \quad \textbf{(2.35)}$$

After setting $n=m+l$ in (2.35), the equation in (2.36) is obtained.

$$R_{m(m+l)}(k) = r_k^{m(m+l)} = \begin{cases} \lambda^l W_N^{M(m+l)k} \sum_{i=0}^{N-1-k} d_{i+1}^* d_{i+k+1} W_N^{Mli}, & 0 \le k \le N-1 \\ \lambda^l W_N^{Mmk} \sum_{i=0}^{N-1+k} d_{i-k+1}^* d_{i+1} W_N^{Mli}, & -(N-1) \le k < 0 \end{cases} \quad \textbf{(2.36)}$$

The ACV of the $c_m$ and $c_{(m+l)}$ is the vector of elements given in (2.37).

$$c_m^* * \tilde{c}_{m+l} = R_{m(m+l)} = \left\{ r_{-(N-1)}^{m(m+l)}, r_{-(N-2)}^{m(m+l)}, ..., r_0^{m(m+l)}, ... r_{(N-2)}^{m(m+l)}, r_{(N-1)}^{m(m+l)} \right\} \quad \textbf{(2.37)}$$

The vector summation of the ACV's for all m values is given in (2.38).

$$\begin{aligned} \sum_{m=0}^{N-1} c_m^* * \tilde{c}_{m+l} &= \sum_{m=0}^{N-1} R_{m(m+l)}(k) = \sum_{m=0}^{N-1} r_k^{m(m+l)}, \quad k = -(N-1), ..., 0..., (N-1) \\ &= \left\{ \sum_{m=0}^{N-1} r_{-(N-1)}^{m(m+l)}, \sum_{m=0}^{N-1} r_{-(N-2)}^{m(m+l)}, ... \sum_{m=0}^{N-1} r_0^{m(m+l)}, ... \sum_{m=0}^{N-1} r_{(N-2)}^{m(m+l)}, \sum_{m=0}^{N-1} r_{(N-1)}^{m(m+l)} \right\} \\ &= \left\{ q_{-(N-1)}^l, q_{-(N-2)}^l, ... q_0^l, ... q_{(N-2)}^l, q_{(N-1)}^l \right\} \end{aligned} \quad \textbf{(2.38)}$$

The elements of the vector summation of the ACV's for all $m$ values are calculated in (2.39).

$$\begin{aligned} q_k^l &= \sum_{m=0}^{N-1} r_k^{m(m+l)} \\ &= \begin{cases} \left( \sum_{m=0}^{N-1} W_N^{Mmk} \right) \times \lambda^l W_N^{Mlk} \times \left( \sum_{i=0}^{N-1-k} d_{i+1}^* d_{i+k+1} W_N^{Mli} \right), & 0 \le k \le N-1 \\ \left( \sum_{m=0}^{N-1} W_N^{Mmk} \right) \times \lambda^l \times \sum_{i=0}^{N-1+k} d_{i-k+1}^* d_{i+1} W_N^{Mli}, & -(N-1) \le k < 0 \end{cases} \end{aligned} \quad \textbf{(2.39)}$$

If $M$ is relatively prime to $N$, the expression of $q_k^l$ given in (2.39) is equal to zero;

- for $k \neq 0$, since

$$\sum_{m=0}^{N-1} W_N^{Mmk} = 0, \quad if \ k \neq 0 \tag{2.40}$$

- for k=0 and l≠0, since

$$\begin{aligned} \sum_{i=0}^{N-1+k} d_{i+1}^{*} d_{i+k+1} W_N^{Mli} &= \sum_{i=0}^{N-1+k} d_{i-k+1}^{*} d_{i+1} W_N^{Mli} = \sum_{i=0}^{N-1+k} \left| d_{i+1} \right|^2 W_N^{Mli} \\ &= \left| d_{i+1} \right|^2 \sum_{i=0}^{N-1+k} W_N^{Mli} = 0, \quad \text{for } l \neq 0 \end{aligned} \tag{2.41}$$

However $q_k^{\,l}$ is non-zero if $k=l=0$, hence the condition given in (2.33) is obtained.

In Figure 2-7 the summations of the normalized correlation vectors of a 6x6 ZCC-Complementary code matrix are shown. As seen in the figure, only the matched point in the matched channel is non-zero, all the other elements of the summation vectors are zero.

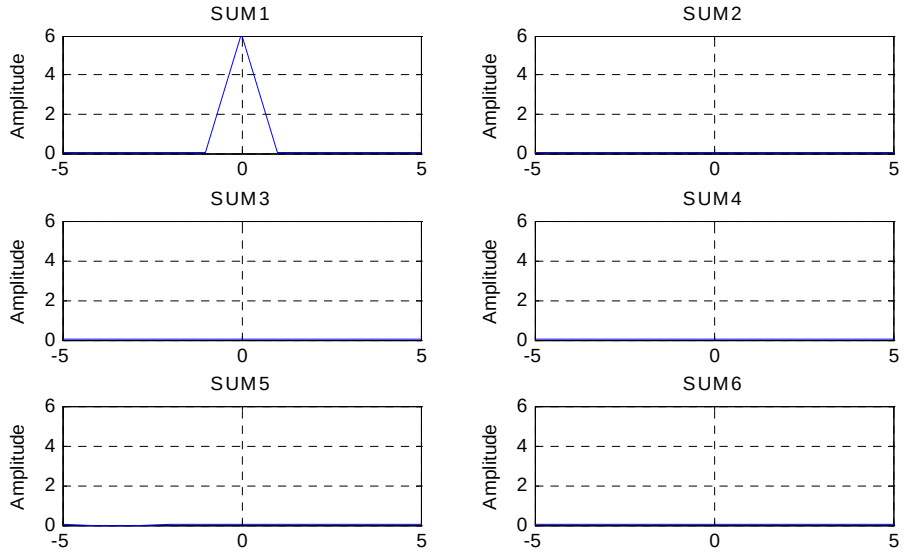


**Figure 2-7** ZCC-Complementary code example

#### 2.2.1.2.5 Comparison

There are various phase codes available in the literature for coding single-pulse waveforms. However, in the literature there is not enough study on codes for coding pulse-burst waveforms.

The studies done in the scope of this thesis is mostly focused on coding pulse-burst radar signals and processing these signals. Therefore, the code types given in Section 2.2.1.2 are the ones that can be used for coding pulse-burst waveforms. These codes that can be used for coding pulse-burst waveforms are defined in matrix format. Each row of the codes defined in matrix format is used for coding a pulse in the burst. So, the number of rows in the code matrix is equal to the number of pulses in the pulse-burst waveform and the number of columns is equal to the code length used in a single pulse.

Many issues may be considered while evaluating the performance of the code matrices. However, in the thesis studies, code matrices are expected to have high PSL value. Therefore, PSL is considered while evaluating the codes used. The highest sidelobe level can appear in matched channel as well as the mismatched channels in applications where pulse-burst waveform is used. Therefore, two ratios should be checked while the performance of the code matrices are evaluated in the thesis. One of these is the ratio of the signal level at matched point to the maximum time sidelobe level in the matched channel. This ratio will be named as inter-channel PSL from now on and will be symbolized with $PSL_{inter}$. The other ratio that should be considered is the ratio of the signal level at the matched point to the highest signal level appearing in the mismatched channel. This ratio will be named as intra-channel PSL from now on and will be symbolized with $PSL_{intra}$. The mathematical definitions of $PSL_{inter}$ and $PSL_{intra}$ are given in (2.42).

$$PSL_{inter} = \frac{|s_{MC}(t_0)|}{\max\{|s_{MC}(t)|\}} \quad where\ t \neq t_0$$
$$PSL_{intra} = \frac{|s_{MC}(t_0)|}{\max\{|s_{MMC}(t)|\}} \qquad \textbf{(2.42)}$$

where $t_0$ : time of matched point in the matched channel; $s_{MC}$(t) : signal in the matched channel; $s_{MMC}$(t) : signal in the mismatched channel.

In Section 2.2.1.2, four main types of code matrices are stated. These are orthogonal code matrices, complementary code matrices, ZCC code matrices and ZCC-Complementary code matrices.

The cross-correlation of the orthogonal codes with each other should be low. The signals appearing in the mismatched channels at the pulse-burst matched filter output, are made up of the sum of the cross-correlation of the codes in the code matrix. Therefore, the signal levels appearing in mismatched channels for orthogonal codes are expected to be low. This situation means that the orthogonal codes can have high $PSL_{intra}$ value. However, there is no limitation to get high $PSL_{inter}$ values in orthogonal code matrices.

Complementary codes have zero sidelobe level in matched channel. Therefore, $PSL_{inter}$ value is very high, theoretically infinite in complementary codes. However, there is no feature in complementary codes to decrease the signal level in mismatched channels. On the other hand, the signal level for ZCC codes in mismatched channels is nearly 0. So, ZCC codes have very high, even infinite $PSL_{intra}$ value. However, there is no limitation in ZCC codes to increase its $PSL_{inter}$ value. ZCC codes and complementary codes complete each other. One of them has a very high $PSL_{inter}$ value and the other has a very high $PSL_{intra}$ value. ZCC-Complementary codes, carrying both of these features of complementary codes and ZCC codes, have high $PSL_{inter}$ and

$PSL_{intra}$ values at the same time. Consequently, ZCC-Complementary code matrices are suitable for coding pulse-burst waveform in radar applications.

Using code matrices with high $PSL_{inter}$ and $PSL_{intra}$ values will increase the detection capability of the radar. However, the radar systems are designed to detect and track moving targets. Doppler phase shift will be observed in the reflected waveform from moving targets between the pulses in the burst and even between the code elements used in the pulse. The performances of these codes under different Doppler phase shifts are discussed in Chapter 3.

# CHAPTER 3

# THE PERFORMANCE EVALUATION OF PHASE CODES IN PULSE DIVERSITY

## 3.1 RADAR APPLICATIONS WITH STANDARD CODES

A lot of issues depending on the needs should be taken into account while a code to be used in a radar application is chosen. The ISL value of the codes that are used in the applications, where distributed clutter is dominant, is checked. The PSL value is preferred to be high in applications where discriminating close targets and detecting targets under high clutter background [50]. ISL and PSL are generally related concepts. Making improvement for a code in one causes improvement in the desired way in the other. Some studies are done in the scope of the thesis to get successful results in target detection in high clutter signal. Therefore, codes with high PSL value are used in the radar model.

A lot of matrices, that can be used to code pulse-burst waveform, have high PSL values for zero Doppler shift. Whereas, radar systems are generally used for detecting and tracking moving targets. Therefore, the radar codes that will be used in radar applications are expected to show the same high performance when they are also reflected from moving targets.

It is easy to compensate for the distortion that is caused by the Doppler frequency in situations where a single pulse is processed to gather

information. However, even small Doppler frequency shifts may cause serious distortions in pulse-burst waveforms. The signal is affected only from the phase shift inside the pulsewidth in the single-pulse processing. However, the signal that will be processed in the pulse-burst waveforms is affected from the phase shift during the whole burst duration. The expression of the phase shift that is caused by the Doppler frequency in a signal in a certain time interval is given in (3.1).

$$\phi_s = \int_{t_0}^{t_0+\Delta t} 2\pi f_d dt = 2\pi f_d \Delta t \qquad \textbf{(3.1)}$$

where $f_d$ : Doppler frequency; $\Delta t$ : the width of the interested time interval; $\Phi_s$ : phase shift due to Doppler frequency; $t_0$ : start time of the interested time interval.

When a single-pulse is processed, the maximum value of $\Delta t$ is equal to the pulsewidth. However, in pulse-burst waveform processing, $\Delta t$ is equal to ($n$-1)PRI for the $n^{th}$ pulse. PRI is generally 500-1000 times the pulsewidth in practical radar applications. Therefore, the phase difference between the pulses in the burst is much larger than the one between the code elements in the pulse.

When the pulse-burst waveform, in which $C_{TX}$ code matrix is used, is transmitted; the phase of each element of the received waveform is as in $C_{RX}$ code matrix. The phase shift, indicated in the $C_{RX}$ code matrix, is due to target movement.

$$C_{TX} = \left\{ c_{mn} \right\}_{[m,n]=[0,0]}^{[m,n]=[M-1,N-1]}$$
$$C_{RX} = \left\{ c_{mn} e^{jn\phi_1} e^{jm\phi_2} \right\}_{[m,n]=[0,0]}^{[m,n]=[M-1,N-1]} \qquad \textbf{(3.2)}$$
$$where\ \phi_1 = 2\pi f_d \frac{\tau}{N}\ and\ \phi_2 = 2\pi f_d T_r$$

where $C_{TX}$ : transmitted code matrix; $C_{RX}$ : received code matrix; $c_{mn}$ : $n^{th}$ element of the $m^{th}$ code sequence in the code matrix; $M$ : total number of pulses in the burst; $N$ : the length of code sequence used in a pulse; $f_d$ : Doppler frequency; $\tau$ : pulsewidth; $T_r$ : PRI; $\Phi_1$ : the phase shift between the consecutive code elements in the pulse due to Doppler shift; $\Phi_2$ : the phase shift between the consecutive pulses in the burst due to Doppler shift.

In Figure 3-1, the result of an experiment is displayed. This experiment shows that the phase shift between the code elements does not affect the signal significantly at the output of pulse-burst matched filter. In this experiment, a burst waveform consisting of 4 pulses is used. PRI is equal to 1 ms and the pulsewidth is equal to 1 μs. The pulse-burst waveform is coded with a random code matrix consisting of 4x64 elements. Two different echoes of the coded pulse-burst waveform, reflected from a target that caused 20.5 kHz Doppler shift, are created. While $Echo_1$ is being created, only the phase shift between the pulses is considered. On the other hand; while $Echo_2$ is being created, the phase shift between the code elements in the pulse is considered as well as the phase shift between the pulses. Afterwards; both two echoes are processed through the filter matched to the transmitted pulse-burst waveform. When the amplitudes of the $Echo_1$ and $Echo_2$ at the matched filter output are compared, the graph shown in Figure 1-5 is obtained for each channel.

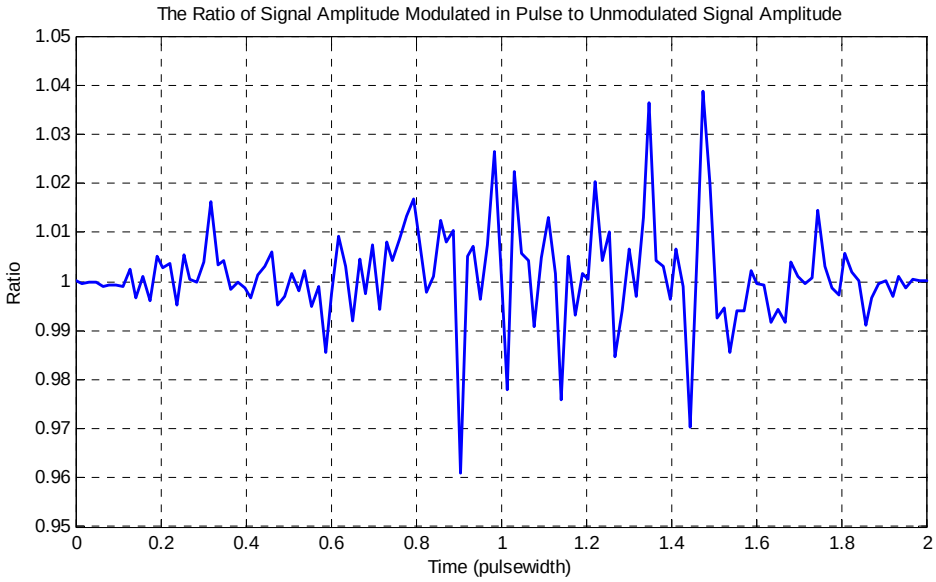


**Figure 3-1** The ratio of $Echo_1$ envelope to $Echo_2$ envelope

The ratio given in Figure 3-1 shows that there is not any significant difference between Echo1 and Echo2 amplitudes. While the performance of the different code matrices under the Doppler phase shift is evaluated in scope of thesis studies, the Doppler phase difference between the code elements in the pulse is ignored. The Doppler frequency values resulting from the possible target velocities are larger than the PRF value. The baseband Doppler signal has more than one cycle throughout the PRI. Therefore, different Doppler frequency values may cause the same phase shift between consecutive pulses. In order to ease the grouping, the performance of the code matrices is evaluated under the different phase shifts between consecutive pulses instead of under different Doppler frequencies.

Ambiguity diagrams are composed to evaluate the performance of the code matrices used for coding pulse-burst waveforms for different Doppler phase shift values. The correlation functions for each channel are calculated while ambiguity diagram is composed. Doppler axis of the calculated correlation functions is not evaluated according to the Doppler frequency shift but the

Doppler phase shift between the pulses as mentioned above. The mathematical expression of the ambiguity diagram defined for a code matrix is given in (3.3).

$$\left|\chi_{n+1}(t_d,\phi)\right| = \left|\sum_{m=0}^{M-1}\left(\int_{-\infty}^{\infty} p_m(t)e^{jm\phi}p^*_{((m-n))M}(t+t_d)dt\right)\right|$$

$$= \left|\begin{array}{l}\int_{-\infty}^{\infty} p_0 p^*_{((-n))M}(t+t_d)dt + \int_{-\infty}^{\infty} p_1 e^{j\phi} p^*_{((1-n))M}(t+t_d)dt\ldots \\ \qquad\qquad \ldots + \int_{-\infty}^{\infty} p_{M-1}e^{j(M-1)\phi}p^*_{((M-1-n))M}(t+t_d)dt\end{array}\right| \qquad \textbf{(3.3)}$$

where $0 \le n \le M-1$

where $\chi_n$ : correlation function of $n^{th}$ channel in the ambiguity diagram; $p_m(t)$ : $m^{th}$ pulse in the burst; $t_d$ : time delay; $\Phi$ : Doppler phase shift between consecutive pulses; $M$ : number of code sequence in the code matrix.

First channel is always the matched one in the calculation of correlation functions. The ambiguity diagrams of code matrices that will be used for coding pulse-burst waveforms are expected to have the characteristics listed below.

- The signal level for all Φ values to be high, while td=0 in correlation function calculated for matched channel.
- The signal level in correlation function calculated for matched channel to be low for $t_d \neq 0$.
- The correlation function levels calculated for mismatched channels to be low.

### 3.1.1 Use of Random Codes in Pulse Diversity

Transmitted pulses in the burst can be coded with random codes. In this condition, the peak at the output of pulse-burst matched filter is observed at

the expected time in the expected channel for zero Doppler shift. However, the $PSL_{inter}$ and $PSL_{intra}$ values show difference according to the used random code, number of the pulses in the burst and the length of the codes used in pulses. In Figure 3-2 the $PSL_{inter}$ and $PSL_{intra}$ values for different sizes of the random code matrices, used in the pulse-burst waveforms, are given. In order to construct these figures $PSL_{inter}$ and $PSL_{intra}$ values of 1000 different code matrices are calculated and the averages of these values are taken.

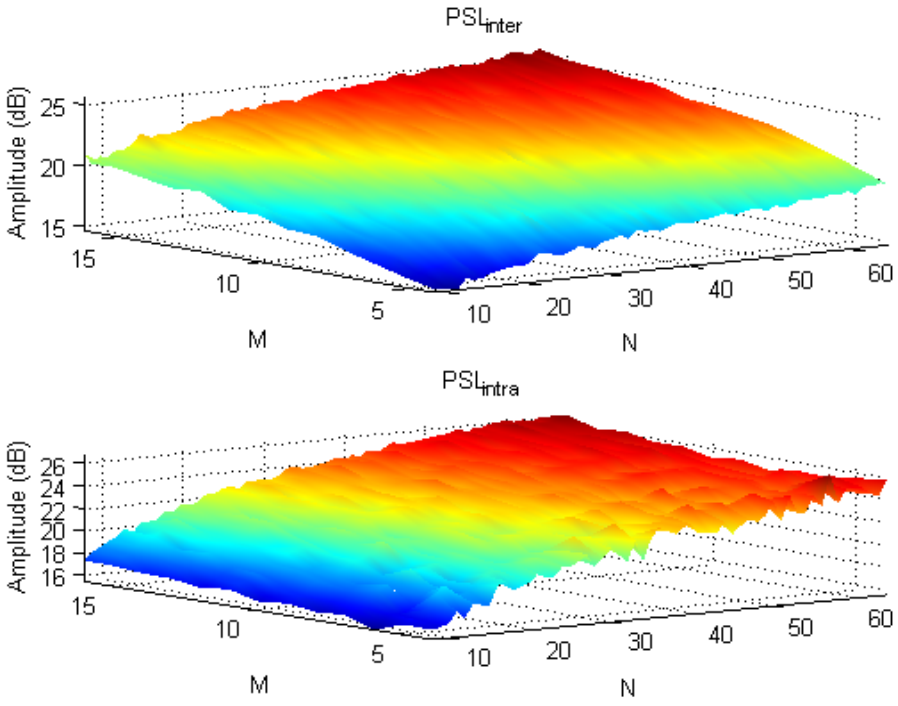


**Figure 3-2** $PSL_{inter}$ and $PSL_{intra}$ values for code matrices in different sizes with zero Doppler

When the graphs given in Figure 3-2 is examined, it is obvious that increasing the number of the pulses in the burst and the length of code used in the pulse, will make the target echo more obvious. Increasing the number of the pulses in the burst increases particularly the $PSL_{intra}$ value and increasing the length of code used in the pulse increases particularly the $PSL_{inter}$ value. However, there are factors in radar applications limiting the code length used in the pulse and the number of the pulses used in the burst.

Using 4 pulses in the burst and coding each pulse with a 64 element code sequence is assumed. In Figure 3-3 the ambiguity diagram of a 4x64 random code matrix is displayed.

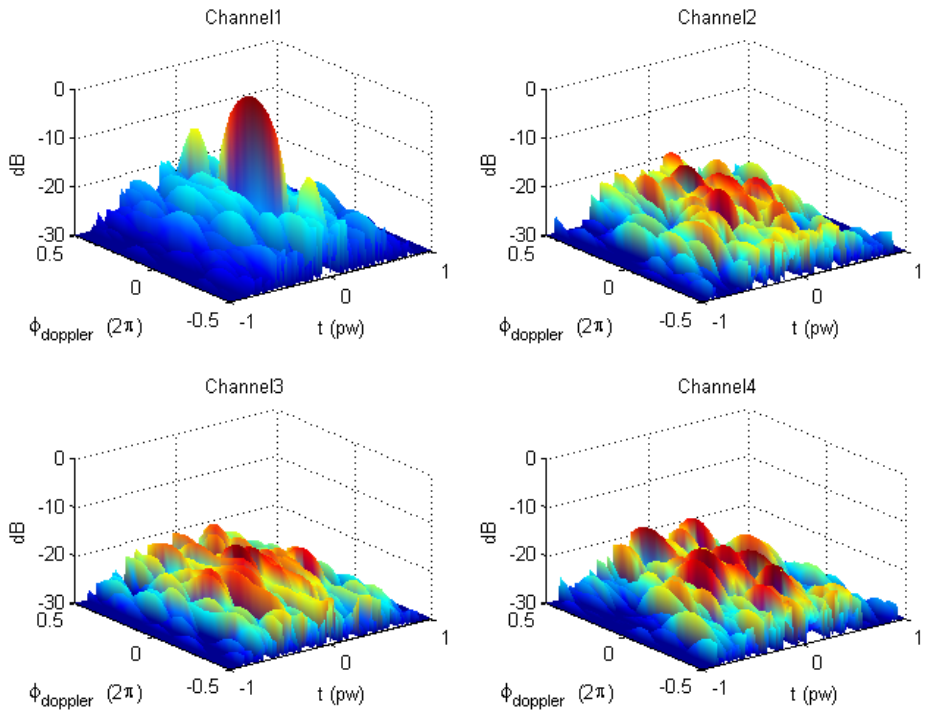


**Figure 3-3** Ambiguity diagram of a 4x64 random code matrix

The ambiguity diagram displayed in Figure 3-3 shows that the random code reflected from a moving target, could not achieve a desired result at the output of the pulse-burst matched filter. As seen in the figure, when the phase shift is different from zero, the signal level at matched point decreases considerably. Moreover; the signal level in matched and mismatched channels at undesired times increases, it even exceeds the signal level at the matched point.

In Figure 3-4, the performance of the random code matrices of different sizes under specific Doppler phase shifts are evaluated. The same codes used in Figure 3-2 are used in calculation of this figure. In this figure; it is accepted

that there is a 0.6π and 1.0π phase difference between the consecutive code sequences, processed in the pulse-burst matched filter. Then, the averages of the calculated $PSL_{inter}$ and $PSL_{intra}$ values are taken.

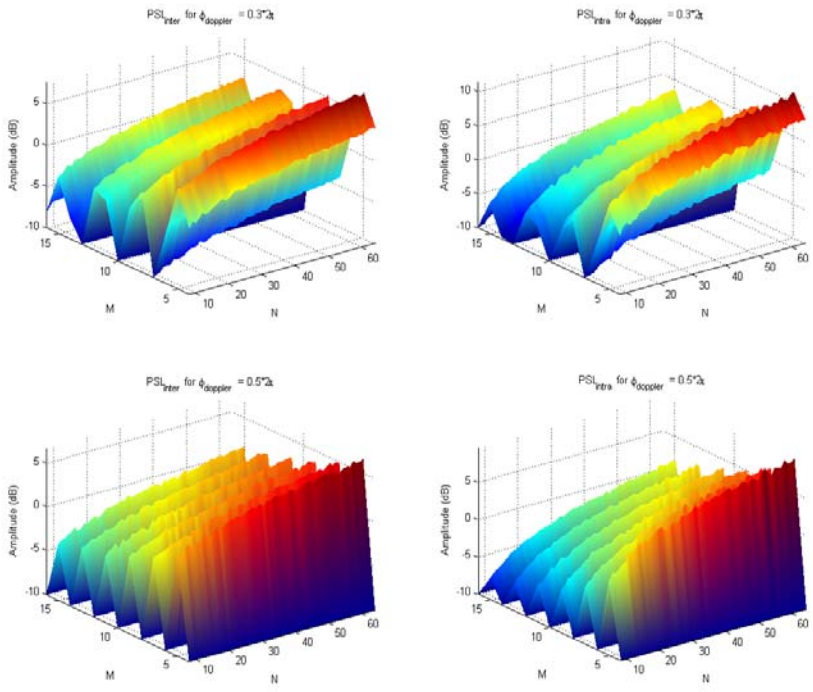


**Figure 3-4** The $PSL_{inter}$ and $PSL_{intra}$ values under non-zero Doppler phase shifts

Figure 3-4 shows that the Doppler phase shift affects the random code matrices of various sizes; and decreases $PSL_{inter}$ and $PSL_{intra}$ values, dramatically. For this reason, it is not appropriate to use random code matrices for coding pulse-burst signals.

### 3.1.2 Use of Codes with Low Correlation in Pulse Diversity

The signal appearing in the matched channel at the pulse-burst matched filter output depends on the sum of auto-correlations of the pulses in the burst.

Therefore using codes, with low auto-correlation sidelobe levels, for coding the pulse-burst waveforms increases the $PSL_{inter}$ value. On the other hand, the signal level appearing in the mismatched channels depends on the sum of cross-correlations of pulses in the burst. Therefore, using codes with low cross-correlation levels is a method to get high $PSL_{intra}$ value. Composing the code matrix with codes having low cross-correlation levels draws this code matrix closer to the orthogonal specifications. There are no matrices consisting of codes having low auto-correlation sidelobe level and low cross-correlation level in the literature. The codes used in this study, are obtained through optimization. The codes are produced randomly and they are optimized so that they have low auto-correlation sidelobe level and low cross-correlation level.

The mathematical expression of the constructed cost function is given in (3.4).

$$CF = \max\left\{\left|R_{ij}(k)\right|\right\} \quad \text{except for } \{k = 0 \ \& \ i = j\} \quad \text{where } i = 0,1,2...M\text{-}1;\ j = 0,1,2...M\text{-}1 \tag{3.4}$$

where $CF$ : cost function; $|R_{ij}(k)|$ : magnitude of $k^{th}$ element of ACF between $i^{th}$ code sequence and j$^{th}$ code sequence; $M$ : number of code sequence in the code matrix.

In the cost function defined in (3.4), the maximum sidelobe level of AACF and maximum level of ACCF of code sequences in the code matrix are minimized. In order to implement the optimization, whose cost function is given in (3.4), the standard function ‘fminimax’ of MATLAB program is used. fminimax uses a Sequential Quadratic Programming (SQP) method, [46]. Modifications are made to the line search and Hessian. In the line search an exact merit function is used together with the merit function proposed by [48] and [51]. The line search is terminated when either merit function shows improvement. The function uses a modified Hessian that takes advantage of

the special structure of this problem [52]. Detailed information about optimization algorithm, used in fminimax function, can be found in MATLAB Help Documentation [53].

In Figure 3-5 the optimization results of a 4x64 random code matrix is given. In the figure, the plots in blue indicate the results of the code matrix before optimization and the ones in red indicate the results of the code matrix after optimization.

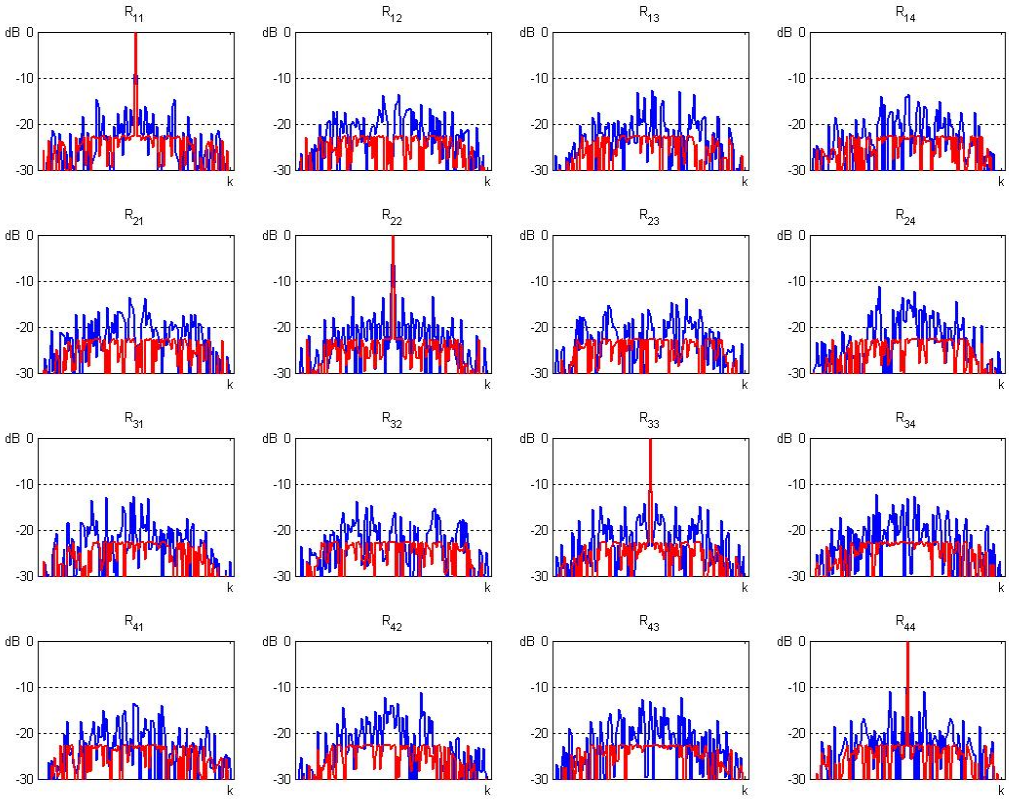


**Figure 3-5** Correlations between codes in a 4x64 optimized code matrix

In Figure 3-5 it can be seen that the sidelobe level in the auto-correlation results and signal level in the cross-correlation results decrease. In order to determine the $PSL_{inter}$ and $PSL_{intra}$ values of the code matrices that are before

and after the optimization, their matched filter outputs are composed under zero Doppler shift.

The $PSL_{inter}$ and $PSL_{intra}$ values of the 4x64 optimized code matrix under zero Doppler phase shift are both equal to 22.6424 dB. The $PSL_{inter}$ and $PSL_{intra}$ values of the code matrix before optimization are equal to 17.1228dB and 15.3459dB, respectively. The ambiguity diagram for the optimized code matrix is given in Figure 3-6.

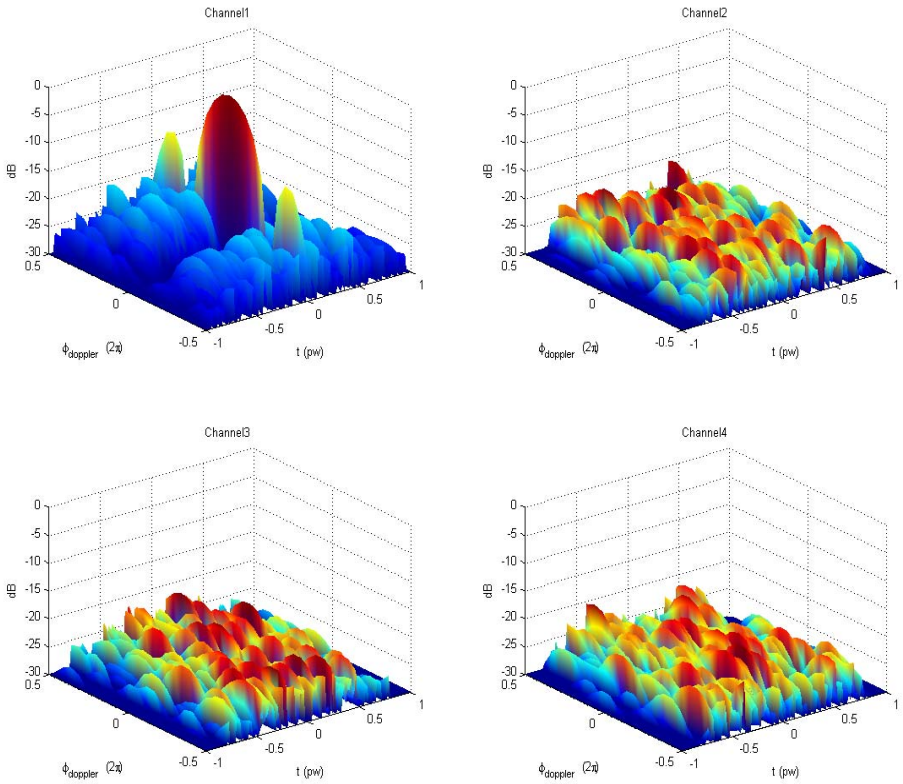


**Figure 3-6** Ambiguity diagram of a 4x64 optimized code matrix

The code matrix with low auto-correlation sidelobe level and low cross-correlation level gives quite satisfactory results for zero Doppler phase shift. However, as it can be inferred from the ambiguity diagram, the $PSL_{intra}$ and

$PSL_{inter}$ values of these codes also decrease under various Doppler phase shifts. For this reason, it is not appropriate to code the pulse-burst waveform with this type codes.

### 3.1.3 Use of ZCC Codes in Pulse Diversity

When the pulse-burst waveform is coded with ZCC codes and processed through its own matched filter, it has a fairly good $PSL_{intra}$ value. ZCC codes having quite high $PSL_{intra}$ value ensures each channel to be matched to a certain delay time at the end of pulse-by-pulse processing. This property is very important for radar applications. In radar applications, the advantages listed below are obtained due to this property.

1. Each channel is matched to a certain PRI time interval or $c$PRI/2 range interval.
2. The target echo will be formed only in the channel that is matched to its range.
3. In each channel, there will be only the clutter signal that comes from the matched range interval, and the clutter coming from other range intervals will be inherently suppressed at filter output.

In Figure 2-6 matched filter output of a zero time shifted ZCC code matrix, whose size is equal to 4x13, is given. If the same ZCC code matrix, composed of $\{c_0, c_1, c_2, c_3\}$, code sequences is transmitted in a scenario given in Figure 3-7, the received code matrix will be equal to the $\{ c_0+2c_2, c_1+2c_3, c_2+2c_0, c_3+2c_1\}$.

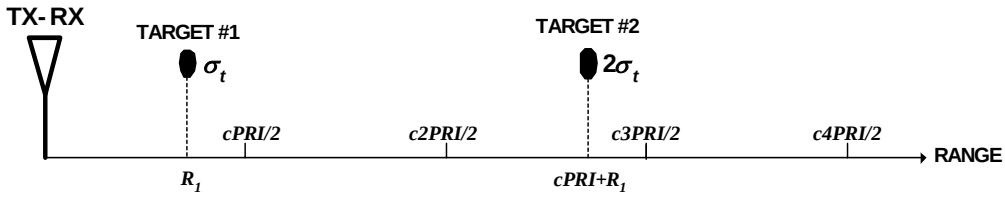


**Figure 3-7** A sample scenario with two targets

When the received code matrix processed through the filter matched to the transmitted code matrix, the result given in Figure 3-8 is obtained at the filter output.

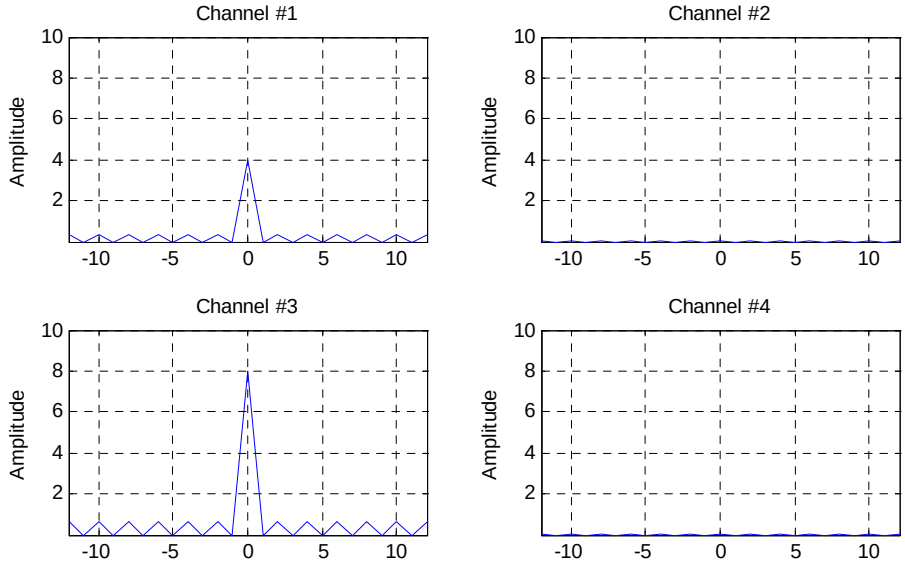


**Figure 3-8** Pulse-Burst matched filter output

When Figure 3-8 is examined the results listed below are observed.

1. The result of the zero time shifted code matrix, $\{c_0, c_1, c_2, c_3\}$, occurred only in Channel #1.
2. The results of the 2 unit delayed code matrix, $\{2c_2, 2c_3, 2c_0, 2c_1\}$, occurred only in Channel #3.

3. Input code matrices didn't affect the results of each other and didn't produce any result in other channels.
4. The characteristics of the fasttime code sequence, used for forming ZCC code matrix, are not disturbed.

ZCC code matrices have fairly good $PSL_{intra}$ values. However, there is no regulation in the ZCC code matrices to increase the $PSL_{inter}$ value. ZCC matrix should be appropriately chosen to get high $PSL_{inter}$ value. If the ZCC code matrix to be used for coding the pulse-burst waveform is chosen in the indicated format in (2.29), the PACF of the slowtime code and the AACF of the fasttime code specify the $PSL_{intra}$ and $PSL_{inter}$ value, respectively. In order to get high $PSL_{inter}$ and $PSL_{intra}$ values; the PACF of the slowtime code sequence and the AACF of the fasttime code sequence should have high PSLs. It is possible to find various codes to satisfy these needs in the literature. However, in the scope of the thesis slowtime and fasttime codes that will be used in the ZCC code matrices are obtained through optimizing random codes according to the needs.

The mathematical expression of the cost function created for optimizing slowtime code sequence is given in (3.5).

$$CF = \max\left\{\left|R_{sc}^{p}(k)\right|\right\} = \max\left\{\left|\sum_{i=0}^{N-1} sc_i^{*}\, sc_{((i+k))N}\right|\right\} \qquad for\ k \neq 0 \qquad \textbf{(3.5)}$$

where $CF$ : cost function; $sc_i$ : $i^{th}$ element of the slowtime code sequence; $|R^{p}_{sc}(k)|$ : magnitude of $k^{th}$ element of PACF of slowtime code sequence; $N$ : length of slowtime code sequence.

In the cost function defined in (3.5), the maximum sidelobe level of PACF of slowtime code sequence is minimized.

The mathematical expression of the cost function created for optimizing fasttime code is given in (3.6).

$$CF = \max\left\{\left|R_{fc}(k)\right|\right\} \qquad for\ k \neq 0$$

$$where\ \ R_{fc}(k) = \begin{cases} \sum_{i=0}^{N-1-k} fc_{i+k} fc_i^{*}, & 0 \le k \le N-1 \\ \sum_{i=0}^{N-1+k} fc_i fc_{i-k}^{*}, & -(N-1) \le k < 0 \end{cases} \qquad \textbf{(3.6)}$$

where $CF$ : cost function; $fc_i$ : $i^{th}$ element of the fasttime code sequence; $|R_{fc}(k)|$ : magnitude of $k^{th}$ element of AACF of fasttime code sequence.

In the cost function defined in (3.6), the maximum sidelobe level of AACF of fasttime code sequence is minimized.

In Figure 3-9, the $PSL_{intra}$ and $PSL_{inter}$ values are gathered as a result of the optimization of slowtime and fasttime codes in various sizes.

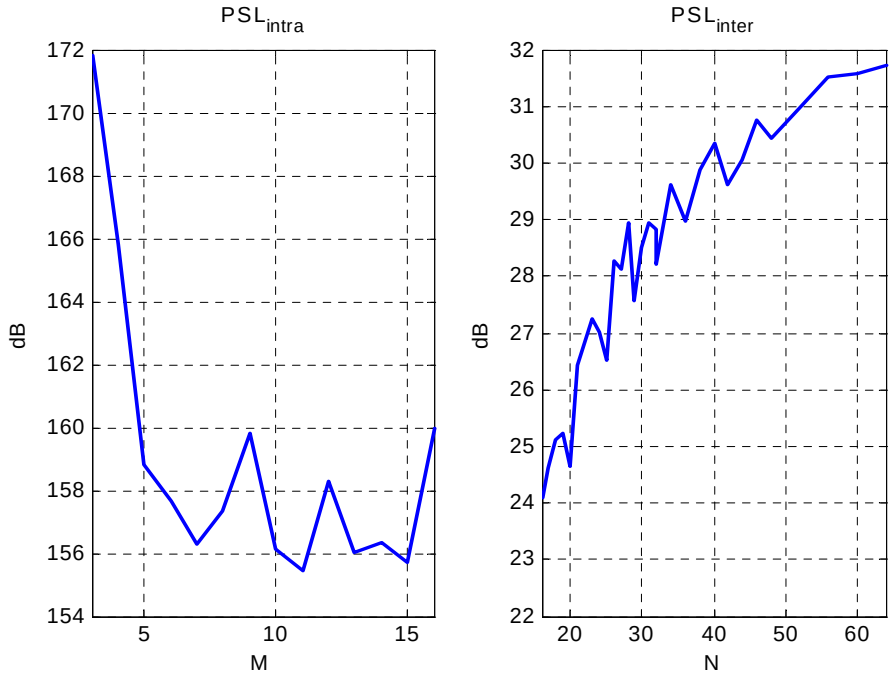


**Figure 3-9** $PSL_{intra}$ and $PSL_{inter}$ values after optimization

It is understood from the Figure 3-9 that ZCC codes have quite low sidelobe levels for zero Doppler shift. Particularly $PSL_{intra}$ is very high. In ZCC code definition $PSL_{intra}$ value is regarded as infinite. However the results, given in Figure 3-9, are obtained through optimization. $PSL_{inter}$ values are not as high as $PSL_{intra}$ values. $PSL_{intra}$ depends on the periodic correlation function; however, $PSL_{inter}$ depends on the aperiodic correlation function of the code sequences. The maximum sidelobe value in the periodic auto-correlation function of any code can be reduced to much smaller value with respect to the maximum sidelobe value in the aperiodic auto-correlation function. To analyze the performance of ZCC codes under various Doppler phase shifts, the ambiguity diagram given in the Figure 3-10 is prepared.

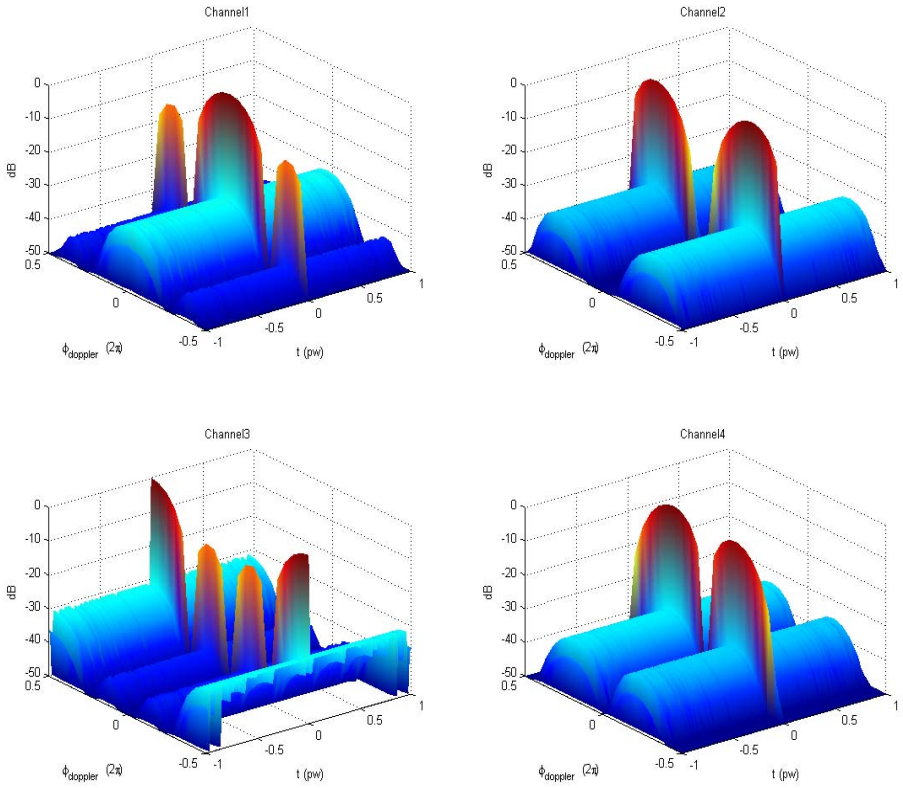


**Figure 3-10** Ambiguity diagram of a 4x64 ZCC code matrix

The ambiguity diagram displayed in Figure 3-10 shows that ZCC codes reflected from a moving target could not achieve the desired result at the pulse-burst matched filter output. As seen in the figure when the phase shift among the pulses is different from zero; the signal level at matched point decreases. On the other hand; the signal levels at undesired times in matched channel and mismatched channels increase. The characteristics of fasttime code sequence, used to form ZCC code matrix, are seen in ambiguity diagram. Doppler effect did not disturb the characteristics that are formed along the time axis. However, it affected the signal ratios between the channels considerably.

In Figure 3-11 the performance of ZCC codes made up of slowtime and fasttime code sequences in various sizes under specific Doppler phase shift is discussed. The same codes used in the Figure 3-9 are used to compose these figures.

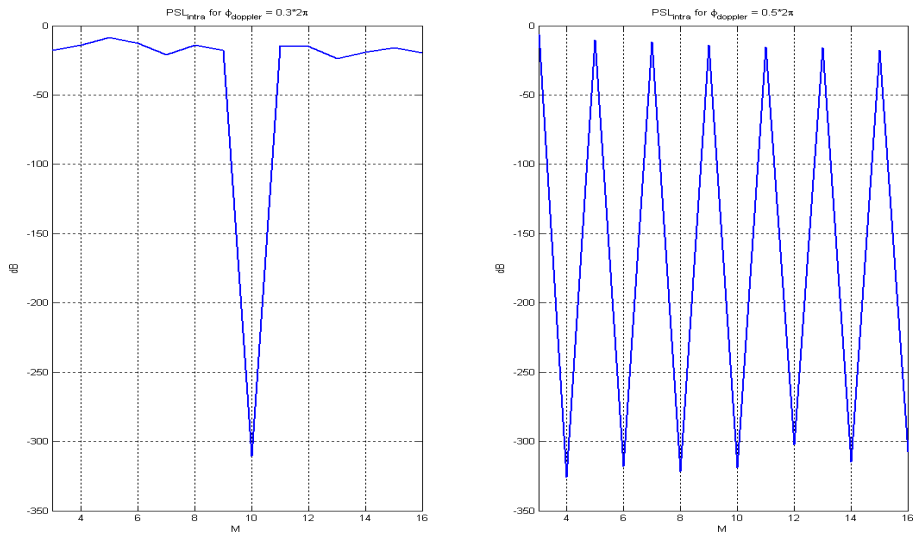


**Figure 3-11** $PSL_{inter}$ and $PSL_{intra}$ values of the ZCC codes under Doppler phase shift

In Figure 3-11 it is seen that Doppler shift negatively affects the performance of ZCC codes. Due to this reason using ZCC code matrices for coding pulse-burst signals is not suitable in radar applications.

### 3.1.4 Use of ZCC-Complementary Codes in Pulse Diversity

ZCC-Complementary codes have the advantages of both complementary codes and ZCC codes. They have high $PSL_{intra}$ values like ZCC codes and they have high $PSL_{inter}$ values like complementary codes. The general form of ZCC codes is given just as it is in (2.34) by Gerlach and Kretschmer. In this condition ZCC-Complementary code matrices are square. Coding the pulse-burst waveform with square code matrix causes some problems in radar applications. The length of code sequences used in pulses is required to be long; on the other hand, the increase in the number of the pulses used in the burst complicates signal processing even decreases the efficiency. However, radar applications have various types and there are radar systems satisfying various needs. Therefore, in some applications square matrices can be preferred for coding pulse-burst waveforms.

ZCC-Complementary code matrices have very high values of $PSL_{inter}$ and $PSL_{intra}$ for zero Doppler shift. In order to analyze the performance of ZCC-Complementary codes under Doppler shift, the ambiguity diagram given in Figure 3-12 is prepared. The codes of 16x16 are used for preparing this diagram. The signal characteristics appearing in the mismatched channels have similar structures with each other. Due to this reason; to increase the intelligibility of the figure, only the signals appearing in 4 channels are displayed.

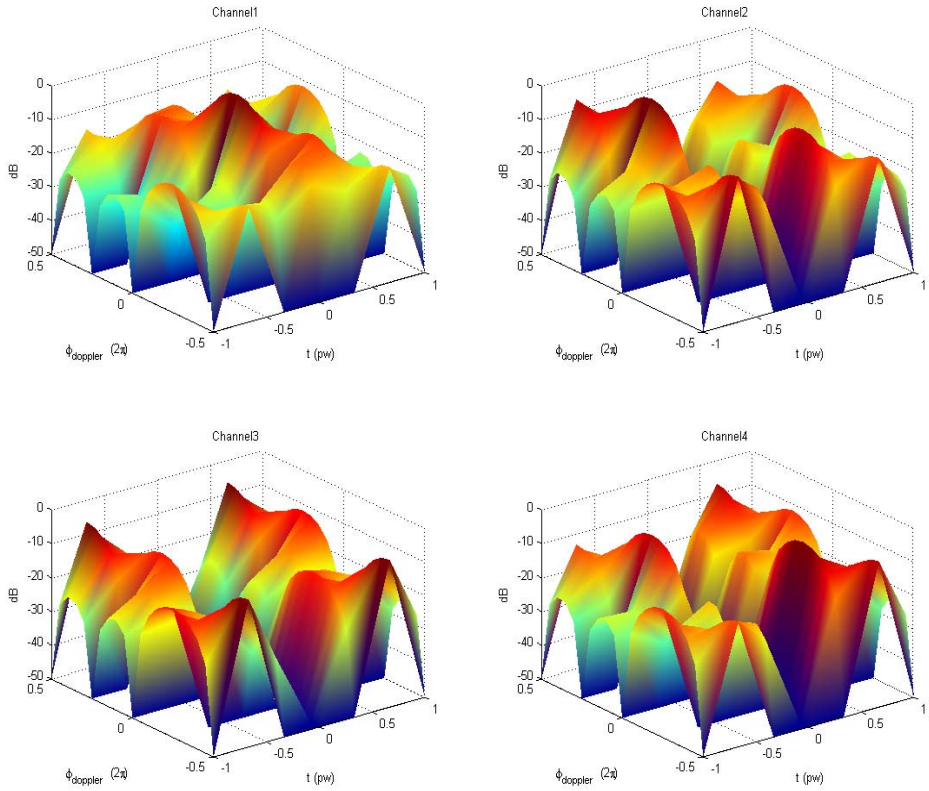


**Figure 3-12** Ambiguity diagram of a 16x16 ZCC-Complementary code matrix

The ambiguity diagram displayed in Figure 3-12, shows that ZCC-Complementary codes reflected from a moving target could not achieve the desired result at the pulse-burst matched filter output.

In Figure 3-11 the performance of ZCC-Complementary code matrices of various sizes under specific Doppler shift is evaluated.

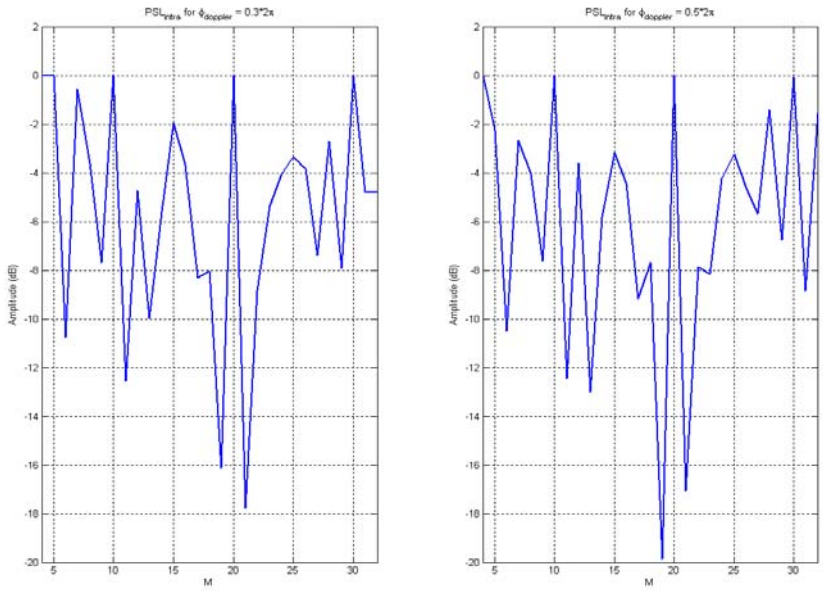


**Figure 3-13** $PSL_{inter}$ and $PSL_{intra}$ values of ZCC codes under Doppler phase shifts

In Figure 3-13 it is seen that Doppler shift between the pulses negatively affects the ZCC codes. Consequently, it is not appropriate to use ZCC code matrices for coding pulse-burst signals.

# CHAPTER 4

# RANGE AMBIGUITY REMOVAL WITH RADAR WAVEFORM OPTIMIZATION

The waveform code matrices, which will be used for coding pulse-burst waveforms in pulse diverse radar systems, are expected to have the following characteristics listed below for all Doppler frequency shifts at the output of pulse-burst matched filter.

1. High signal level at the matched point
2. Low sidelobe level in the matched channel
3. Low signal level in all the mismatched channels

The pulse-burst waveforms, which are used in pulse diverse radar applications, carried out in Chapter 3. These waveforms are coded with code matrices that are defined in literature or optimized with simple methods. These applications show that quite high $PSL_{inter}$ and $PSL_{intra}$ values can be obtained for zero Doppler shift. However, on the condition that the targets move, $PSL_{inter}$ and $PSL_{intra}$ values decrease, so false alarms can occur.

In order to achieve high $PSL_{inter}$ and $PSL_{intra}$ values, it is possible to use mismatched filters. Using mismatched filters causes some SNR loss. However, this loss can be minimized by optimizing the filters. Pulse-burst mismatched filter can be symbolized in the format specified in (4.1).

$$F_{MMF} = \left\{ f_{mn} \right\}_{[m,n]=[0,0]}^{[m,n]=[M\text{-}1,N\text{-}1]} \qquad \textbf{(4.1)}$$

where $F_{MMF}$ : pulse-burst mismatched filter; $f_{mn}$ : $n^{th}$ element of the $m^{th}$ single mismatched filter; $M$ : number of single mismatched filters in the pulse-burst mismatched filter; $N$ : length of single mismatched filter.

The number of single mismatched filters in the pulse-burst mismatched filter is equal to the number of pulses in the pulse-burst waveform. Similarly, the number of elements forming single mismatched filter is the same with the length of the code sequence used in a pulse. The amplitudes of filter elements in the mismatched filter may not be uniform. However, the amplitudes of all code elements forming the pulses are equal to 1.

$$C_{TX} = \left\{ c_{mn} \right\}_{[m,n]=[0,0]}^{[m,n]=[M-1,N-1]}$$
$$C_{RX} = \left\{ c_{mn} e^{jm\phi_1} \right\}_{[m,n]=[0,0]}^{[m,n]=[M-1,N-1]} \qquad \textbf{(4.2)}$$
$$where\ \phi_1 = 2\pi f_d T_r$$

where $C_{TX}$ : transmitted waveform code matrix; $C_{RX}$ : received waveform code matrix; $f_d$ : Doppler frequency; $T_r$ : PRI.

On the condition that the transmitted and the received pulse-burst waveforms are accepted to be in the format given in (4.2), the signal at pulse-burst mismatched filter output becomes as given in (4.3).

$$
\begin{aligned}
\left|\chi_{k+1}[i]\right| &= \left|\sum_{m=0}^{M-1} e^{jm\phi} C^{CF}_{m,((m-k))M}\right| \\
&= \begin{cases} \left|\sum_{m=0}^{M-1}\left(\sum_{n=0}^{N-1-i} c_{m,(n+i)} e^{jm\phi} f_{((m-k))M,n}^{\ *}\right)\right|, & 0 \le i \le N-1 \\ \left|\sum_{m=0}^{M-1}\left(\sum_{n=0}^{N-1+i} c_{m,n} e^{jm\phi} f_{((m-k))M,(n-i)}^{\ *}\right)\right|, & -(N-1) \le i < 0 \end{cases} \qquad \textbf{(4.3)} \\
&= \begin{cases} \left|\sum_{m=0}^{M-1} e^{jm\phi}\left(\sum_{n=0}^{N-1-i} c_{m,(n+i)} f_{((m-k))M,n}^{\ *}\right)\right|, & 0 \le i \le N-1 \\ \left|\sum_{m=0}^{M-1} e^{jm\phi}\left(\sum_{n=0}^{N-1+i} c_{m,n} f_{((m-k))M,(n-i)}^{\ *}\right)\right|, & -(N-1) \le i < 0 \end{cases}
\end{aligned}
$$

where $\left|\chi_k[i]\right|$ : signal envelope of $i^{th}$ sample in the $k^{th}$ channel at the output of pulse-burst mismatched filter; $C^{CF}_{m,n}$ : ACCF between $m^{th}$ code sequence in the transmitted waveform code matrix and $n^{th}$ code sequence in the filter code matrix; $M$ : number of pulses in the burst; $N$ : length of code sequence; $\Phi$ : phase shift between consecutive pulses; $c_{m,n}$ : $n^{th}$ element of $m^{th}$ code sequence in the code matrix.

It is seen that the signal level at pulse-burst mismatched filter output, whose mathematical expression is given in (4.3), changes according to different values of $\Phi$. Therefore, it is not possible for a single pulse-burst mismatched filter to produce the required output for all possible Doppler phase shift values.

In the scope of the thesis work pulse-burst mismatched filter bank is used, in order to get the required result for various Doppler phase shifts. In Figure 4-1 pulse-burst mismatched filter bank structure is given.

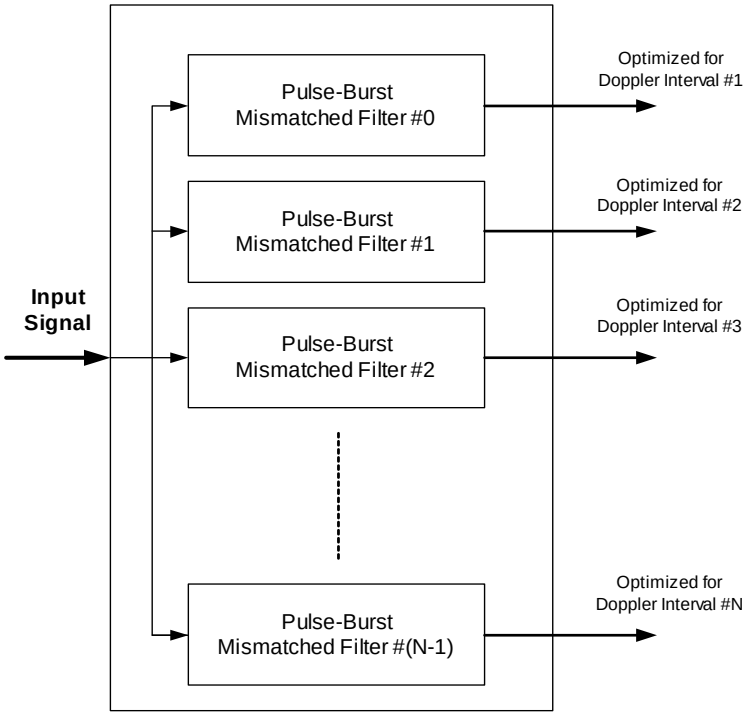


**Figure 4-1** Pulse-burst mismatched filter structure

Each pulse-burst mismatched filter in the filter bank is formed and optimized for a certain Doppler interval. While the number of pulse-burst mismatched filters in the filter bank increases, the Doppler intervals for which each pulse-burst filter is optimized decrease. Consequently; more successful results can be obtained, if more pulse-burst mismatched filters are used in the filter bank. There are channels formed at the pulse-burst mismatched filter output with the same number of the pulses in the burst. Consequently, the filter in which target is detected indicates the Doppler phase information of the target and the channel in which detection is made indicates the target range interval. In the following sections, the filter in which target echo should take place in mismatched filter bank will be called as target filter and, the channel that target echo should take place will be called as target channel.

In the thesis getting high PSL values is aimed. In this chapter optimizations are made in order to get high PSL value in accordance with various needs and

acceptances. In all optimizations the signal level at matched point is attempted to be kept above a certain value, while the maximum signal level at undesired times is minimized. In order to minimize the maximum value at undesired times, the standard function 'fminimax' of MATLAB program is used.

The applied optimizations are divided into 2 main groups. This grouping is done according to the features of the code matrices forming the waveform and the mismatched filters. In the Group A, the optimizations of code matrices, in which there is no dependence between the rows and the columns, are done. Code matrices are concurrently optimized for both high $PSL_{inter}$ and high $PSL_{intra}$ values. In the Group B of optimizations, the waveform and the filter code matrices are composed of the product of slowtime and fasttime code sequences. The slowtime and fasttime code sequences are optimized separately to get high $PSL_{intra}$ and $PSL_{inter}$ values respectively. Both of the groupings are categorized under subgroups. The applied optimizations and the related results are stated in the corresponding sections.

## 4.1 OPTIMIZATION A: OPTIMIZING $PSL_{INTRA}$ AND $PSL_{INTER}$ TOGETHER

The optimizations, in which high $PSL_{inter}$ and $PSL_{intra}$ values are obtained in the same phase, are categorized under 2 subgroups. The common characteristics of these 2 optimization subgroups are listed below.

1. The pulse-burst waveform, in which each pulse is coded with different code sequences, is transmitted from the radar transmitter. Only a single waveform code matrix is produced for the pulse-burst waveform.

2. There are more than one pulse-burst mismatched filter in the radar receiver. Each of them is optimized for a certain Doppler interval. Therefore, there are more than one filter code matrix constructed.
3. The Doppler intervals, for which filters are optimized, intersect with each other. Therefore, PSL is prevented from decreasing for the Doppler values that are between the boundary points of two filters.
4. Waveform code matrix and all filter code matrices are optimized concurrently for both high $PSL_{inter}$ and high $PSL_{intra}$ values.
5. The formats of the waveform and filter code matrices, that are used in optimizations, is as given in (4.4).

$$C_A = \begin{bmatrix} c_0 \\ c_1 \\ \dots \\ c_{M-1} \end{bmatrix} = \begin{bmatrix} c_{00} & c_{01} & c_{02} & \dots c_{0,N-1} \\ c_{10} & c_{11} & c_{12} & \dots c_{1,N-1} \\ \dots & & & \\ c_{M-1,0} & c_{M-1,1} & c_{M-1,2} & \dots c_{M-1,N-1} \end{bmatrix} \quad \textbf{(4.4)}$$

where $C_A$ : code matrix of waveform and filters; $c_{mn}$ : $n^{th}$ element of the $m^{th}$ code sequence; $M$ : number of code sequence in the code matrix; $N$ : number of code element in the code sequence.

6. Each element of the code matrices used in both transmitted pulse-burst waveform and pulse-burst mismatched filters is independent from others.
7. The peak level observed in target channel is constrained to be above a certain level.

### 4.1.1 OPTIMIZATION A1

The optimization done in this section, have the characteristics listed below in addition to the characteristics listed in Section 4.1.

1. Each filter code matrix will be optimized for its own Doppler interval. The outputs of any filter produced for other Doppler phase shifts except for its own interval are ignored.
2. In the optimization maximum peak and minimum sidelobe level in the target channel, and minimum signal level in the other channels of the target filter are aimed. There isn't any optimization done for the other filters apart from the target filter.

In order to be able to use the code matrices, obtained through this optimization, in radar applications another system or operator, which will specify the target filter, is needed. The correlation between the channels leads the operator to specify the target filter. The obtained code matrices are used in radar systems for conforming the detections and measuring the targets' range unambiguously.

The used optimization algorithm can show different performance for different initial codes of same size. In order to compare the results, which the optimization algorithm produced for different initial codes of same size, Table 4 is prepared. The optimization program is run for 10 different initial codes. The initial codes are chosen randomly. In these optimizations a waveform code matrix of 3x32 and three filter code matrices of 3x32 are used. All results given in the table are obtained as a result of filtering the $0.5x2\pi$ Doppler phase shifted waveform with the filter, optimized for $[0.3\ 0.7]x2\pi$ Doppler interval. The expression "maximum sidelobe level in the target filter" used in the table corresponds to the maximum of maximum sidelobe level in the target channel and maximum signal level in all the other channels of the target filter.

**Table 4** Results of Optimization A1 for different initial codes

| Run No | Peak Level at the Target Channel | | Max. Sidelobe Level in the Target Filter | |
|---|---|---|---|---|
| | Before Opt. (dB) | After Opt. (dB) | Before Opt. (dB) | After Opt. (dB) |
| **1** | -31.5586 | -3.3157 | -13.1786 | -32.0203 |
| **2** | -20.6953 | -3.3311 | -12.6162 | -31.6381 |
| **3** | -25.0138 | -3.3407 | -14.8457 | -32.2306 |
| **4** | -26.9649 | -3.3280 | -13.9663 | -31.4153 |
| **5** | -18.7221 | -3.3356 | -15.5593 | -31.9808 |
| **6** | -18.4230 | -3.3372 | -13.9359 | -31.6348 |
| **7** | -26.4596 | -3.3222 | -13.0426 | -32.1292 |
| **8** | -24.9955 | -3.3223 | -14.3898 | -31.9866 |
| **9** | -20.2582 | -3.3367 | -14.5596 | -31.9855 |
| **10** | -20.2086 | -3.3397 | -11.5835 | -31.5122 |

When Table 4 is examined, it is seen that the peak level in target channel increases approximately by 10-15 dB and the maximum sidelobe level in target filter decreases approximately by 15-20 dB for all runs. For all optimized code matrices the peak value at the target channel is close to each other and above a certain level. There is nonlinear condition definition in the optimization algorithm. With this condition, it is ensured that the peak value in the target channel for the optimized code matrices remains above -3.5 dB.

As seen in Table 4, the minimum sidelobe level is obtained in the 3$^{rd}$ run. The results of the code matrices, obtained in the 3$^{rd}$ run, are given in Table 5 under different Doppler phase shifts. While this table is being prepared, different Doppler phase shifts are applied to the waveform. Afterwards, the results of

the waveform at the output of the target filter are observed. Filter #1, Filter #2 and Filter #3 are optimized to have maximum peak level and minimum sidelobe level for [-0.033 0.367]x2π, [0.300 0.700]x2π and [0.633 0.033]x2π Doppler intervals respectively. In Table 5, the Doppler shift applied to the transmitted waveform and the target filter number, which is valid for this Doppler shift, are given. In order to evaluate the success of the optimization, the maximum sidelobe levels in target filter is given in addition to the peak levels in target channel for all Doppler shifts. Besides the peak level that will be obtained at filter output for the given Doppler shift is given on the condition that pulse-burst matched filter for zero Doppler shift is used instead of mismatched filter.

**Table 5** Results of Optimization A1 under different Doppler shifts

| **Doppler Phase Shift (2π)** | **Target Filter No** | **Peak Level at the Target Channel** | | **Max. Sidelobe Level in the Target Filter** | | **Peak Level at the Matched Filter Output (dB)** |
|---|---|---|---|---|---|---|
| | | **Before Opt. (dB)** | **After Opt. (dB)** | **Before Opt. (dB)** | **After Opt. (dB)** | |
| -0.0333 | 1 | -21.281 | -3.5218 | -13.0975 | -32.2306 | -0.8143 |
| 0.1667 | 1 | -18.884 | -3.3391 | -12.6783 | -32.2306 | -3.5218 |
| 0.3667 | 1 | -17.417 | -3.5218 | -12.5515 | -32.2306 | -9.5333 |
| 0.3000 | 2 | -26.272 | -3.5218 | -14.5312 | -32.2306 | -12.2454 |
| 0.5000 | 2 | -25.013 | -3.3407 | -14.8457 | -32.2306 | -9.5424 |
| 0.7000 | 2 | -28.154 | -3.5218 | -15.1232 | -32.2306 | -12.2454 |
| 0.6333 | 3 | -21.377 | -3.5218 | -14.6324 | -32.2306 | -9.5333 |
| 0.8333 | 3 | -20.829 | -3.3392 | -14.2404 | -32.2306 | -3.5218 |
| 1.0333 | 3 | -20.514 | -3.5218 | -14.0665 | -32.2306 | -0.8143 |

As it is seen in Table 5, approximately 30 dB PSL value is obtained for all Doppler shifts in target filter. Besides; the Doppler tolerance of the filter, obtained through the optimization, is quite better than pulse-burst matched filter.

To observe the results of code matrices, obtained in the 3rd run, at the outputs of all filters under 0.5x2π Doppler shift Figure 4-2, Figure 4-3 and Figure 4-4 are prepared. Filter #2 is the target filter for this Doppler value. Therefore, the values given in shaded rows in Table 4 and Table 5 should be observed at 2nd filter output. Since there is no time shift given to the waveform, 1st channel is the target channel. In the figures, the plots in blue symbolize the results of the code matrices before optimization and the ones in red symbolize the results of the code matrices after optimization.

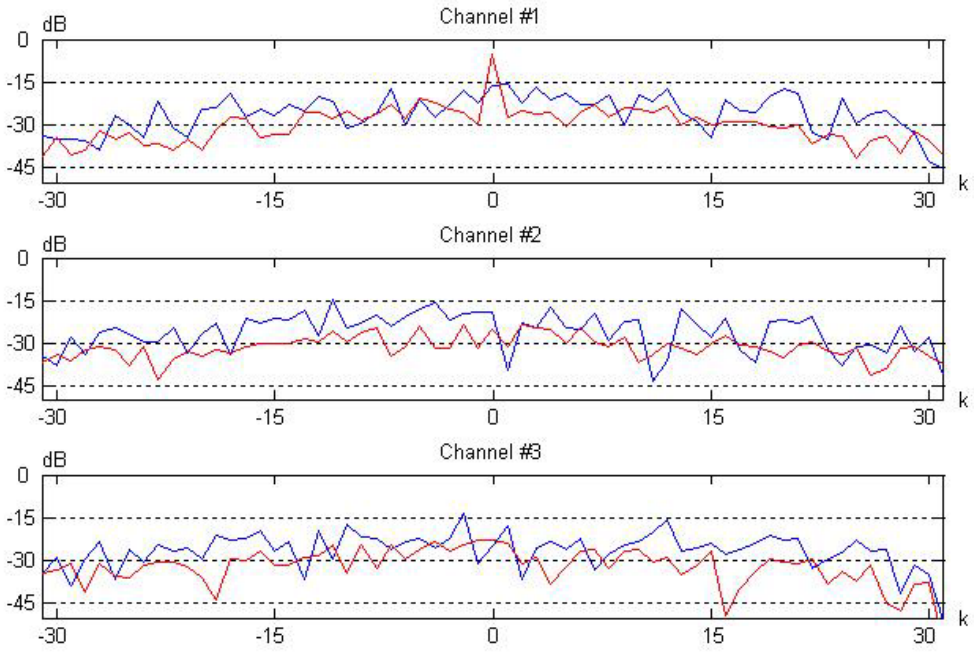


**Figure 4-2** Mismatched filter #1 output

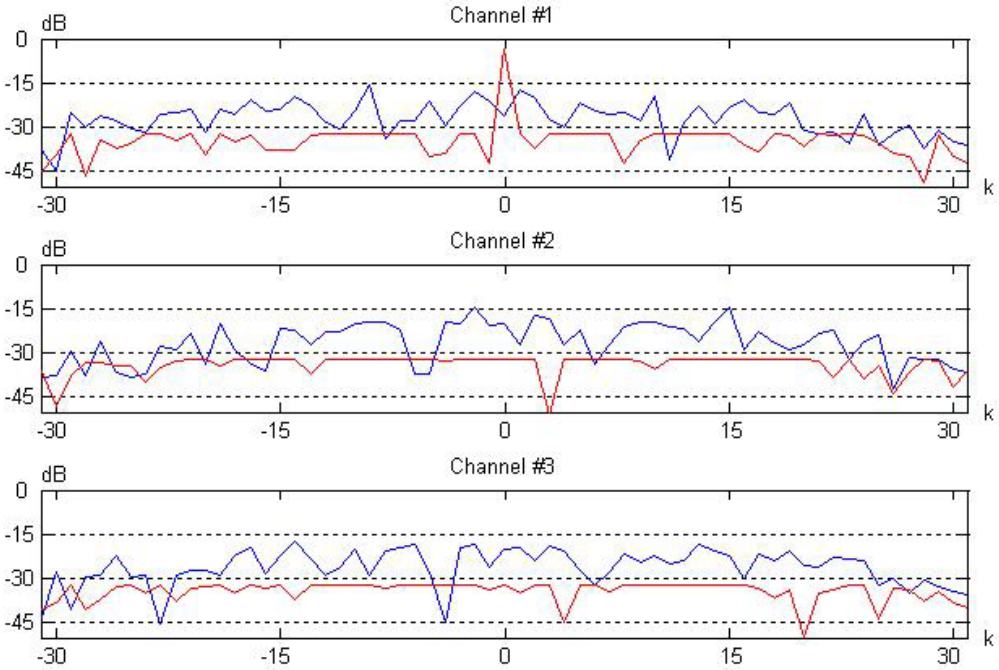


**Figure 4-3** Mismatched filter #2 (target filter) output

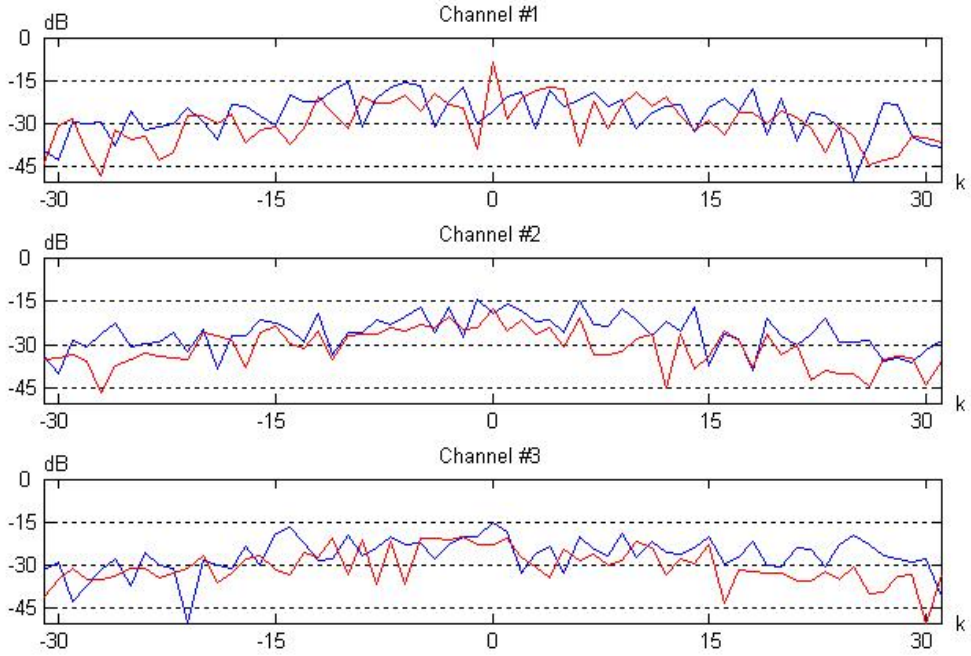


**Figure 4-4** Mismatched filter #3 output

In Figure 4-3, the target filter output is given. In the target filter, the peak value in target channel is quite higher than the sidelobe level in target channel and the signal level in the other channels as well. The peak level obtained in target channel is approximately -3 dB. Maximum sidelobe level, observed in the target filter, is approximately -32 dB. Therefore, approximately 30 dB PSL is obtained under 0.5x2π Doppler shift for the code matrices, obtained in the 3rd run. These values are compatible with the values given for 0.5x2π Doppler shifts in Table 4 and Table 5.

### 4.1.2 OPTIMIZATION A2

The optimization done in this section, have the characteristics listed below in addition to the characteristics listed in Section 4.1.

1. While each filter matrix is optimized for its own Doppler interval, it will also be optimized for other Doppler shifts to produce minimum output.
2. In the optimization, similar to Optimization A1, maximum peak and minimum sidelobe levels in target channel and minimum signal level in the other channels of the target filter are aimed. Besides, minimum sidelobe level in all channels of the filters apart from the target filter is aimed for any Doppler value.

In this optimization method, optimizing all filters for all possible Doppler values ensures the target filter to be specified automatically. Therefore, any Doppler data coming from another radar is not needed. The systems using the codes, which are optimized through this optimization method and succeeded, can run autonomously.

The used optimization algorithm can show different performance for different initial codes of same size. In order to compare the results, which the optimization algorithm produced for different initial codes of same size, Table 6 is prepared. The optimization program is run for 10 different initial codes. The initial codes are chosen randomly. In these optimizations a waveform code matrix of 3x32 and three filter code matrices of 3x32 are used. All results given in the table are obtained as a result of filtering the 0.5x2π Doppler phase shifted waveform with the filter, optimized for [0.3 0.7]x2π Doppler interval. The expression "maximum sidelobe level in all filters" used in the table corresponds to the maximum of maximum sidelobe level in the target channel and maximum signal level in all the other channels of the target filter and maximum signal level in all the other filters.

**Table 6** Results of Optimization A2 for different initial codes

| Run No | Peak Level at the Target Channel | | Max. Sidelobe Level in the all Filters | |
|---|---|---|---|---|
| | Before Opt. (dB) | After Opt. (dB) | Before Opt. (dB) | After Opt. (dB) |
| **1** | -22.1387 | -4.7511 | -13.7857 | -13.8419 |
| **2** | -25.1211 | -4.7511 | -11.0813 | -13.9641 |
| **3** | -39.7894 | -4.7511 | -13.1343 | -13.7333 |
| **4** | -21.7416 | -4.7511 | -12.5739 | -14.6435 |
| **5** | -24.4605 | -4.7511 | -13.4841 | -13.7944 |
| **6** | -29.6286 | -4.7511 | -13.2828 | -13.9725 |
| **7** | -16.3702 | -4.7511 | -13.5186 | -14.0384 |
| **8** | -24.8758 | -4.7511 | -12.6071 | -13.6816 |
| **9** | -20.3617 | -4.7511 | -12.6677 | -13.5976 |
| **10** | -19.7135 | -4.7511 | -12.8959 | -13.5769 |

When Table 6 is examined, it is seen that the peak level in target channel increases by about 15-20 dB. Since, in the optimization it is ensured that the peak value in the target channel for the optimized code matrices remains above -6 dB. However, the same improvement couldn't be observed in decreasing the maximum sidelobe level. The reason is that the optimization method attempts to find out the minimum point of a surface, depending on many variables.

As seen in Table 6, the minimum sidelobe level is obtained in the $4^{th}$ run. The results of the code matrices, obtained in the $4^{th}$ run, are given in Table 7 under different Doppler phase shifts. While this table is being prepared different Doppler phase shifts are applied to the waveform. Afterwards the waveform is processed through all filters and the results obtained at the output of all filters are observed. Filter #1, Filter #2 and Filter #3 are optimized to have maximum peak level and minimum sidelobe level for [-0.033 0.367]x2π, [0.300 0.700]x2π and [0.633 0.033]x2π Doppler intervals respectively. Besides; each filter is optimized in order to produce minimum output signal level to the waveform, shifted with the Doppler values except for its own Doppler interval, in addition to Optimization A1.

**Table 7** Results of Optimization A2 under different Doppler shifts

| Doppler Phase Shift (2π) | Peak Level at the Target Channel | | Max. Sidelobe Level in the all filters | | Peak Level at the Matched Filter Output (dB) |
|---|---|---|---|---|---|
| | Before Opt. (dB) | After Opt. (dB) | Before Opt. (dB) | After Opt. (dB) | |
| -0.0333 | -19.7651 | -13.5666 | -14.0868 | -6.0206 | -0.1275 |
| 0.1667 | -23.9694 | -28.1023 | -14.3728 | -4.7511 | -3.5218 |
| 0.3667 | -35.4107 | -13.5666 | -14.2486 | -6.0206 | -18.9574 |
| 0.3000 | -23.9743 | -6.0206 | -12.6060 | -13.5666 | -17.9019 |
| 0.5000 | -21.7416 | -4.7511 | -12.5739 | -14.6435 | -9.5424 |
| 0.7000 | -23.1283 | -6.0206 | -13.5527 | -13.5666 | -17.9019 |
| 0.6333 | -26.4535 | -13.5666 | -12.4481 | -6.0206 | -18.9574 |
| 0.8333 | -22.1342 | -28.1023 | -12.7218 | -4.7511 | -3.5218 |
| 1.0333 | -19.3299 | -13.5666 | -13.4811 | -6.0206 | -0.1275 |

As it is seen in Table 7, the difference between the peak level in the target channel and maximum sidelobe level, which is observed in any filters, is not stable. This situation hinders the target detection in clutter. Therefore, it is not possible for the codes that are obtained through this optimization method to be used in radar systems.

To observe the results of code matrices, obtained in the $4^{th}$ run, at the outputs of all filters under 0.5x2π Doppler shift, Figure 4-5, Figure 4-6 and Figure 4-7 are prepared. Filter #2 is the target filter for this Doppler value. Therefore, the peak value given in shaded rows in Table 6 and Table 7 should be observed at $2^{nd}$ filter output. However, the maximum sidelobe level can be observed in any channel of any filter. Since there is no time shift given to the waveform,

1st channel is the target channel. In the figures, the plots in blue symbolize the results of the code matrices before optimization and the ones in red symbolize the results of the code matrices after optimization.

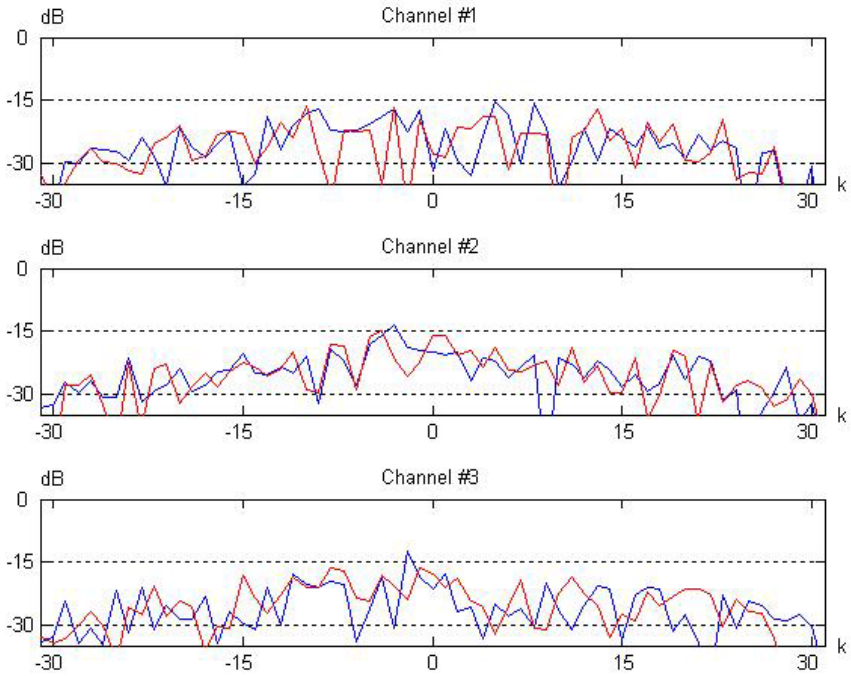


**Figure 4-5** Mismatched filter #1 output

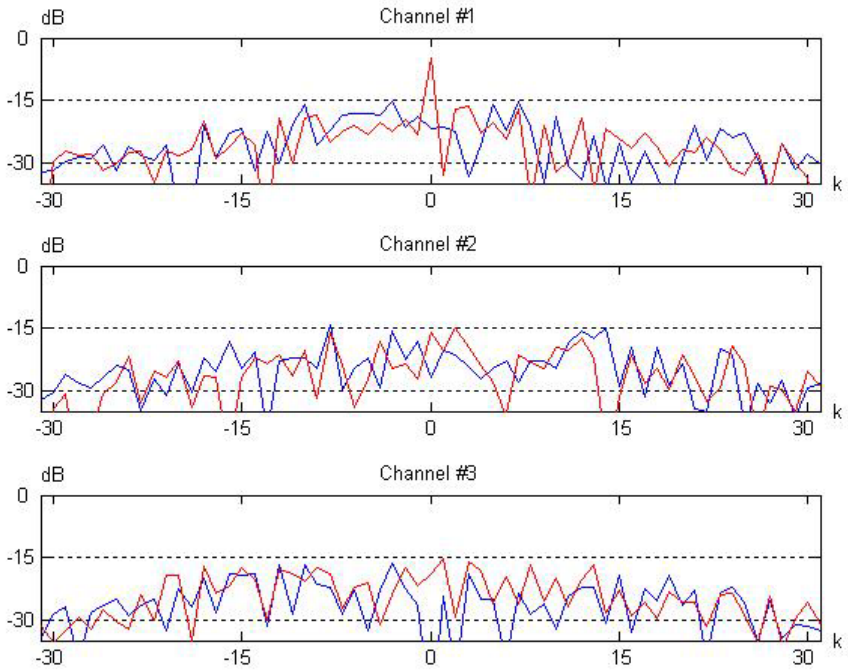


**Figure 4-6** Mismatched filter #2 (target filter) output

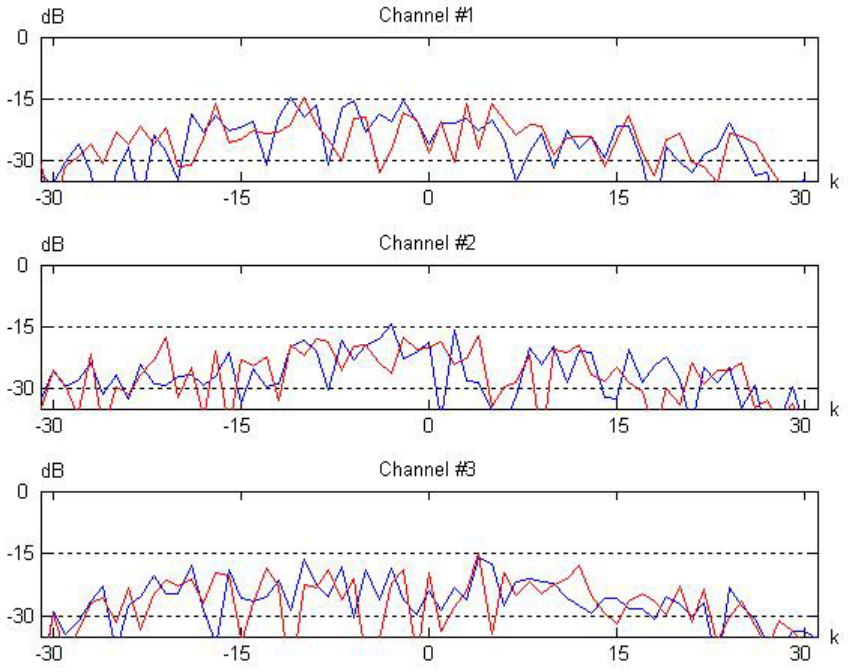


**Figure 4-7** Mismatched filter #3 output

When Figure 4-5, Figure 4-6 and Figure 4-7 are examined, it is seen that the peak level in the target filter transcends the signal level, occurring in the other channels or filters, approximately by 10 dB for 0.5x2π Doppler value. However, same results cannot be obtained for other Doppler values as seen in Table 4. Consequently; the codes that are obtained by Optimization A2 methods is not acceptable to be used in radar applications.

## 4.2 OPTIMIZATION B : OPTIMIZING $PSL_{INTRA}$ AND $PSL_{INTER}$ INDIVIDUALLY

In the optimizations done in this section the $PSL_{inter}$ and $PSL_{intra}$ values of the signal, produced at the output of mismatched filter bank, are optimized seperately. These optimizations are categorized under 2 subgroups. The common characteristics of these 2 subgroups are listed below.

1. The pulse-burst waveform, in which each pulse is coded with different code sequences, is transmitted from the radar transmitter. Only a single waveform code matrix is produced for pulse-burst waveform.
2. There are more than one pulse-burst mismatched filter in the radar receiver. Each of them is optimized for a certain Doppler interval. Therefore, there are more than one filter code matrix constructed.
3. The Doppler intervals for which filters are optimized intersect with each other. Therefore, PSL is prevented from decreasing for the Doppler values that are between the boundary points of two filters.
4. The formats of the waveform and filter code matrices that are used in optimization is as given in (4.5).

$$C_B = a^T b = \begin{bmatrix} a_0 \\ a_1 \\ \dots \\ a_{M-1} \end{bmatrix} \begin{bmatrix} b_0 & b_1 & \dots & b_{N-1} \end{bmatrix} = \begin{bmatrix} a_0 b_0 & a_0 b_1 & \dots & a_1 b_{N\text{-}1} \\ a_1 b_0 & a_1 b_1 & \dots & a_1 b_{N\text{-}1} \\ \dots & & & \\ a_{M\text{-}1} b_0 & a_{M\text{-}1} b_1 & \dots & a_{M\text{-}1} b_{N\text{-}1} \end{bmatrix} \quad \textbf{(4.5)}$$

where $C_B$ : code matrix of waveform and filters; $a$ : slowtime code sequence; $b$: fasttime code sequence; $M$ : number of code sequence in the code matrix; $N$ : number of code element in the code sequence.

5. The fasttime code sequences used in all code matrices are the same. However, different slowtime code sequences are formed for each code matrix.

6. Fasttime code sequence will be optimized to have the minimum auto-correlation sidelobe level. Consequently, $PSL_{inter}$ value in any channel is determined by the optimization of fasttime code sequence.

7. All slowtime code sequences used in waveform and filters will be optimized concurrently to get high $PSL_{intra}$ value in any filter. The optimizations in this category are grouped according to the differences in the optimization of slowtime code sequences.

8. The peak level observed in target channel is constrained to be above a certain level.

### 4.2.1 OPTIMIZATION B1

The optimization done in this section, have the characteristics listed below in addition to the characteristics listed in Section 4.2.

1. Waveform and filters slowtime code sequences are optimized for their own Doppler phase interval. During the optimization, the outputs of any filter produced for other Doppler phase shifts except for its interval are ignored.
2. In the optimization maximum peak and minimum sidelobe level in the target channel, and minimum signal level in the other channels of the target filter are aimed. There isn't any optimization done for the other filters apart from the target filter.

This optimization method resembles Optimization A1 in functionality. The difference between Optimization A1 and Optimization B1 is the structure of the code matrices. The codes obtained by this method can be used in radar for confirming the detections or measuring the targets' range unambiguously. However, in order to be able to use these codes, the radar system needs Doppler information coming from another radar or it needs operator aid.

The used optimization algorithm can show different performance for different initial codes of same size. In order to compare the results that the optimization algorithm produced for different initial codes of same size, Table 8 is prepared. The optimization program is run for 10 different initial codes. The fasttime code, used in all runs, is same. Different optimization results are obtained as a result of the slowtime code optimization. At the end of the optimizations of fasttime and slowtime code sequences, a waveform code matrix of 4x64 and four filter code matrices of 4x64 are obtained. All results given in the table are obtained as a result of filtering the 0.375x2π Doppler

phase shifted waveform with the filter optimized for [0.225 0.525]x2π Doppler interval. The expression "maximum sidelobe level in the target filter" used in the table corresponds to the maximum of maximum sidelobe level in target channel and maximum signal level in all the other channels of the target filter.

**Table 8** Results of Optimization B1 for different initial codes

| Run No | Peak Level at the Target Channel | | Max. Sidelobe Level in the Target Filter | |
|---|---|---|---|---|
| | Before Opt. (dB) | After Opt. (dB) | Before Opt. (dB) | After Opt. (dB) |
| **1** | -8.6312 | -2.5911 | -7.7005 | -28.2169 |
| **2** | -8.6406 | -2.5909 | -9.1037 | -28.2321 |
| **3** | -9.1972 | -3.0819 | -7.0554 | -28.0600 |
| **4** | -9.7847 | -2.6156 | -2.7185 | -25.8300 |
| **5** | -13.6450 | -2.5909 | -5.0369 | -28.2275 |
| **6** | -8.5080 | -2.8398 | -7.3917 | -28.5578 |
| **7** | -23.5200 | -2.8398 | -8.7454 | -28.6486 |
| **8** | -17.4876 | -2.8399 | -9.6824 | -28.6440 |
| **9** | -11.2328 | -2.5908 | -11.3698 | -28.2239 |
| **10** | -4.9496 | -2.8398 | -8.1165 | -28.6461 |

When Table 8 is examined, it is seen that the peak level in target channel increases by 5 dB to 20 dB for 0.375x2π. Moreover, at the end of the optimization maximum sidelobe level in the target filter decreases approximately by 20 dB. In the optimization it is ensured that the peak value in the target channel for the optimized code matrices remains above -3 dB.

As seen in Table 8, the minimum sidelobe level is obtained in the 7$^{th}$ run. The results of the code matrices, obtained in the 7$^{th}$ run, are given in Table 9 under different Doppler phase shifts. While this table is being prepared different Doppler phase shifts are applied to the waveform. Afterwards, the results of the waveform at the output of the target filter are observed. Filter #1, Filter #2, Filter #3 and Filter #4 are optimized to have maximum peak level and minimum sidelobe level for [0.975 0.275]x2π, [0.225 0.525]x2π, [0.475 0.775]x2π and [0.725 0.025]x2π Doppler intervals respectively.

**Table 9** Results of Optimization B1 under different Doppler shifts

| **Doppler Phase Shift (2π)** | **Target Filter No** | **Peak Level at the Target Channel** | | **Max. Sidelobe Level in the Target Filter** | | **Peak Level at the Matched Filter Output** |
|---|---|---|---|---|---|---|
| | | **Before Opt. (dB)** | **After Opt. (dB)** | **Before Opt. (dB)** | **After Opt. (dB)** | |
| 0.975 | 1 | -16.769 | -2.7308 | -7.4576 | -24.5428 | -3.3970 |
| 0.125 | 1 | -15.584 | -2.7340 | -7.4636 | -24.3915 | -4.3857 |
| 0.275 | 1 | -14.402 | -2.8053 | -7.5453 | -23.9138 | -5.8273 |
| 0.225 | 2 | -22.871 | -2.6209 | -9.5125 | -23.8657 | -38.9775 |
| 0.375 | 2 | -23.520 | -2.8398 | -8.7454 | -28.6486 | -19.6967 |
| 0.525 | 2 | -23.756 | -3.0980 | -8.1242 | -23.8657 | -15.0740 |
| 0.475 | 3 | -21.442 | -3.0980 | -6.1714 | -23.8657 | -15.0740 |
| 0.625 | 3 | -18.366 | -2.8399 | -5.8100 | -28.6448 | -19.6967 |
| 0.775 | 3 | -16.037 | -2.6210 | -5.5568 | -23.8657 | -38.9775 |
| 0.725 | 4 | -19.000 | -2.3350 | -11.2272 | -23.8697 | -5.8273 |
| 0.875 | 4 | -17.965 | -2.3495 | -11.3552 | -23.9488 | -4.3857 |
| 0.025 | 4 | -16.891 | -2.4321 | -11.4595 | -23.8778 | -3.3970 |

As it is seen in Table 9, approximately 25 dB PSL value is obtained for all Doppler shifts in target filter. Besides; Doppler tolerance of the codes, obtained by Optimization B1, is quite better than pulse-burst matched filter.

To observe the results of code matrices, obtained in the 7$^{th}$ run, at the outputs of all filters under 0.375x2π Doppler shift Figure 4-8, Figure 4-9, Figure 4-10 and Figure 4-11 are prepared. Filter #2 is the target filter for this Doppler value. Therefore, the values given in shaded rows in Table 8 and Table 9 should be observed at 2$^{nd}$ filter output. In the figures, the plots in blue symbolize the results of the code matrices before optimization and the ones in red symbolize the results of the code matrices after optimization.

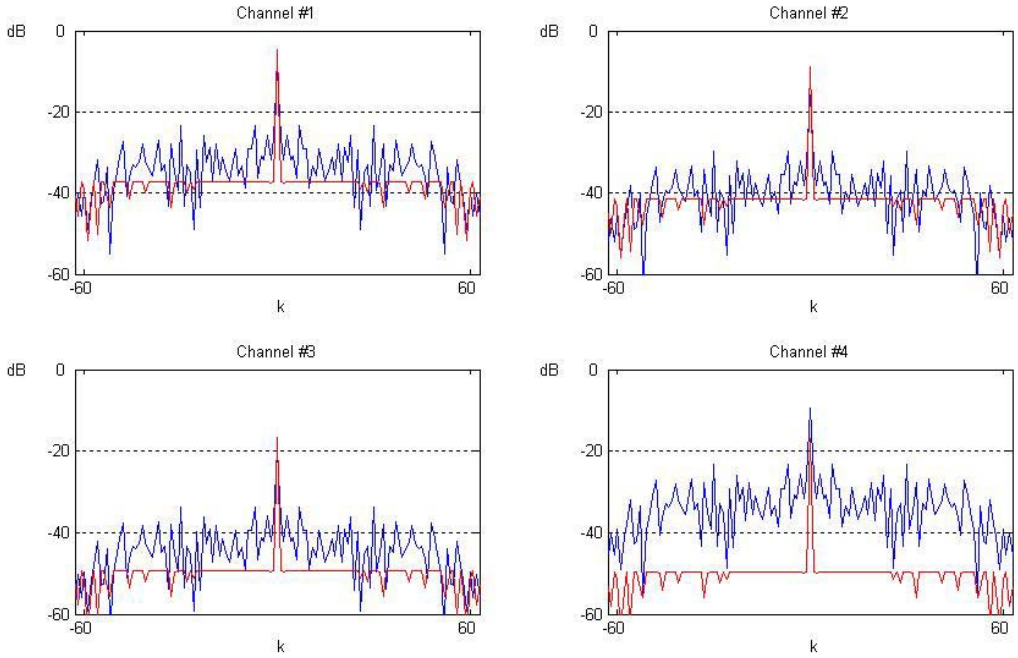


**Figure 4-8** Mismatched filter #1 output

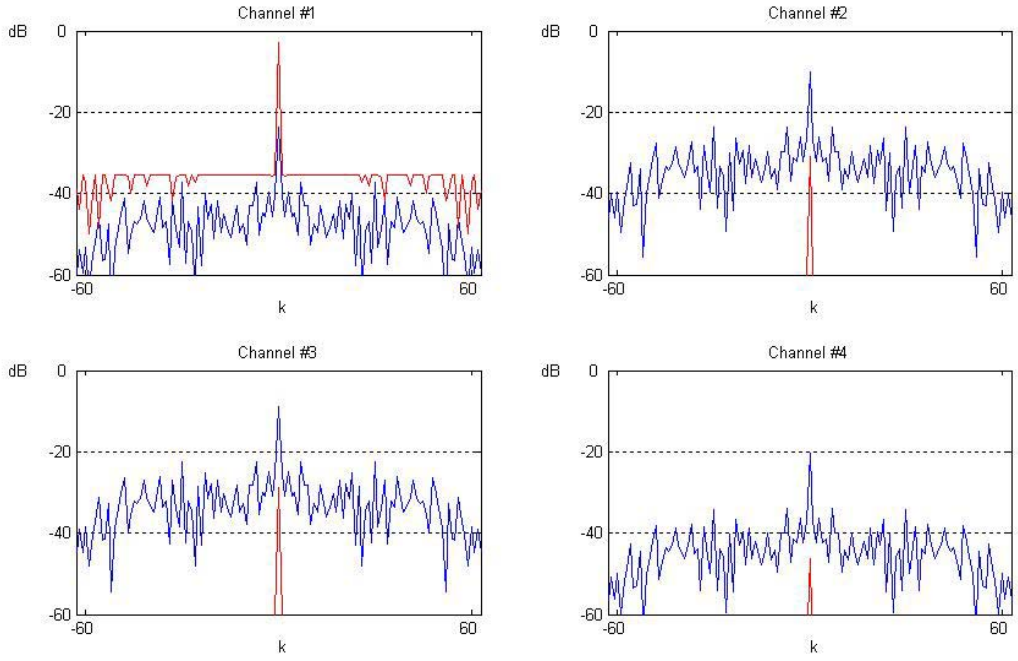


**Figure 4-9** Mismatched filter #2 (target filter) output

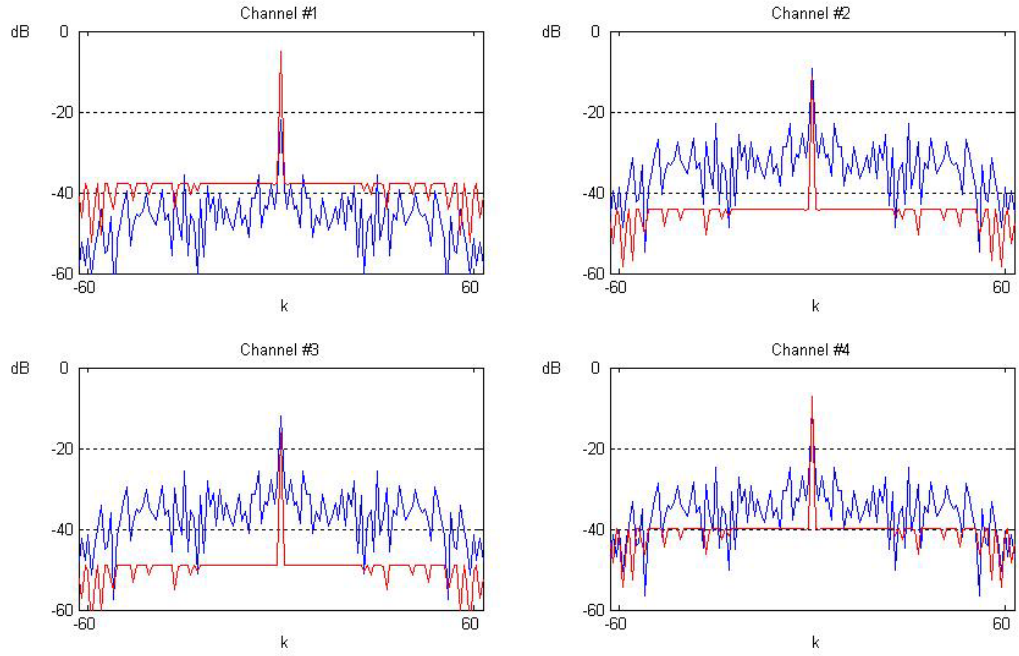


**Figure 4-10** Mismatched filter #3 output

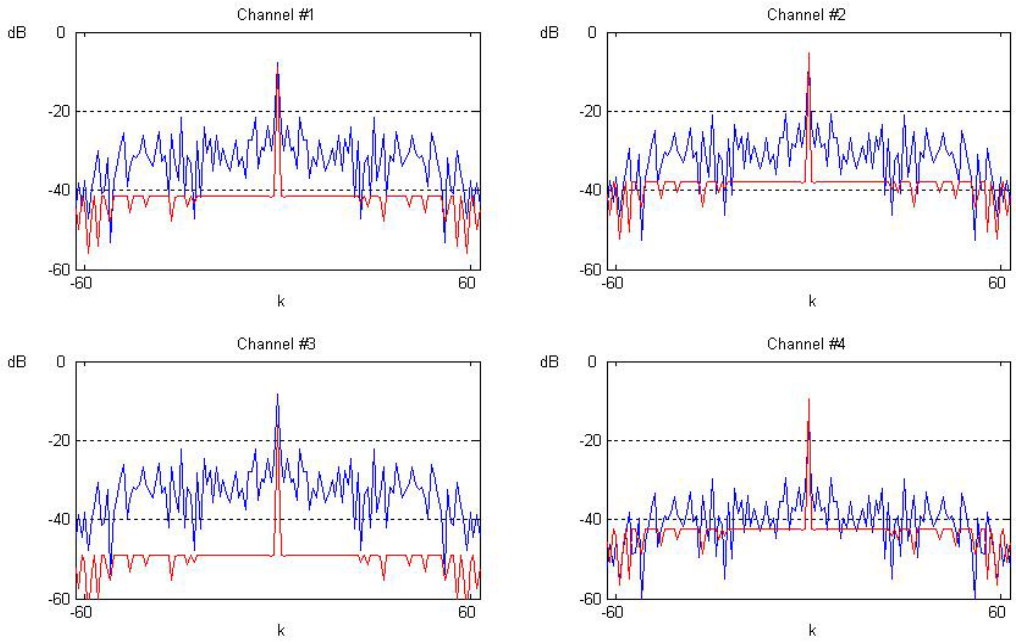


**Figure 4-11** Mismatched filter #4 output

In Figure 4-9 the target filter output is given. In the target filter, the peak level in target channel is relatively higher than the maximum signal levels in the other channels. The peak level obtained in target channel is -2.8 dB. The highest signal level in the other channels is observed in Channel #3 and its value is –28.6 dB as given in Table 9. Therefore, the PSL value that is obtained for 0.375x2π Doppler shift in target filter is approximately 26 dB.

When Figure 4-8, Figure 4-9, Figure 4-10 and Figure 4-11 are examined, it is seen that all correlation lags are minimized except for the samples in the middle of the signals that occur in all channels of all filters. However, according to Optimization B1 method, only Filter #2 is needed to be optimized. The reason of this situation is using the same optimized fasttime code vector for the waveform and all filter code matrices. Therefore, a characteristic depending on the auto-correlation vector of the optimized fasttime code vector is formed in all channels. The auto-correlation vector of

the fasttime code sequence before and after the optimization is given in Figure 4-12.

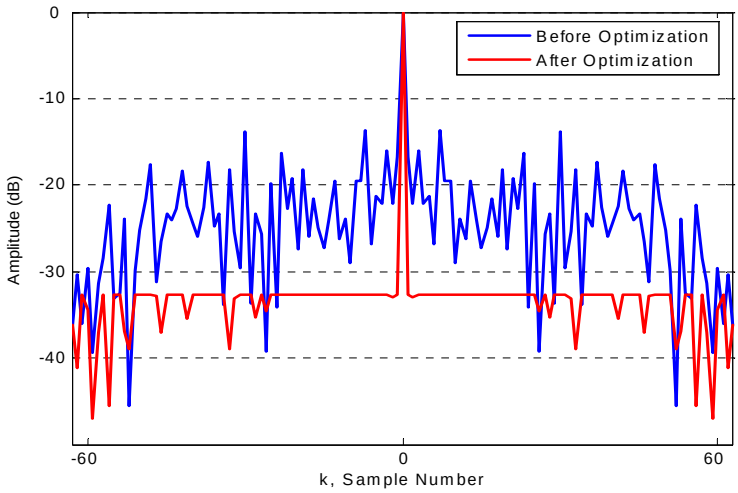


**Figure 4-12** Auto-correlation of fasttime code sequence

The characteristics given in Figure 4-12 can be obviously observed at the filter outputs given in Figure 4-8, Figure 4-9, Figure 4-10 and Figure 4-11. However, in each channel it is multiplied with a different scalar. The weighting in the channels depends on the used slowtime code. In the optimization of the slowtime code sequences, the weighting in the target channel attempted to be kept high and the weighting in other channels low.

### 4.2.2 OPTIMIZATION B2

The optimization done in this section, have the characteristics listed below in addition to the characteristics listed in Section 4.2.

1. While each filter code matrix is optimized for its own Doppler interval, it will also be optimized for other Doppler shifts to produce minimum output.

2. In the optimization, similar to Optimization B1, maximum peak and minimum sidelobe levels in target channel and minimum signal level in the other channels of the target filter are aimed. Besides, minimum signal level in all channels of the filters apart from the target filter is aimed for any Doppler value.

This optimization method resembles the Optimization A2 method in terms of functionality and it also resembles Optimization B1 in terms of the structure of its code matrices. The difference between Optimization A2 and Optimization B2 is the structure of the code matrices. In Optimization B2 the $PSL_{intra}$ and $PSL_{inter}$ values are optimized at different steps. In Optimization B2 method all filters are optimized for all Doppler values, different from Optimization B1. The code matrices, optimized through this method and succeeded, can be used in all radars without needing the Doppler information.

The used optimization algorithm can show different performance for different initial codes of same size. In order to compare the results, which the optimization algorithm produced for different initial codes of same size, Table 10 is prepared. The optimization program is run for 10 different initial codes. The fasttime code, used in all runs, is same. Different optimization results are obtained as a result of the slowtime code optimization. At the end of the optimizations of fasttime and slowtime code sequences, a waveform code matrix of 4x64 and four filter code matrices of 4x64 are obtained. All results given in the table are obtained as a result of filtering the 0.375x2π Doppler phase shifted waveform with the filter optimized for [0.225 0.525]x2π Doppler interval. The expression “maximum sidelobe level in all filters” used in the table corresponds to the maximum of maximum sidelobe level in target channel and maximum signal level in all the other channels of the target filter and maximum signal level in all the other filters.

**Table 10** Results of Optimization B2 for different initial codes

| Run No | Peak Level at the Target Channel | | Max. Sidelobe Level in the all filters | |
|---|---|---|---|---|
| | Before Opt. (dB) | After Opt. (dB) | Before Opt. (dB) | After Opt. (dB) |
| **1** | -21.8693 | -2.8158 | -13.0788 | -10.2505 |
| **2** | -19.2449 | -2.8158 | -12.1488 | -10.2505 |
| **3** | -13.9259 | -2.8158 | -14.0421 | -7.1711 |
| **4** | -12.0433 | -2.8158 | -9.7415 | -7.1648 |
| **5** | -16.5190 | -2.8158 | -7.2591 | -7.1711 |
| **6** | -9.0110 | -2.8158 | -8.6828 | -7.1711 |
| **7** | -15.3518 | -2.8158 | -8.6321 | -7.1711 |
| **8** | -17.6920 | -2.8158 | -17.4010 | -6.8892 |
| **9** | -17.2277 | -2.8158 | -15.9687 | -10.2506 |
| **10** | -13.6828 | -2.8158 | -9.2546 | -7.5689 |

When Table 10 is examined, it is seen that the peak level in target channel increases approximately by 10-15 dB. Since, in the optimization it is ensured that the peak value in the target channel for the optimized code matrices remains above -3 dB. However, the same improvement couldn't be observed in decreasing the maximum sidelobe level. The reason is that the optimization algorithm attempts to find out the minimum point of a surface, depending on many variables.

As seen in Table 10, the minimum sidelobe level is obtained in the $9^{th}$ run. The results of the code matrices, obtained in the $9^{th}$ run, are given in Table 11 under different Doppler phase shifts. While this table is being prepared, different Doppler phase shifts are applied to the waveform. Afterwards the

waveform is processed through all filters and the results obtained at the output of all filters are observed. Filter #1, Filter #2, Filter #3 and Filter #4 are optimized to have maximum peak level and minimum sidelobe level for [0.975 0.275]x2π, [0.225 0.525]x2π, [0.475 0.775]x2π and [0.725 0.025]x2π Doppler intervals respectively. Besides; each filter is optimized in order to produce minimum output signal level to the waveform, shifted with the Doppler values except for its own Doppler interval, in addition to Optimization B1.

**Table 11** Results of Optimization B2 under different Doppler shifts

| **Doppler Phase Shift (2π)** | **Peak Level at the Target Channel** | | **Max. Sidelobe Level in the all filters** | | **Peak Level at the Matched Filter Output (dB)** |
|---|---|---|---|---|---|
| | **Before Opt. (dB)** | **After Opt. (dB)** | **Before Opt. (dB)** | **After Opt. (dB)** | |
| -0.0250 | -13.4512 | -3.0980 | -9.7951 | -10.0836 | -3.3970 |
| 0.1250 | -10.6569 | -2.8158 | -9.7302 | -10.2506 | -4.3857 |
| 0.2750 | -9.0411 | -3.0980 | -9.7326 | -9.6178 | -5.8273 |
| 0.2250 | -15.9643 | -3.0980 | -14.2101 | -10.0836 | -38.9775 |
| 0.3750 | -17.2277 | -2.8158 | -15.9687 | -10.2506 | -19.6967 |
| 0.5250 | -20.7784 | -3.0980 | -13.9743 | -9.6178 | -15.0740 |
| 0.4750 | -14.4858 | -3.0980 | -8.5942 | -10.0836 | -15.0740 |
| 0.6250 | -16.2325 | -2.8158 | -10.3950 | -10.2506 | -19.6967 |
| 0.7750 | -16.7514 | -3.0980 | -10.0225 | -9.6178 | -38.9775 |
| 0.7250 | -7.5443 | -3.0980 | -15.9286 | -10.0836 | -5.8273 |
| 0.8750 | -9.9028 | -2.8158 | -13.3472 | -10.2506 | -4.3857 |
| 1.0250 | -13.8261 | -3.0980 | -11.0759 | -9.6178 | -3.3970 |

As it is seen in Table 11, for all Doppler values there is a difference around 7 dB between the peak level in target channel and the maximum sidelobe level after optimization. This difference is not enough for ambiguity resolution. Therefore, it is not possible for the codes that are obtained in this optimization to be used in radar applications.

To observe the results of code matrices, obtained in the 9th run, at the outputs of all filters under $0.375 \times 2\pi$ Doppler shift Figure 4-13, Figure 4-14, Figure 4-15 and Figure 4-16 are prepared. Filter #2 is the target filter for this Doppler value. Therefore; the peak value, given in shaded rows in Table 10 and Table 11, should be observed at 2nd filter output. However, the maximum sidelobe level can be observed in any channel of any filter. Since there is no time shift given to the waveform, $1^{st}$ channel is the target channel. In the figures, the plots in blue symbolize the results of the code matrices before optimization and the ones in red symbolize the results of the code matrices after optimization.

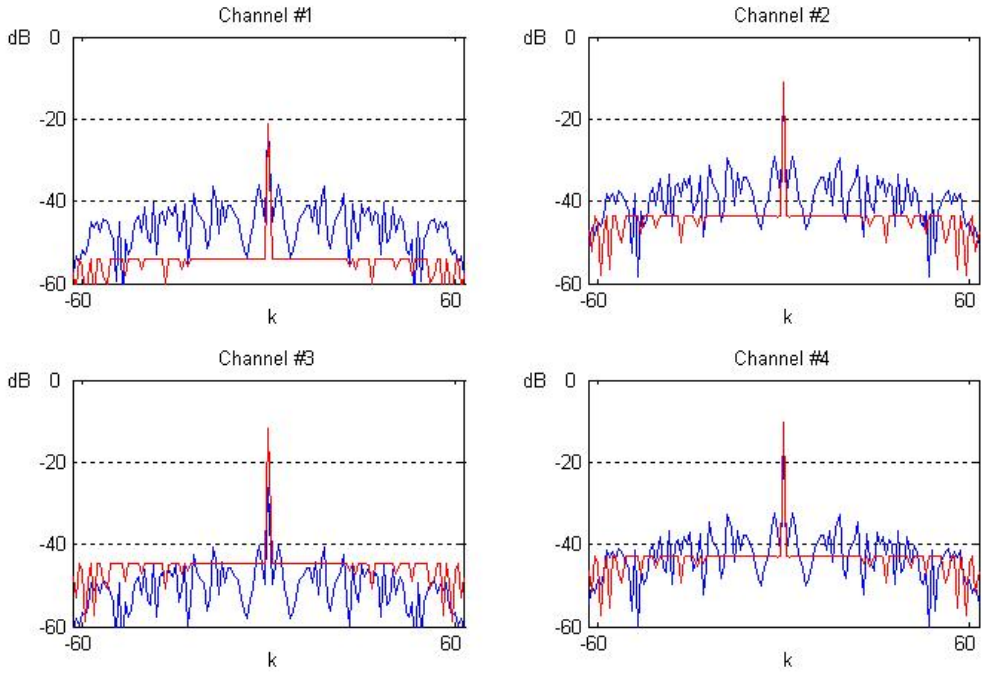


**Figure 4-13** Mismatched filter #1 output

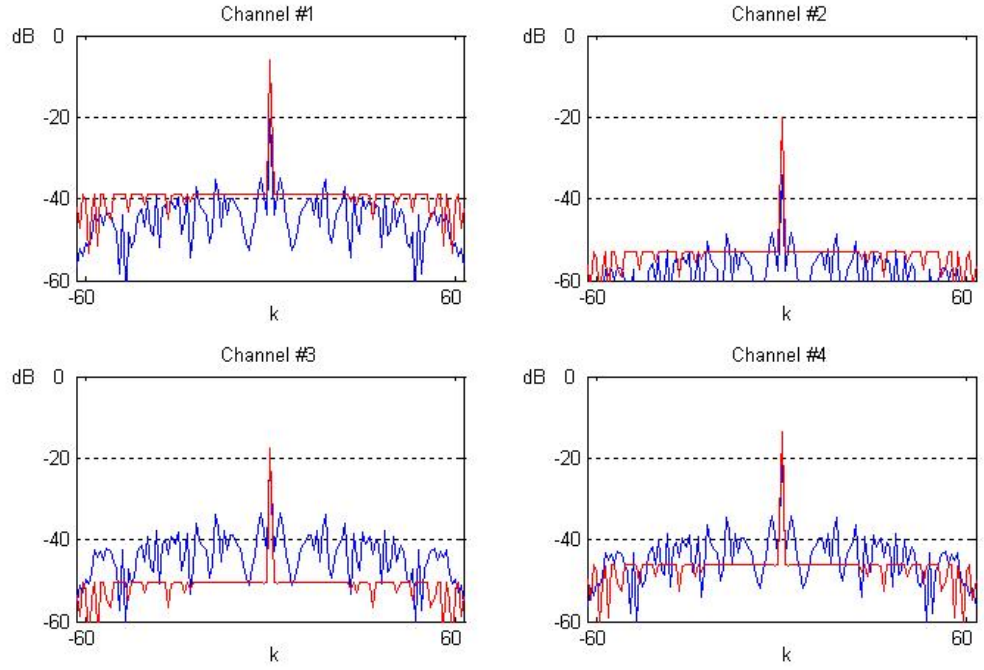


**Figure 4-14** Mismatched filter #2 (target filter) output

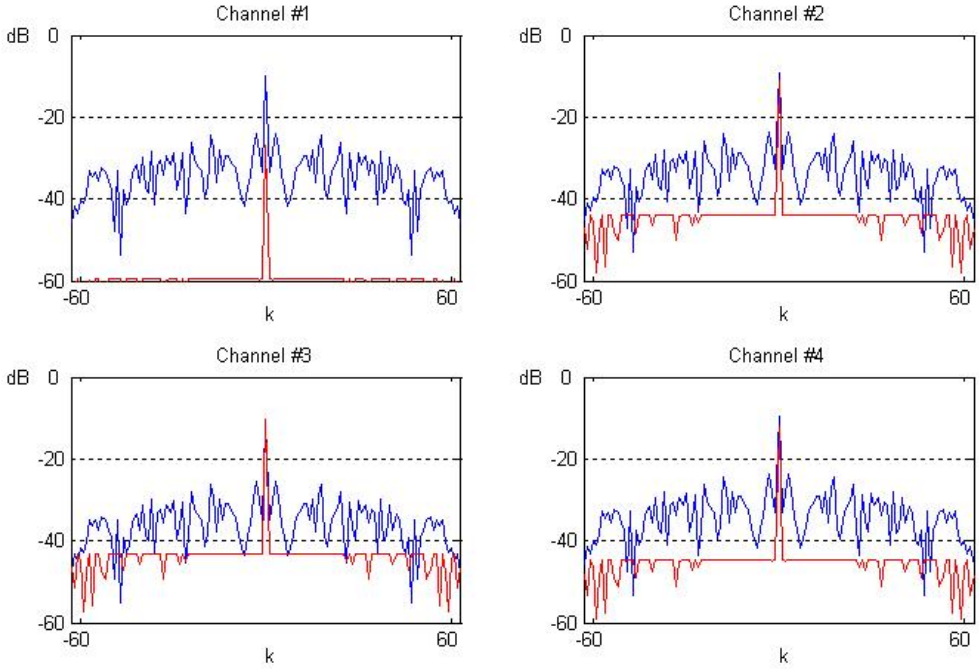


**Figure 4-15** Mismatched filter #3 output

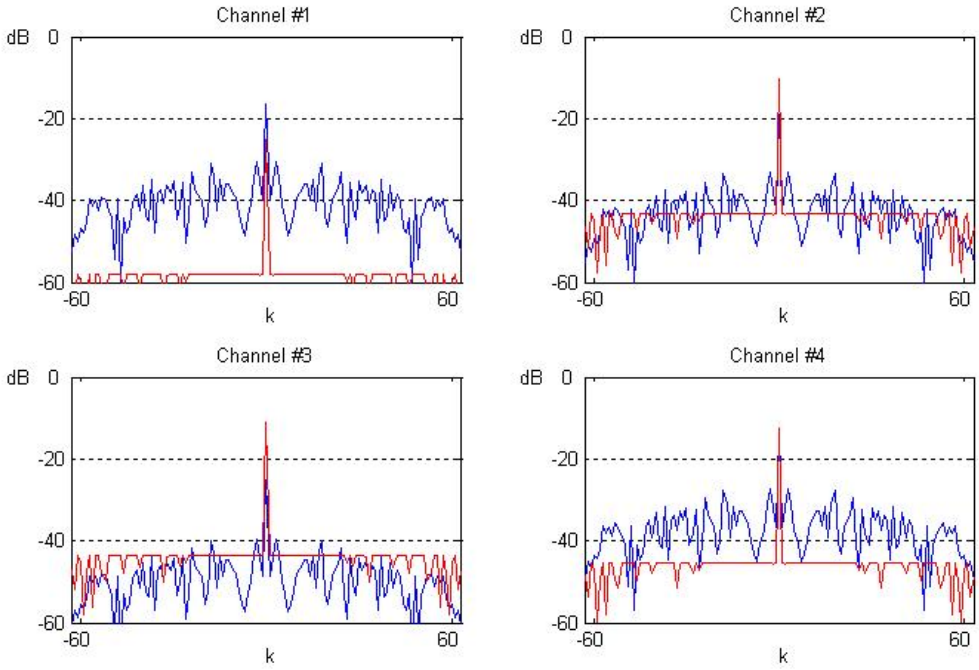


**Figure 4-16** Mismatched filter #4 output

Figure 4-14 is the target filter for the given Doppler value. However, there isn't a significant difference between the signal level in the 1st channel in Figure 4-14 and the signal level in the channels of other filters. The peak level in target channel is -2.8 dB. The maximum sidelobe level is observed in Channel #2 of Filter #1. The value of the maximum sidelobe is –10.2 dB as given in Table 11. At the outputs of Filter#1, Filter#2, Filter#3 and Filter #4 the characteristics given in Figure 4-12 is observed. However, the required weighing of the channel could not be obtained at the end of the slowtime code sequences optimization.

## 4.3 COMPARISON

In this chapter, four different optimization methods are defined. These methods are implemented through fminimax function. Afterwards; the results of defined optimization methods are produced by means of these implementations.

The code matrices are optimized concurrently for high $PSL_{intra}$ and $PSL_{inter}$ values in the Optimization A1 and the Optimization A2 methods. The minimum point of a surface, which depends on many variables, is attempted to be found in these methods. Therefore, it takes quite a long time for these optimizations to give results. To exemplify, it took the 10 runs whose results are given in Optimization A1 150 hours to culminate on a high performance computer.

Since the Optimization B1 and the Optimization B2 are carried out in two phases and they control less parameters, they give result more quickly. As a result of these optimizations, the characteristics of the auto-correlation function of the fasttime code is observed in all channels. Any code sequence,

used for coding single pulses, can be used as the fasttime code sequence in the code matrix in Optimization B1 and Optimization B2.

When the successes of the optimization methods are compared, it is seen that Optimization A1 and Optimization B1 methods produce quite satisfying results. The codes, obtained in these optimizations, can be used in radar systems by taking Doppler information from another system or by the help of an operator.

In the Optimization A2 and the Optimization B2, the expected results couldn't be obtained since the optimization algorithms control a very sensitive and a rapidly varying surface. fminimax function may result in a local minimum instead of a global minimum. In order to prevent this, the optimization methods can be run with different initial codes many times. However, in the studies of the thesis, the results of the optimization methods for all possible initial codes could not be calculated due to computer source limitation. Besides; it is possible to get relatively successful results by using different optimization algorithms. Since the studies in the scope of this thesis mostly consist of the needs of pulse diversity and the improvements that will be gained in accordance with these needs, different optimization algorithms were not implemented.

# CHAPTER 5

# RADAR APPLICATIONS

## 5.1 RADAR MODEL

In order to be able to analyze the performance of the code matrices given in Section 2.2.1.2, when radar signals are reflected from moving targets, a radar model is implemented. The radar model implemented in the scope of this thesis consists of a transmitter, a pulse-burst matched filter, MTI and CFAR systems. The structure of the radar receiver model used in the thesis studies is given in Figure 5-1.

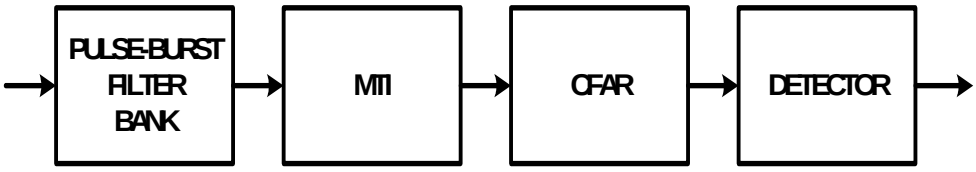


**Figure 5-1** Radar receiver structure

In the radar model the burst waveforms in which each pulse is coded with different code sequences are transmitted from the transmitter. In the receiver, firstly, the pulse-burst matched filter output of the received signal is created. The output of a pulse-burst matched filter is processed to get rid of the clutter signal through filtering it in MTI. Afterwards, it is entered the detection procedure to compare with the threshold which was specified by CFAR. Cell Averaging CFAR (CA-CFAR) model [52] is implemented in the radar model.

Threshold is calculated for each range resolution cell in CA-CFAR model. When threshold is calculated for any range resolution cell, range guard gates and range signal gates are formed in both sides of the interested range cell. Guard gates are constructed between the interested cell and the signal gates. The gated signal is calculated before the calculation of threshold for the interested range cell. When the gated signal level is calculated, only the signals in the target gates are summed but the ones in the guard gates are ignored. The expression of the gated signal for any range cell is given in (5.1).

$$s_G[n] = \sum_{i=n-GL-SL}^{n-GL-1} s[n] + \sum_{i=n+GL+1}^{n+GS+SL} s[n] \qquad \textbf{(5.1)}$$

where $s_G[n]$ : gated signal level for the interested range cell; $s[n]$ : signal level in the $n^{th}$ range cell; $GL$ : number of range cell in one guard gate; $SL$ : number of range cell in one signal gate.

The expression of the threshold calculated for the interested range cell is given in (5.2).

$$e[n] = s_G[n] \times \left( PFA^{-1/4(GL+NL)} - 1 \right) \qquad \textbf{(5.2)}$$

where $e[n]$ : threshold level; $PFA$ : probability of false alarm.

All of the signals, used in the radar model, are modeled in the complex envelope format. The radar signal, which is actually in the form identified in (5.3), is created in the form identified in (5.4) in the simulation model.

$$x(t) = a(t) \sin\left(2\pi ft + \theta(t)\right) \qquad \textbf{(5.3)}$$

where $f$ : carrier frequency in Hz; $a(t)$ : amplitude modulation of the carrier signal; $\theta(t)$ : phase or frequency modulation of the carrier signal.

$$x(t) = a(t) e^{j\theta(t)} \qquad \textbf{(5.4)}$$

All of the frequency and phase modulations in the signal are modeled in the $\theta(t)$.

Since the pulse-by-pulse process is done in the radar model; at the output of the pulse-burst matched filter, the number of channels created is equal to the number of pulses in the burst. The time duration of the each channel has the same length with PRI. In the radar model, the time in which the target echo exists and a certain interval around this time is concerned during a PRI. Therefore the signals, which can only be observed in this time interval, are displayed in the simulation outputs for each channel.

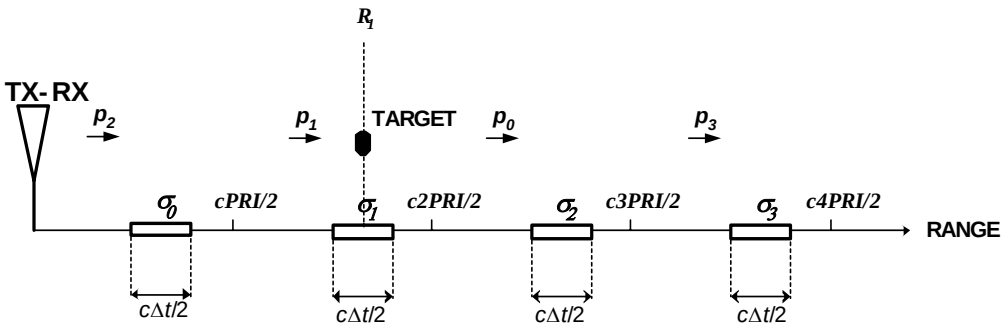


**Figure 5-2** A sample scenario used in radar model

The transmitted pulses are received after being reflected from the point target and the clutter sources. The width of the clutter sources in range is specified by the user. The features of a sample scenario given in the Figure 5-2 are listed below.

- The burst signal consists of [$p_0$, $p_1$, $p_2$, $p_3$] pulses.
- The target is range $R_1$ between the $PRI$ and $2PRI$.
- The time interval having $\Delta t$ width around the target is concerned.

The signals listed below are received in the PRI in which $p_2$ pulse is transmitted for this sample scenario.

- The echo of $p_2$ reflected from the clutter source in the [$R_1$-$cPRI$/2-$c\Delta t$/2, $R_1$-$cPRI$/2+$c\Delta t$/2] range interval.
- The echo of $p_1$ reflected from the target at the $R_1$ range.
- The echo of $p_1$ reflected from the clutter source in the [$R_1$-$c\Delta t$/2, $R_1$+$c\Delta t$/2] range interval.
- The echo of $p_0$ reflected from the clutter source in the [$R_1$+$cPRI$/2-$c\Delta t$/2, $R_1$+$cPRI$/2+$c\Delta t$/2] range interval.
- The echo of $p_3$ reflected from the clutter source in the [$R_1$+$cPRI$-$c\Delta t$/2, $R_1$+$cPRI$+$c\Delta t$/2] range interval.

By this way the target echo and clutter echoes of each pulse used in the burst is received. Besides; both the clutter signal coming from the unambiguous range and the clutter signal coming from the ambiguous range, having the same length with the burst waveform, are modeled.

At the input of the pulse-burst matched filter in the receiver, phasor summation of the received signals is done. The summed signal is processed through the single-pulse matched filters of each pulse in a parallel way. Until all of the pulses in the burst are transmitted, the signals at the output of the single-pulse matched filters are kept inside the buffers. The signals kept in the buffers are time aligned and summed after all of the pulses in the burst are transmitted. By this way, the pulse-burst matched filter doing pulse-by-pulse processing is implemented and the coherent integration for all of the pulses in the burst is done in pulse-burst matched filter.

In Table 12 the signals inside each buffer for a pulse-burst waveform, that is reflected from a target in the [$kPRIc$/2, ($k$+1)$PRIc$/2] range interval, are indicated. The number of the pulses in the burst is $M$. Consequently; $M$

number of single-pulse matched filter and $M$ number of buffers are used to build the pulse-burst matched filter. At the output of the pulse-burst matched filter, $M$ number of channels are constructed.

**Table 12** The contents of the buffers

| **Buffer Number** | **Output of the Single-Pulse Matched Filter between** | | | | |
|---|---|---|---|---|---|
| | **[0,PRI]** | ... | **[nPRI, (n+1)PRI]** | **...** | **[(M-1)PRI, MPRI]** |
| **Buffer #0** | $p_{((M-k))M} * h_0$ | **...** | $p_{((M-k+n))M} * h_0$ | **...** | $p_{((M-k-1))M} * h_0$ |
| **Buffer #1** | $p_{((M-k))M} * h_1$ | **...** | $p_{((M-k+n))M} * h_1$ | **...** | $p_{((M-k-1))M} * h_1$ |
| **...** | **...** | **...** | **...** | **...** | **...** |
| **Buffer #(M-2)** | $p_{((M-k))M} * h_{M-2}$ | **...** | $p_{((M-k+n))M} * h_{M-2}$ | **...** | $p_{((M-k-1))M} * h_{M-2}$ |
| **Buffer #(M-1)** | $p_{((M-k))M} * h_{M-1}$ | **...** | $p_{((M-k+n))M} * h_{M-1}$ | **...** | $p_{((M-k-1))M} * h_{M-1}$ |

The signals given in Table 13 are constructed after the contents of each buffer are circularly shifted according to the amounts specified in Figure 2-4. Considering the $((M))M$ value is equal to 0, the second $M$ in the modulo process is left out while giving the signal numbers.

**Table 13** The contents of the buffers after time aligning

| **Output of the Pulse-Burst Matched Filter at** | | | | |
|---|---|---|---|---|
| **1$^{st}$ channel** | **...** | **($n$+1)$^{th}$ channel** | **...** | **$M^{th}$ channel** |
| $p_{((M-k))M} * h_0$ | ... | $p_{((M-k+n))M} * h_0$ | ... | $p_{((M-k-1))M} * h_0$ |
| $p_{((M-k+1))M} * h_1$ | ... | $p_{((M-k+n+1))M} * h_1$ | ... | $p_{((M-k))M} * h_1$ |
| ... | ... | ... | ... | ... |
| $p_{((M-k-2))M} * h_{M-2}$ | ... | $p_{((M-k+n-2))M} * h_{M-2}$ | ... | $p_{((M-k-3))M} * h_{M-2}$ |
| $p_{((M-k-1))M} * h_{M-1}$ | ... | $p_{((M-k+n-1))M} * h_{M-1}$ | ... | $p_{((M-k-2))M} * h_{M-1}$ |

As seen in the Table 13, the constructed filter order in each channel is as $[h_0, h_1, h_2, \ldots h_{M-1}]$. Therefore, for a channel to be matched to the received pulse-burst waveform, the aligned signal order in the corresponding channel should be as $[p_0, p_1, p_2, \ldots p_{M-1}]$. The order of the pulse-burst waveform reflected from the $[kPRIc/2, (k+1)PRIc/2]$ range interval in the n$^{th}$ channel is as $[p_{((M-k+n))M}, p_{((M-k+n+1))M}, \ldots p_{((M-k+n-1))M}]$. Consequently; the ($n$+1)$^{th}$ channel is matched to the $[nPRIc/2, (n+1)PRIc/2]$ range interval.

To summarize; peak is observed for a target at the $R_1$ range in the specified channel and time in (5.5).

$$\text{if } \frac{cnPRI}{2} < R_1 < \frac{c(n+1)PRI}{2}, \text{ then}$$
$$\bullet \ \#\ of\ MC = n$$
$$\bullet \ time\ of\ MP\ in\ the\ MC = \frac{2R_1}{c} - nPRI \quad \text{where } 0 \le n \le M-1 \qquad \textbf{(5.5)}$$

where $MC$ : matched channel; $MP$ : matched point; $M$ : number of pulses in the burst.

It is easy to discriminate the echo of a target in the $R_1$ range from the echo of another target in the $R_1+cPRI/2$ range. The use of $M$ pulses in pulse-burst waveform and coding each pulse with different codes pushes the unambiguous range from $cPRI/2$ to $cMPRI/2$.

## 5.2 CLUTTER CHARACTERISTICS

Clutter can be classified into two main categories: surface clutter and volume clutter. Surface clutter includes the echoes from trees, vegetation, ground terrain, man-made structures and sea surface [3]. In the radar model, implemented in this thesis, only surface clutter is modeled.

In many cases, the clutter signal level is much higher than the receiver noise level. Thus, the radar's ability to detect targets embedded in high clutter background depends on the signal-to-clutter ratio (SCR) rather than the signal-to-noise ratio (SNR) [3]. As a result, in the radar model, noise is not modeled since signals are processed under high clutter levels.

The following steps are carried out in turn while the clutter signal is being produced.

- The range intervals in which the clutter sources exist are divided into resolution cells.
- Each resolution cell is considered as a point clutter scatterer and the radar cross section (RCS) is calculated for each point clutter scatterer.
- For each point clutter scatterer, the reflections of the relevant pulse from them in each PRI are calculated.

The average clutter RCS for an area having a specific size is defined as in (5.6).

$$\sigma_C = \sigma_0 A_C \tag{5.6}$$

where $\sigma_0$ : clutter RCS per unit area; $\sigma_c$ : RCS of the clutter occupying an area $A_c$.

The geometry of ground based radar and surface clutter is shown in Figure 5-3.

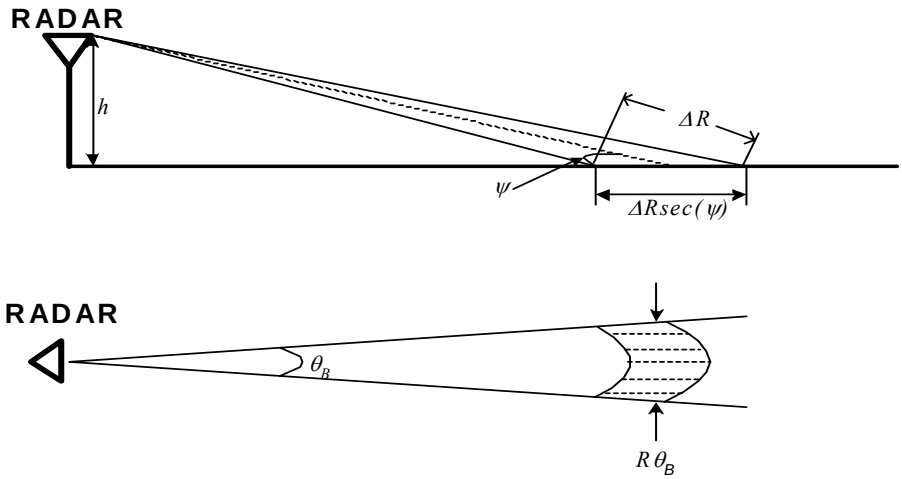


**Figure 5-3** The geometry of ground based radar and area of clutter source

Considering the geometry, given in the Figure 5-3, the area of the radar resolution cell is calculated as in (5.7).

$$A_C = R\theta_B \frac{\Delta R}{\cos\psi} \tag{5.7}$$

where $\theta_B$ : two-way azimuth beamwidth; $\Delta R$ : resolution cell width in range domain; $\Psi$ : grazing angle.

$\psi$ is proportional to the height of the radar. Since the modeled radar is ground based, its height is low enough to assume $\psi = 0$. Also the resolution element of the radar in time domain is chipwidth. So, in the simulation the average clutter RCS for each resolution cell is calculated as in (5.8).

$$\sigma_C = \sigma_0 R \theta_B \frac{c\tau}{2N} \tag{5.8}$$

where $c$ : velocity of propagation; $\tau$ : pulsewidth; $N$ : the length of code sequence used in a pulse.

The RCS value of each point clutter scatterer is directly proportional to its range. However, received signal power is inversely proportional with the 4th order of the range. Therefore, signal power, being reflected from a point clutter scatterer, in the receiver changes in an inversely proportional way with the 3rd order of its range. The value of a signal power, being reflected from a point clutter scatterer, is given in (5.9).

$$S = \frac{P_t G A_e \sigma_C}{(4\pi)^2 R^4} = \frac{P_t G A_e}{(4\pi)^2 R^3} \frac{\sigma_0 \theta_B c\tau}{2N} \tag{5.9}$$

where $P_t$ : transmitted signal power; $G$ : antenna gain; $A_e$ : antenna effective aperture.

Due to the fact that the terrestrial formations changes suddenly, the RCS values of the clutter sources change abruptly. Clutter echoes are random and have thermal-noise like characteristics in fasttime because of the individual clutter components or scatterers have random phases and amplitudes. However, in (5.8) the average RCS is modeled and the average RCS values of consecutive point clutter scatterers slightly change.

In order to observe the rapid changes in the fasttime clutter signal in the radar model, the average RCS vector is multiplied with normally distributed random

variables. The mean value of normally distributed random variables is equal to 0, its variance is equal to 1 and its standard deviation is equal to 1. In this way, the instantaneous clutter RCS vector is obtained. Its mean value is equal to 0, its variance is equal to $\sigma_c^2$ and its standard deviation is equal to $\sigma_c$. In Figure 5-4 the normalized instantaneous RCS vector for [25km 55km] range interval and corresponding average RCS vector is given.

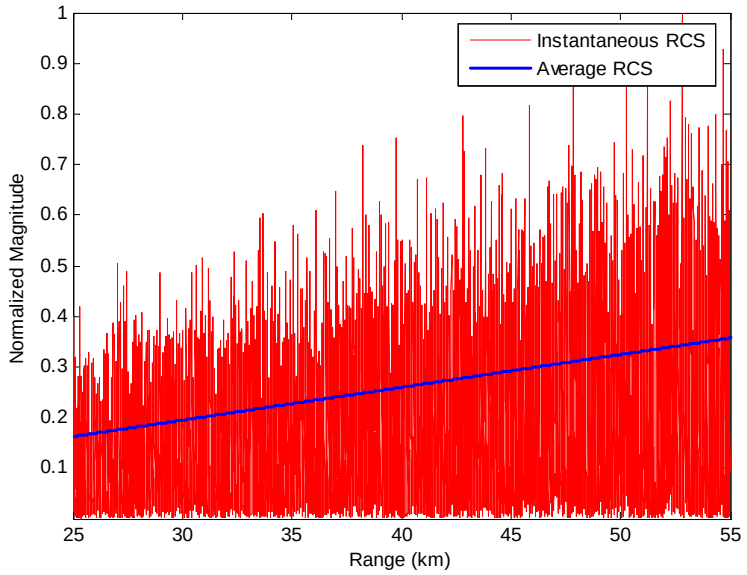


**Figure 5-4** Normalized instantaneous RCS and corresponding average RCS of each point clutter scatterer for a range interval [25km-55km]

Multiplying the average RCS vector with different normally distributed random variable for each pulse, means that the instantaneous RCS value of the same point clutter scatterer has different and uncorrelated values in consecutive pulses. However, the change of the point clutter scatterer RCS value in different pulses results from only internal fluctuations and antenna rotation. Therefore, there is a predicted limit in the change of the same point clutter scatterer RCS value according to time. The change of the same point clutter scatterer RCS value according to time identifies the slowtime characteristics of the clutter signal. If the clutter slowtime frequency response

is of large width, the point clutter scatterer RCS value changes rapidly according to time; and if it is of narrow width, the point clutter scatterer RCS value changes slowly according to time. As the width of the clutter slowtime frequency response widens, the clutter energy going through the MTI or Doppler filters increases. Consequently; the improvement factor decreases.

The slowtime clutter power spectral density can be expressed as a Gaussian function with a standard deviation in frequency domain. The standard deviation of the Gaussian function is inversely proportional to the time duration of the signal received from a clutter scatterer [3].

The time duration of the signal received from a clutter scatter is as in (5.10).

$$t_0 = \frac{\theta_B}{\dot{\theta}_S} \tag{5.10}$$

where $t_0$ : time duration of the signal received; $\dot{\theta}_S$ : antenna scanning rate; $\theta_B$ : antenna beamwidth.

The standard deviation of the clutter spectrum caused by antenna scanning modulation is as in (5.11) [3].

$$\sigma = \frac{1}{3,77t_0} = \frac{0,265\dot{\theta}_S}{\theta_B} \tag{5.11}$$

where $\sigma$ : standard deviation of the clutter spectrum.

Then the clutter power spectral density in slowtime is as in (5.12).

$$W(f) = W_0 \exp\left(-\frac{f^2}{2\sigma^2}\right) = W_0 \exp\left(-\frac{(f\theta_B)^2}{2\left(0,265\dot{\theta}_S\right)^2}\right) \tag{5.12}$$

where $f$ : frequency.

In order to limit the change of the clutter signal, it needs to be filtered in slowtime. The filter frequency response should be as in (5.12). To be able to carry out the filtering process, the filter input must have a certain length. Consequently; instantaneous RCS vectors with the same amount of the pulses that are to be used in the simulation are created. Afterwards, RCS matrix is created as concatenating these vectors and filtering through columns of it. As a result of filtering the RCS matrices, the clutter RCS values that can be used in the radar model are obtained. Since in the radar model the clutter signals coming from the ambiguous range are modeled too, a RCS matrix is created for each interval of *cPRI/2* wide of the modeled ambiguous range. Each line of the created RCS matrices defines a RCS vector that will be used in a PRI. Each element of this vector defines RCS value of a point clutter scatterer.

The radar signal, reflected from the clutter sources, is created by convolving the transmitted pulses with the related line of the RCS matrix. The summation of the signals, reflected from the clutter sources in each cPRI/2 range interval, is equal to the received summed clutter signals for the related PRI.

## 5.3 RADAR APPLICATIONS WITH OPTIMIZED CODES

In this chapter the results of the waveform and filter code matrices, optimized in Chapter 4, in the radar receiver under clutter and Doppler effect are evaluated. To make evaluations the radar model, described in Section 5.1, is used. In the simulations the performance of the codes, obtained in Optimization A2 and Optimization B2, are not tested. Because, it is decided in Chapter 4 that the codes which are obtained through Optimization A2 and Optimization B2 methods will not be used in radars.

Optimization results should be evaluated under the same scenario conditions. Therefore, a general scenario is composed and the same scenario is used in all simulations. The properties of this scenario are given in Table 14.

**Table 14** Sample scenario properties

| Parameter | Value |
|---|---|
| Pulsewidth | 0.6 μsec |
| PRI | 0.3 msec |
| Antenna Beamwidth | 2 degree |
| Antenna Rotation Velocity | 60 rpm |
| SCR | -20 dB |
| Clutter Source Intervals for 3 pulses waveform | [ 18.92 21.08] km<br>[ 63.92 66.08] km<br>[108.92 111.08] km |
| Clutter Source Intervals for 4 pulses waveform | [ 18.92 21.08] km<br>[ 63.92 66.08] km<br>[108.92 111.08] km<br>[153.92 156.08] km |
| MTI Type | 3-Pulse Canceller |
| Target Range | 20 km |
| CFAR Type | Cell Averaging |
| CFAR PFA | 1e-6 |
| CFAR Guard Gatewidth | 4xChipwidth |
| CFAR Signal Gatewidth | 10xChipwidth |

There are more than one filter in the radar receiver. In Optimization A1 and Optimization B1 only the target filter output is optimized. Therefore, the outputs of the other filters are not given in the following sections.

### 5.3.1 USING CODES OBTAINED BY OPTIMIZATION A1

In this section the use of the code matrices, optimized with Optimization A1 method, in radar receiver are evaluated. The code matrices whose results are given in Section 4.1.1 are used for coding the waveform and the filters. The size of the waveform and the filter code matrices is 3x32. Other scenario parameters of radar application are given in Table 14. 0.5x2π Doppler phase shift is applied to the target echo. Filter #2 is the target filter for this Doppler value. The results are given in Figure 5-5, Figure 5-7 and Figure 5-8. All of the given figures are normalized according to the maximum envelope value of the signal formed at the Filter #2 output. Therefore, none of the given results are higher than 0 dB or 1. Target range is 20km and the width of the range of interest is equal to 2.16 km.

In Figure 5-5 the envelope of the signal, formed at the Filter #2 output, is given. Since the target is at 20 km range, the target echo is supposed to occur in Channel #1. At the input of the filter, the clutter signal power is relatively higher than the target echo power. Therefore, the target echo can't be distinguished at this step.

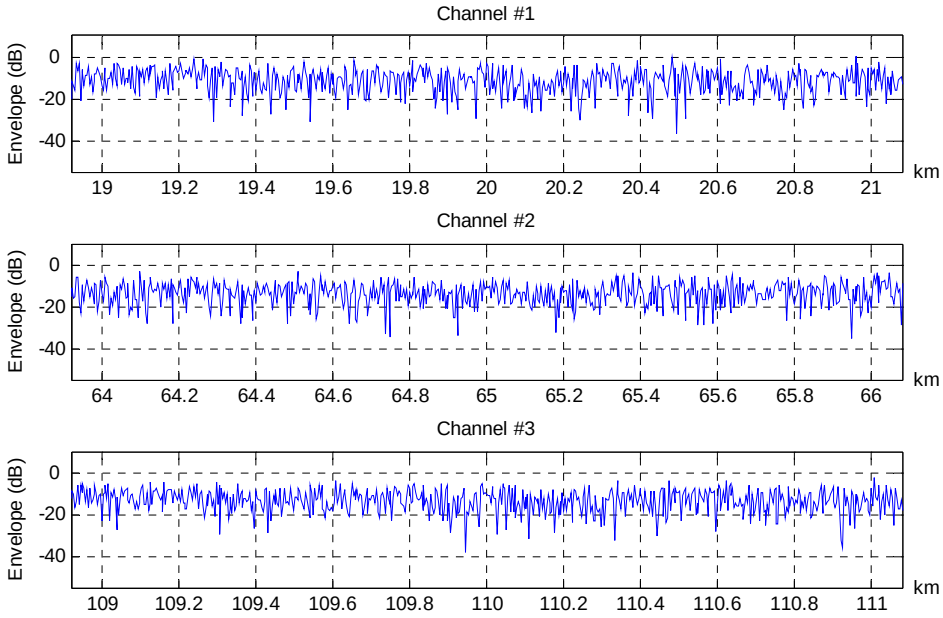


**Figure 5-5** Filter #2 output in logarithmic scale

Filter output is processed through MTI filter to make the target echo more obvious. MTI processor applies a gain between 0 and 1 to the signals in accordance with their slowtime frequency characteristics. The slowtime characteristics of the clutter signal will designate the amount of the clutter signal that will remain after MTI processing. In Figure 5-6 the slowtime frequency response of the clutter signal is given.

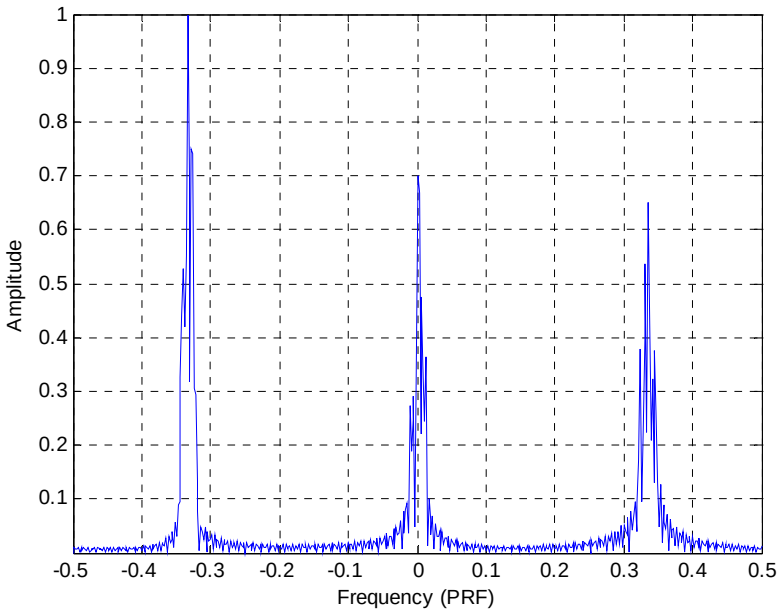


**Figure 5-6** Clutter slowtime frequency response

In Figure 5-6 it is seen that clutter signal has components at 3 different frequencies. Using 3 different pulses is the reason for this situation. However, MTI has the stopband characteristics for a single frequency interval. In order to do the MTI processing properly, the pulses that undergo cancellation process must have the same characteristics. Therefore, cancellation process must be done between the pulses in the same order in consecutive bursts, instead of consecutive pulses. In this situation the slowtime sampling frequency of the signals, which will be used in the MTI, decreases to PRF/3. When slowtime sampling frequency decreases to PRF/3, there will be only one of the components, that is observed in Figure 5-6 , in clutter slowtime frequency response. Consequently; cancellation of the clutter signal will be done properly. However, sampling interval's increasing will also increase the time interval between the clutter signals in cancellation process. This situation will increase the amount of clutter signal passing through MTI. The envelope of the signal at MTI output is given in Figure 5-7.

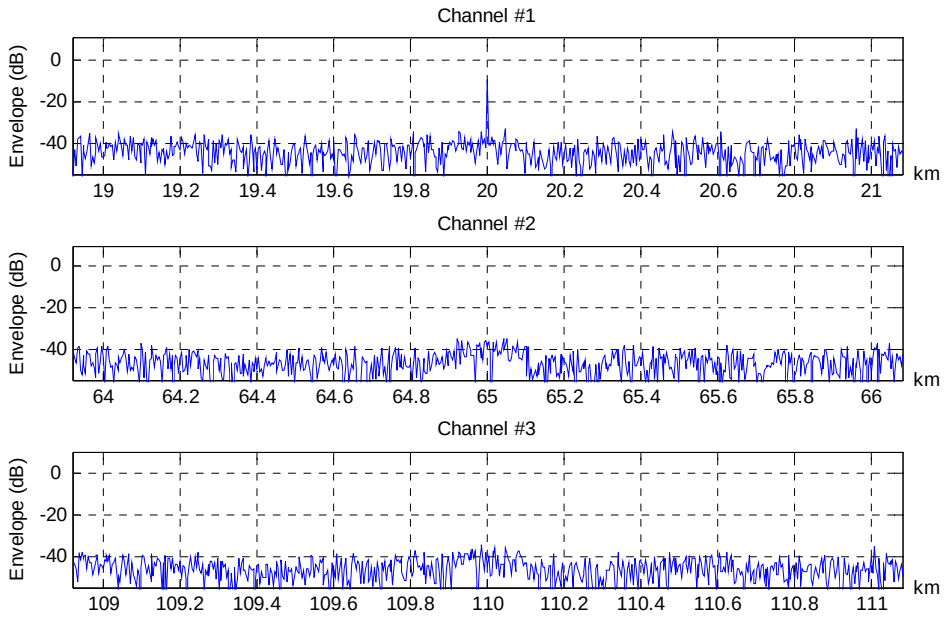


**Figure 5-7** MTI output in logarithmic scale

In Figure 5-7 the envelope of target echo is 25 dB higher than the envelope of the clutter signal at MTI output. At the beginning of the scenario, the target signal in the receiver is defined approximately 20 dB lower than the total clutter signal for the target range. The signal level at Filter #2 output is approximately 0 dB. Therefore, the target echo at the input of Filter #2 must be at maximum -20 dB. However, the target echo is measured around –10 dB in the results given in Figure 5-7. The reason for this is that Filter #2 is matched to [0.3 0.7]x2π Doppler interval, and Channel #1 is matched to 0-45 km range interval. The signals, coming from intervals apart from 0-45 km range interval, are attenuated in the 1$^{st}$ channel by the filter. Therefore, SCR increases at the filter output according to the code matrix that is used in the waveform and the filters.

The target echo at MTI output being 25 dB higher than the clutter signal level seems enough for detection. In Figure 5-8 CA-CFAR threshold, calculated

with respect to the signal at MTI output, is given in linear scale. The graphic in blue indicates the signal envelope at the MTI output, and the one in red indicates the CA-CFAR threshold.

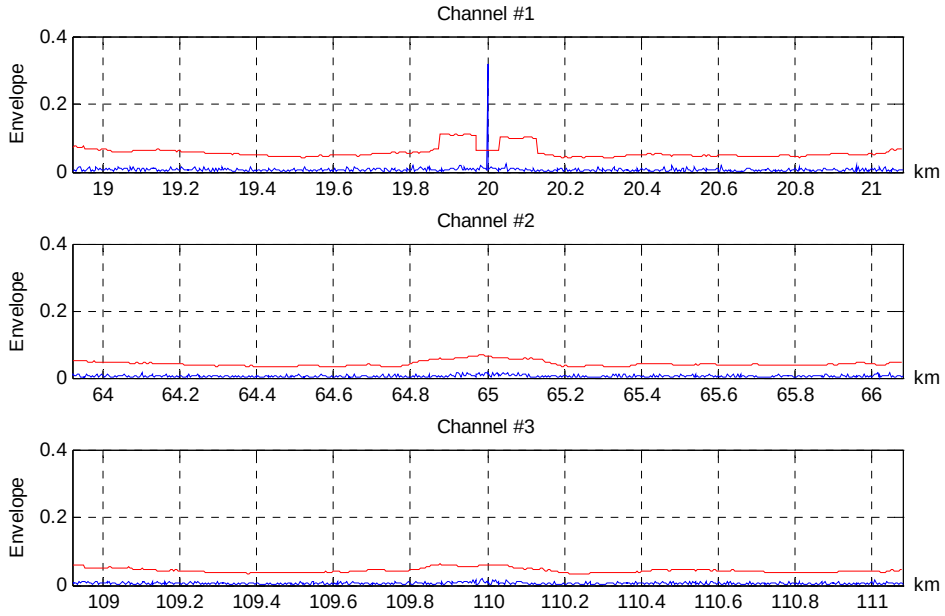


**Figure 5-8** MTI output in linear scale

As it is seen in Figure 5-8, target echo exceeds the threshold and detection is made successfully. The graphics given in Figure 5-5, Figure 5-7 and Figure 5-8 indicate that the codes, optimized with Optimization A1 method, produced successful results in the radar receiver. Target echo is 20 dB lower than the clutter signal at filter input. After mismatched filtering and MTI processing, the target echo becomes around 25 dB higher than the clutter signal. This implies that filter and MTI have totally 45 dB improvement factor.

### 5.3.2 USING CODES OBTAINED AFTER OPTIMIZATION B1

In this section the results of the code matrices, optimized with Optimization B1 method, in radar receiver are evaluated. The code matrices whose results are given in Section 4.2.1 are used for coding waveform and filters. The size of the waveform and the filter code matrices is 4x64. Other scenario parameters of radar application are given in Table 14. 0.625x2π Doppler phase shift is applied to the target echo. Filter #3 is the target filter for this Doppler value. The results of the waveform and the filter code matrices in the receiver are given in Figure 5-9, Figure 5-10 and Figure 5-11. All of the given figures are normalized according to the maximum envelope value of the signal formed at the Filter #3 output. Therefore, none of the given results are higher than 0 dB or 1. Target range is 20 km and the width of the range of interest is equal to 2.16 km.

In Figure 5-9 the envelope of the signal, formed at the Filter #3 output, is given. Since the target is at 20 km range, the target echo is supposed to occur in Channel #1. At the input of the filter, the clutter signal power is relatively higher than the target echo power. Therefore, the target echo can't be distinguished at this step.

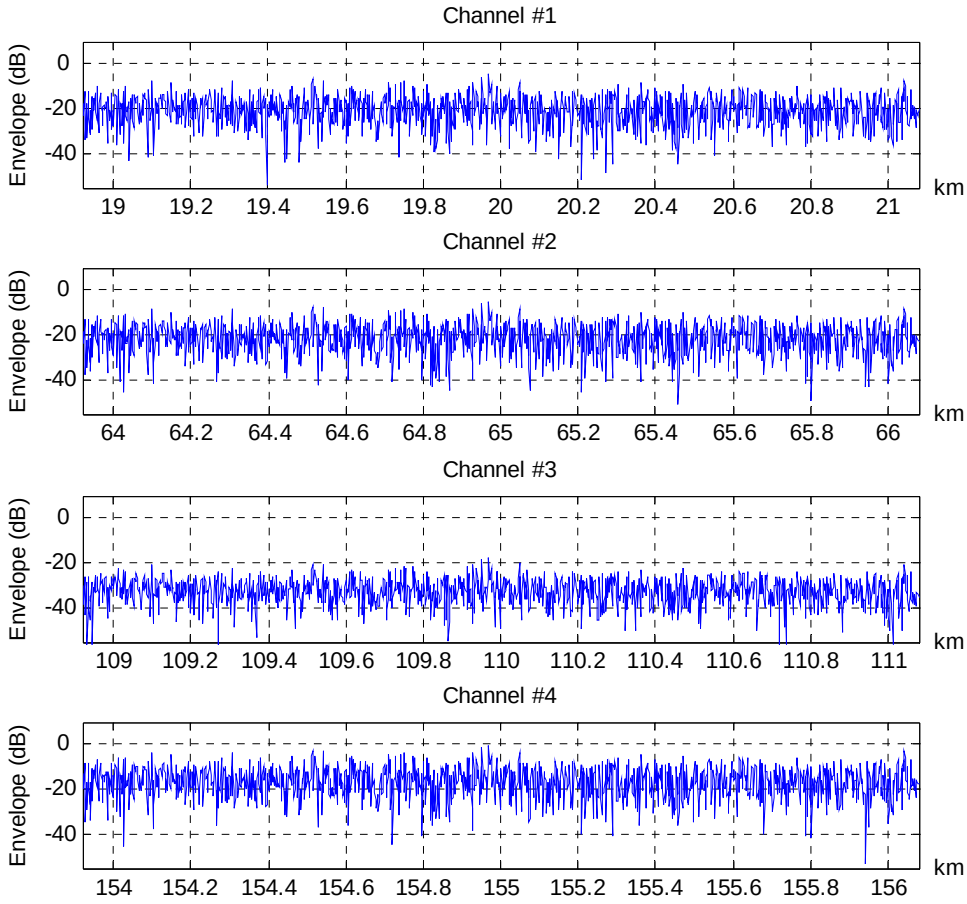


**Figure 5-9** Filter #3 output in logarithmic scale

The filter output, given in Figure 5-9, is processed through MTI to supress clutter signal. In Figure 5-10 the signals occurring at MTI output is displayed in logarithmic scale.

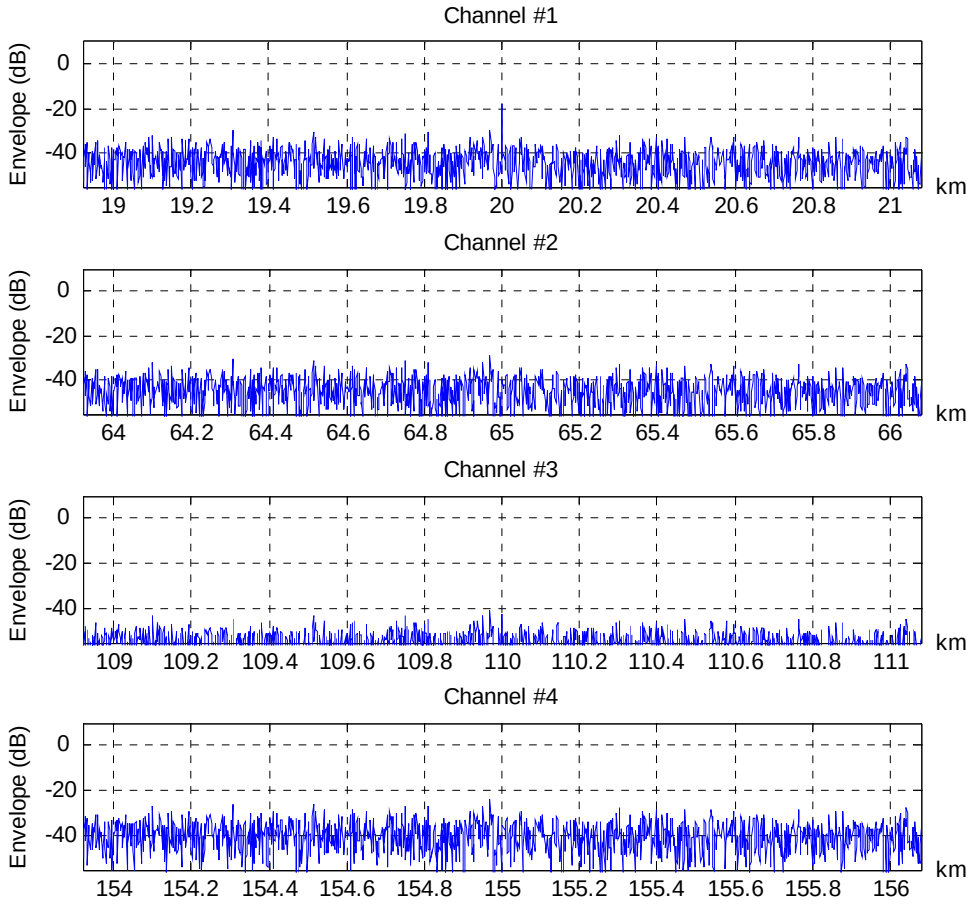


**Figure 5-10** MTI output in logarithmic scale

As it is seen in Figure 5-10, target echo is above the clutter signal by about 15 dB. In Figure 5-11 CA-CFAR threshold, calculated with respect to the signal at MTI output, is given in linear scale. The graphic in blue indicates the signal envelope at the MTI output, and the one in red indicates the CA-CFAR threshold.

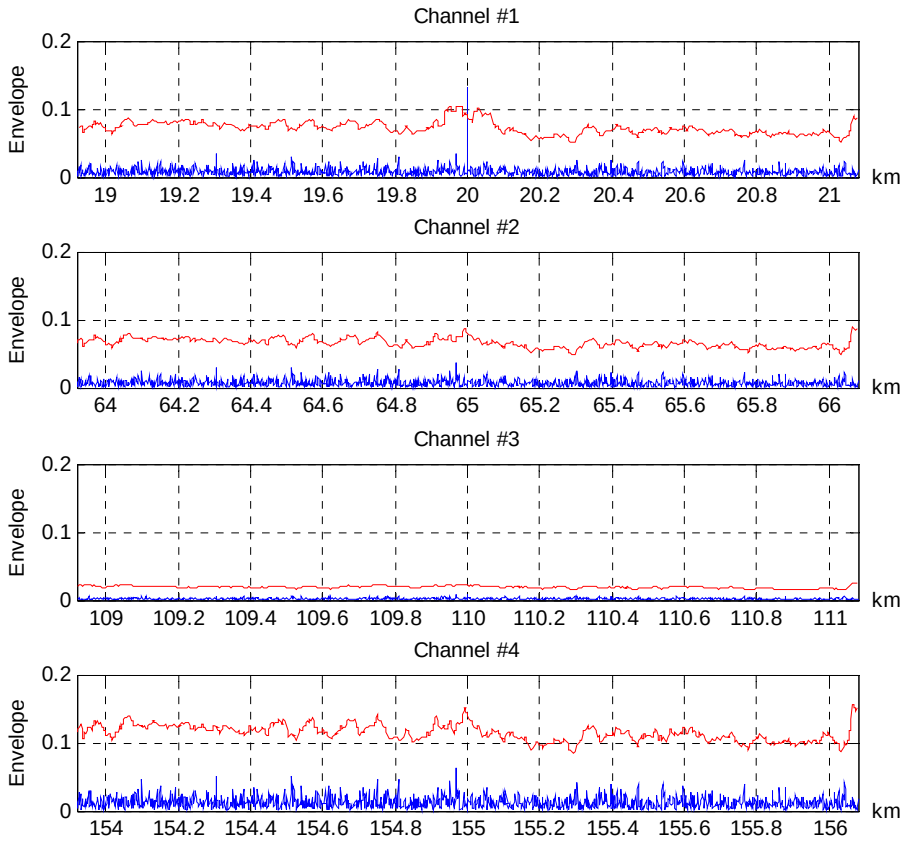


**Figure 5-11** MTI output in linear scale

As it is seen in Figure 5-11 the target signal exceeds threshold. Besides; there isn't another threshold crossing that might cause a false alarm. The graphics given in Figure 5-9, Figure 5-10 and Figure 5-11 indicate that the codes, optimized with Optimization B1 method, produced successful results in the radar receiver. Target power is 20 dB lower than the clutter signal power at filter input. After mismatched filtering and MTI processing, the envelope of target echo becomes around 15 dB higher than the envelope of the clutter signal. This implies that filter and MTI have 35 dB improvement factor. This improvement is lower than the one that is obtained in Section 5.3.1 since, in Section 5.3.1 there are 3 pulses between the pulses used in the MTI.

# CHAPTER 6

# RESULTS AND DISCUSSION

It is a general need to increase unambiguous range without increasing PRI value in radar systems. In this thesis, some studies were carried out to increase the unambiguous range with pulse diversity method without changing PRI value. In pulse diversity method pulse-burst waveform should be transmitted from the transmitter. Furthermore, the received signal should be processed through the pulse-burst filter and range information should be extracted at the end of processing of each burst. In pulse diversity method, it has been understood that the filter in the receiver is as important as transmitted waveform.

The studies show that pulse-burst filtering can be done with a filter group that is composed of single-pulse filters. The number of single-pulse filters used in the filter group is equal to the number of pulses used in the burst. This method is called as pulse-by-pulse processing. In the pulse-by-pulse processing, total filter length is decreased considerably. At the output of pulse-burst filter, processes pulse-by-pulse, there are as many channels as the number of different pulses used in the burst. It has been shown that each of these channels is matched to a certain time (hence range interval) shift in the transmitted signal. Target echo occurred in the channel, matched to its delay time. Therefore, target range could be measured unambiguously even if delay time of the target echo was bigger than PRI.

In order to measure the target range unambiguously, matched channel must be identified. The studies reveal that the signal level in matched channel must be

higher than the signal level in any of the other channels to identify the matched channel. Besides; high value of PSL in matched channel ensures that target is detected more easily. There are code matrices in literature showing these characteristics at the matched filter output. These code matrices are the ones that are composed of complementary, ZCC and ZCC-Complementary code series. Evaluating the performance of these code matrices in radar applications and modify these code matrices according to the needs has been the main aims of the thesis studies.

The sum of the auto-correlation functions of the complementary codes has zero sidelobe level. It has been shown that the signal occurring in matched channel at pulse-burst filter output is equal to the sum of the auto-correlations of the codes used in the burst. Therefore, it has been considered that high PSL value can be obtained in the matched channel at the pulse-burst matched filter output by using the complementary codes in the pulse-burst waveform. When the signal in matched channel has zero sidelobe level, the clutter sources around the target will be prevented from suppressing the target echo.

The shifted sums of the cross-correlations of the ZCC codes are equal to zero. It has been shown that the signals occurring in mismatched channels at pulse-burst filter output are equal to the shifted sums of the cross-correlations of the code sequences used in the burst. Therefore it has been considered that zero signal level can be obtained in the mismatched channels at the pulse-burst matched filter output by using the ZCC codes in the pulse-burst waveform. Obtaining zero signal level in mismatched channels eased identifying the matched channel and consequently detecting the target unambiguously. Besides; obtaining zero signal level in mismatched channels has indicated that a signal occurring in a channel does not have any component in other channels. In this condition, in each channel there will occur the clutter signal coming only from the interval that is matched to the channel. Therefore the

clutter signal, came from the mismatched intervals, would be suppressed inherently in the filtering process while the target echo was being made more evident. This property is the condition particularly expected in high PRF radars.

ZCC-Complementary codes have the properties of both ZCC and complementary codes. Therefore, it has been considered that zero-sidelobe level in the matched channel and zero signal level in the mismatched channels are obtained at the pulse-burst matched filter output by using the ZCC-Complementary codes in the pulse-burst waveform. Getting this property in the receiver will bring in an excellent detection ability to the radar system.

The codes used in the radar applications must be Doppler tolerant. Therefore, the codes defined in the literature have been examined under Doppler effect. When the performance of ZCC and ZCC-Complementary codes in radar applications was examined, it has been observed that these codes do not produce the required results at the matched filter output under Doppler effect. Moreover, new codes have been optimized for having low sidelobe level in auto-correlations and low signal level in cross-correlations by taking into consideration that they could be used in coding the pulse-burst waveform in radar applications. These codes have been observed to be successful at the pulse-burst matched filter output for zero Doppler shift but unsuccessful for non-zero Doppler shifts like ZCC and ZCC-complementary codes. The reason for the codes, which can be used for coding pulse-burst waveform, being so much effected by Doppler shift has been defined. In the applied examinations it has been understood that a single pulse-burst filter will not be able to tolerate all possible Doppler values. Therefore using filters, each of which would produce the required results for a certain Doppler interval, was decided. Moreover, in order to obtain high PSL values single-pulse mismatched filters instead of single-pulse matched filters were used in the pulse-burst filters.

Four different optimization methods, that would optimize one waveform code matrix and more than one filter code matrix simultaneously, were defined to obtain the required results at the end of the filtering process. The usage and properties of the code matrices obtained through these optimization methods were discussed. Afterwards, these methods were implemented with fminimax function of MATLAB. When the codes, obtained through the optimizations, were tested under Doppler effect, it has seen that two of the optimization methods produce the required results.

In order to observe the usage of the codes, obtained through optimization, in the pulse diversity method with high clutter signal, a radar model was implemented. The problems encountered in the suppression of clutter due to pulse diversity were identified and the techniques for solving these problems were mentioned. The results that the codes produced in MTI and CFAR applications were examined. At the end of the simulations, it has been observed that the codes, obtained through the implemented optimization methods, show successful results in the radar model.

In the optimizations done in scope of the thesis MATLAB standard function ‘fminimax’ was used. Since it is not related with the main aim of the thesis studies, the defined optimization methods were not implemented in different optimization algorithms. Implementation of the defined optimization methods with different algorithms was left for the future studies.

# REFERENCES


[1] Mark A. Richards, **Fundamentals of Radar Signal Processing**, McGrawHill, 2005.

[2] Bassem R. Mahafza, Atef Z. Elsherbeni, **Matlab Simulations for Radar Systems Design**, Chapman & Hall/CRC, 2004.

[3] Merrill I. Skolnik, **Introduction to Radar Systems**, Third Edition, McGrawHill, 2001.

[4] Merrill I. Skolnik, **Radar Handbook**, Second Edition, McGrawHill, 1990.

[5] Nadav Levanon, Eli Mozeson, **Radar Signals**, Wiley-InterScience, 2004

[6] Charles E. Cook, Marvin Bernfeld, **Radar Signals**, Artech House, 1993.

[7] G. Morris, Linda Harkness, **Airborne Pulsed Doppler Radar**, Artech House, 1996.

[8] George W. Stimson, **Introduction to Airborne Radar**, SCITECH, 1998.

[9] Fred E., Nathanson, **Radar Design Principles**, McGraw-HILL, 1991.

[10] Bernard L. Lewis, Wesley W. Shelton, Frank F. Kretschmer, **Aspects of Radas Signal Processing**, Artech House, 1986.

[11] Fuqin Xiong, **Digital Modulation Techniques**, Artech House, 2000.

[12] Alan V. Oppenheim, Alan S. Willsky, **Signals and Systems**, Second Edition, Phipe, 1983.

[13] Alan V. Oppenheim, Ronald W. Schafer, **Discrete-Time Signal Processing**, Second Edition, Phipe, 1999.

[14] Simon Haykin, **Communication Systems**, John Wiley and Sons, 1994.

[15] John G.Proakis, **Digital Communications**, McGraw-HILL, 1995.

[16] L. R. Welch, **Lower Bounds on the Maximum Cross Correlation of Signals**, IEEE Transactions on Information Theory, Volume: 20, Issue: 3, pp 397-399, May 1974.

[17] D. V. Sarwate, **Bounds on Crosscorrelation and Autocorrelation of Sequences**, IEEE Transactions on Information Theory, Volume: 25, Issue: 6, pp 720- 724, Nov 1979.

[18] Marcel J. E. Golay, **Complementary Series**, IEEE Transactions on Information Theory, Volume: 7, Issue: 2, pp 82-87, Apr 1961.

[19] C. C. Tseng, C. L. Liu, **Complementary Sets of Sequences**, IEEE Transactions on Information Theory, Volume: 18, Issue: 5, pp: 644-652, Sep 1972.

[20] R. Sivaswamy, **Multiphase Complementary Codes**, IEEE Transactions on Information Theory, Volume: 24, Issue: 5, pp 546-552, Sep 1978.

[21] S. Z. Budisin, **New Complementary Pairs of Sequences**, Electronics Letters, Volume: 26, Issue: 13, pp 881-883, Jun 1990.

[22] B. M. Popovic, **Complementary Sets Based on Sequences with Ideal Periodic Autocorrelation**, Volume 26, No. 18, pp 1428-1430, 1990.

[23] Karl Gerlach, Frank F. Kretschmer, **General Forms and Properties of Zero Cross-Correlation Radar Waveforms**, Aerospace and Electronic Systems, IEEE Transactions, Volume: 28, Issue: 1, pp 98-104, Jan 1992.

[24] Karl Gerlach, Frank F. Kretschmer, **New Radar Pulse Compression Waveforms,** IEEE National Radar Conference, pp 194-199, Apr1988.

[25] Karl Gerlach, Frank F. Kretschmer, **Low Sidelobe Radar Waveforms Derived from Orthogonal Matrices**, IEEE Transactions on Aerospace and Electronic Systems, Volume: 27, Issue: 1, pp 92-102, Jan 1991.

[26] Jon M. Anderson, Micheal A. Temple, William M. Brown, Benjamin L. Crossley, **A Nonlinear Suppression Technique for Range Ambiguity Resolution in Pulse Doppler Radars**, IEEE National Radar Conference, pp 141-146, 2001

[27] Eli Mozeson, Nadav Levanon, **Diverse Radar Pulse-Train with Favourable Autocorrelation and Ambiguity Functions**, IEEE National Radar Conference, pp 172-176, Oct. 2002.

[28] Eli Mozeson, Nadav Levanon, **Removing Autocorrelation Sidelobes by Overlaying Orthogonal Coding on any Train of Identical Pulses**, IEEE Transactions on Aerospace and Electronic Systems, Volume: 39, Issue: 2, pp 583-603, April 2003.

[29] Graeme Nash, **Preliminary Report on Pulse Compression Waveforms and their Application to Waveform Agility**, Australian Government Department of Defence, Weapons Systems Division Systems Sciences Laboratory, 2005

[30] W. Lei, T. Long, W. Han, **Resolution of Range and Velocity Ambiguity for a Medium Pulse Doppler Radar**, IEEE International Radar Conference, pp 560-564, 2000.

[31] Xiang-Gen Xia, **Doppler Ambiguity Resolution Using Optimal Multiple Pulse Repetition Frequencies**, IEEE Transactions on Aerospace and Electronic Systems, Volume 35, No.1, pp 371-179, Jan. 1999.

[32] E. Buckley, **Ambiguity Suppression in a Multiple Beam Radar**, IEEE International Radar Conference, pp 492-496, Oct. 2002.

[33] Lin Feng-ling, M. Steiner, **New Techniques for Radar Coherent Range Ambiguity Resolution**, IEEE International Radar Conference, pp 99-104, 2001.

[34] Yong Liang Zhao, **The Relationship between the Resolution of Radar Imaging and the Condition Number of the Transformation Matrix**, M.Sc., Hong Kong University of Science and Technology, A thesis submitted in partial fulfillment of the requirements for the degree of master of science in the Department of Mathematics, 1997.

[35] Nadav Levanon, **Train of Diverse Multifrequency Radar Pulses**, IEEE Radar Conference, pp 93-98, 2001.

[36] Nadav Levanon, Eli Mozeson, **Multicarrier Radar Signal - Pulse Train and CW**, IEEE Transactions on Aerospace and Electronic Systems, Volume: 38, Issue: 2, pp 707-720, Apr 2002.

[37] Branislav M. Popovic, **Efficient Matched Filter for the Generalized Chirp-Like Polyphase Sequences**, IEEE Transactions on Aerospace and Electronic Systems, Volume: 30, Issue: 3, pp 769-777, Jul 1994.

[38] Karl R. Griep, James A.Ritcey, John J. Burlingame, **Poly-Phase Codes and Optimal Filters for Multiple User Ranging**, IEEE Transactions on Aerospace and Electronic Systems, Volume 31, No 2, pp 752-767, April 1995.

[39] Aleksa Zejak, Ervin Zentner, Predag Rapajic, **Doppler Optimized Sidelobe Suppression in Phase-coded Pulse Compression Radars**, IEEE Electrotechnical Conference, Vol.1, pp 480-483, May 1991.

[40] A. J. Zejak, E. Zentner, P. B. Rapajic, **Doppler Optimized Mismatched Filters, Electronics Letters**, Volume: 27, Issue: 7, pp 558-560, Mar 1991.

[41] Hermann Rohling, **Mismatched Filter Design for Pulse Compression**, IEEE Radar Conference, pp 253-257, May 1990.

[42] Martin H. Ackroyd, F. Ghani, **Optimum Mismatched Filters for Sidelobe Suppression**, IEEE Transactions on Aerospace and Electronic Systems, Volume AES-9, March 1973.

[43] Nadav Levanon, **Cross-Correlation of Long Binary Signals with Longer Mismatched Filters**, IEEE Proceedings Radar, Sonar and Navigation, Volume: 152, Issue: 6, pp 377- 382, Dec. 2005.

[44] Carroll Nunn, **Constrained Optimization Applied to Pulse Compression Codes and Filters**, IEEE International Radar Conference, pp 190-194, May 2005.

[45] J. M. Baden, M. N. Cohen, **Optimal Peak Sidelobe Filters for Biphase Pulse Compression**, IEEE International Radar Conference, pp 249-252, May 1990.

[46] R. K. Brayton, S. W. Director, G. D. Hachtel, L. Vidigal, **A New Algorithm for Statistical Circuit Design Based on Quasi-Newton Methods and Function Splitting**, IEEE Transactions Circuits and Systems, Volume: 26, Issue:9, pp. 784-794, Sept. 1979.

[47] A. C. W. Grace, **Computer-Aided Control System Design Using Optimization Techniques**," Ph.D. Thesis, University of Wales, Bangor, Gwynedd, UK, 1989.

[48] S. P. Han, **A Globally Convergent Method for Nonlinear Programming**, Journal of Optimization Theory and Applications, Vol. 22, pp 297-309, July 1977.

[49] K. Madsen, H. Schjaer-Jacobsen, **Algorithms for Worst Case Tolerance Optimization**, IEEE Transactions of Circuits and Systems, Volume: 26, Issue: 9, pp 775-783, Sep 1979.

[50] C. Nunn, **Constrained Optimization Applied to Pulse Compression Codes and Filters**, IEEE International Radar Conference, pp 190-194, May 2005.

[51] M. J. D. Powell, **A Fast Algorithm for Nonlinearly Constrained Optimization Calculations, Numerical Analysis**, Lecture Notes in Mathematics, Vol. 630, 1978.

[52] P. P. Gandhi, S. A. Kassam,, **Analysis of CFAR Processors in Nonhomogeneous Background**, IEEE Transactions on Aerospace and Electronic Systems, Volume: 24, Issue: 4, pp 427-445, July 1988.

[53] **MATLAB**, Language of Technical Computing Online Help Documentation.